SEISMIC ANALYSIS OF PIPELINES WITH YIELDING SUPPORTS.

by

C. A. Ibell

a thesis submitted in partial fulfilment for the degree of Master of Science in Engineering.

September 1984.

Department of Civil Engineering,
University of Cape Town.

ABSTRACT

Pipelines in structures such as a nuclear reactor can be analysed separately when the structure is subjected to seismic type loading. The pipeline is modelled with various types of supports, such as a rigid support or an elastic support. The pipeline is analysed and designed so that stresses in the pipeline and at the supports are acceptable. When the pipeline is subjected to a larger intensity earthquake than that designed for, the stresses at some supports may exceed the yield stresses, causing the support to yield. The yielding of a support can influence the response at the other supports in the pipeline, and in some cases cause failure of the supports to occur.

This thesis investigates the effect yielding of an internal pipe hangar support in a two-span pipeline has on the adjacent end supports. Essentially the findings are that the yielding of the pipe hangar support is not detrimental to the overall stability of the pipeline, as long as the support does not yield excessively.

DECLARATION

I, Christopher Anthony Ibell, declare that this is essentially my own work and has not been submitted for a degree at another university.

C. A. Ibell
September 1984.

Signed by candidate

ACKNOWLEDGEMENTS

I would like to express my gratitude to the following

Professor J. B. Martin - my supervisor and invaluable source of help

Postgraduate colleagues - Mr. C. Mercer
Mr. L. Resende
Mr. G. Duffett, for their help.

To Tony and Judy for their devotion.

To my fiance Kim, for her typing and patience.

The Civil Engineering staff for their friendship.

The Council for Scientific and Industrial Research for their financial assistance.

TABLE OF CONTENTS

NOMENCLATURE

Characters

A	a gravity multiplier, area of a cross-section
[C]	damping matrix
D	absolute relative displacement
{F}	force vector
g	gravitational acceleration
[K]	stiffness matrix
ℓ	length
M	moment
[M]	mass matrix
O	centre of curvature
P	plastic element
r	arbitrary radius of circular bend
$\bar{r}$	radius of circular bend to centroidal axis
R	radius of circular bend to neutroidal axis
R^*	increment in R
r_o	outer radius of circular bend
r_i	inner radius of circular bend
r_{po}	outer radius of pipe section
r_{pi}	inner radius of pipe section
t	time
[T]	transformation matrix
u	displacement
$\dot{u}$	velocity
$\ddot{u}$	acceleration
V	pseudovelocity
x,y,z	co-ordinate directions

Greek Characters

β	angle
γ	angle
κ	curvature

ϕ	angle
δ	displacement
Δ	increment in
ζ	degree of critical damping
ξ	mode amplitude
ω_0	natural circular frequency
ω	natural frequency
β, γ	Newmark factors

Superscripts

$\cdot$	first derivative with respect to time
$\cdot\cdot$	second derivative with respect to time
-1	inverse of a matrix
T	transpose of a matrix
max	maximum value of

Subscripts

0	initial conditions
t	time
i	the i-th iteration

Special Symbols

[ ]	matrix
{ }	vector
d	differentiation with respect to
∂	partial differentiation with respect to

CHAPTER ONE

1. Introduction

The field of structural engineering has been broadened extensively with the advent of the utilisation of nuclear energy. By the very nature of the contents of a nuclear reactor, various components of a nuclear power station are required to satisfy stringent safety requirements in the design procedure; examples of such components are the piping systems. The piping systems form an integral part of the safe operation of a nuclear power station, and hence it is essential that in event of an earthquake the pipe and pipe support stresses do not attain their ultimate failure values.

Relatively long pipelines require supports along their length to keep the pipe stresses relatively low i.e. to increase the rigidity and to decrease the flexibility of the pipeline. Typical types of supports are hangar supports, where the pipe is restrained in one direction only, and rigid supports, where the pipe may be held in position and rotation. Fig. [1.1] illustrates two extreme types of pipe supports.

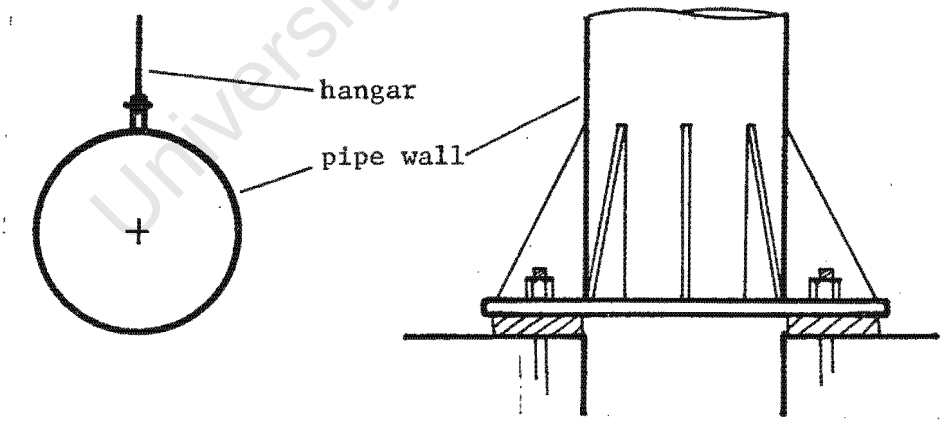

Fig. 1.1 Hangar and Rigid Pipe Support

In a seismic analysis, the fixity conditions of these piping restraints have a significant effect on the response of a piping system to a specific vibration. In most instances, the fundamental

frequency of a pipeline ranges approximately from 1Hz to 30Hz. The range of frequencies over which most earthquakes operate is approximately 0.1Hz to 40Hz which effectively means that the pipeline is likely to be severely affected by an earthquake. This is because the exciting frequency is approximately the same as the natural frequency of the pipeline. A method of reducing the effect the earthquake has on a structure is to shift the natural frequency of the structure out of the range of the earthquake. A method of moving the frequency out of the range of the earthquake is to make the structure more rigid; more supports would have to be added in a pipeline or the fixity conditions would have to change from simply supported to rigid supports. This is a costly method of solving the problem.

A pipeline is usually designed to withstand an earthquake elastically. In the event of an earthquake causing greater support reactions than designed for, inelasic deformations can occur in the pipe support. When inelastic deformations occur in a pipe support, energy is dissipated through plastic work. When an internal pipe support yields in a static analysis, the load is redistributed to adjacent pipe supports, resulting in an increase in adjacent pipe support forces. The question arose of whether the maximum forces at adjacent supports, in a dynamic analysis, would also increase during the response, and if so, would yielding of the adjacent support occur and thus lead to a total collapse of the pipeline system.

Previous work in this field was done by POWELL and ROW [1]. In their work, various pipelines were analysed with in-phase shaking with a number of yielding internal supports. Their results showed that, for piping systems with moderate amounts of restraint, there was a consistent trend towards a reduction in pipe stresses and pipe support reactions as the yield stress of the restrainer decreased. Conversely, for heavily restrained pipelines, the pipe stresses and pipe support reactions increased as the restrainer yield stress decreased. In most examples it was found that the addition of an energy absorbing support was preferable to the absence of any

support.

The overall aim of this thesis was to investigate further the effect the reduction in yield stress in an internal pipe hangar support had on adjacent rigid pipe supports, as well as to investigate trends which could lead to setting up a simple design procedure for the earthquake analysis of pipelines with yielding supports. For this purpose, two two-span simulated pipelines were set up, so that this effect of progressive yielding of the internal elasic-plastic support under earthquake conditions could be studied. In the two pipeline configurations three wall thicknesses for the first and two thicknesses for the second were considered. Five earthquake records were used for each different pipeline. The method that was followed to model the progressive reduction in yield stress of an internal support was to procede with a fully elastic analysis of the pipeline with the internal support in position. The maximum force in the hangar was found, hence the maximum elastic stress was found. The maximum stress was then set equal to a yield stress for the hangar.

Five more analyses were then carried out for each pipeline and for each earthquake record, reducing the yield stress form its maximum value to zero. At zero yield stress, the pipe acted as if the support was non-existent, which was to be expected. The general results showed a consistent trend that as the yield stress in the hangar decreased so the adjacent pipe support forces increased. However, if the yield stress was zero, the adjacent pipe support reactions usually rose above that of the elastic system with the elastic hangar.

The finite element method of analysis was chosen to model the simulated pipelines, for the reasons that it can model straight and curved sections of a pipeline separately, it can model the response of the pipeline accurately and it carries out transient analyses efficiently. A finite element computer program was required to analyse pipe loops under earthquake loading; it had to thus incorporate transient analysis capabilities, both time history and

frequency analyses, as well as have a complete structural element library.

The program chosen was NOSTRUM, a non-linear finite element program, developed as a research program by the UCT/CSIR APPLIED MECHANICS RESEARCH UNIT at the University of Cape Town. At the start of the investigation, the structural element library within NOSTRUM contained truss, beam and spring elements. It did not contain a curved pipe element, essential for modelling pipe bends efficiently. A large number of discreet straight pipe elements would be necessary to obtain a similar degree of accuracy to that of a single curved pipe element; furthermore, a large number of discreet straight pipe elements should not generally be used to model a curve because the strain distribution across a straight and across a curved pipe element is radically different. Thus a suitable formulation for a curved pipe element had to be derived and implemented into NOSTRUM. This involved the formulation of the stiffness matrices for the straight and curved pipe elements, with the stiffness matrix co-ordinate systems of the respective elements matching that of other structural elements within the computer program.

The inclusion of the effect of an internal support yielding in a seismic analysis requires the use of a time history analysis. The response spectrum approach cannot include the effect of any inelastic behaviour of the structure. For a time-history analysis, the earthquake acceleration-time record is input into the program. The simulated pipelines were subjected to a variety of earthquake records, four of them being actual earthquake records and the fifth an artificially generated one. All the peak accelerations were scaled to a peak ground acceleration of 0.3g. Even though the peak accelerations of the different earthquake records were the same, the response of the pipelines varied greatly from earthquake to earthquake. Various single degree of freedom mode approximation systems were set up to simulate the multi-degree of freedom system. It was hoped that similar trends would occur in both the multi-degree and single degree of freedom systems so that predictions of the

multi-degree of freedom behaviour could be extrapolated from the single degree of freedom results.

In summary, the thesis consists firstly of the formulation of the curved and straight pipe stiffness matrices in Chapter 2, followed by a discussion on NOSTRUM. Chapter 3 describes time history and the modal superposition with response spectrum approach. Chapter 4 describes the simulated pipeline configurations followed by the discussion of the results and conclusions in Chapter 5.

CHAPTER TWO

2. Finite Element Modelling of Pipelines

2.1 The Finite Element Method

The finite element method of structural analysis is, as the name implies, the discretisation of a structure into finite parts. These separate parts or elements make up a finite element mesh. Each element within the mesh has a certain stiffness and certain external loading functions, and by assembling all the element stiffnesses and load terms a system stiffness matrix K and a load vector F can be found.

The equilibrium equation Ku = F can then be solved for the unknown displacement variables u. Using the evaluated total displacements the elemental stresses, strains and reactions can be calculated.

This method is a natural extension of the displacement method where equilibrium equations were found at each node and a set of simultaneous equations are solved to obtain the nodal displacements. In this generalised displacement method, the finite element method, stiffness matrices and load vectors are calculated element by element, and thus it is convenient to assemble a global stiffness matrix and load vector also in an element by element fashion. In this way global equilibrium equations are found.

In a finite element model of a pipe loop, two types of elements are required to discretize the structure. They are a straight pipe element and a curved pipe element, the latter for modelling circular bends in the pipe loop. The formulation of each element stiffness matrix is necessary so that the global stiffness matrix for the total pipe loop can be assembled and solved using the above procedures.

Since the computational work involved in this thesis required the

setting up of simulated pipe loops under earthquake loading, it was necessary to formulate both element stiffness matrices. The curved pipe element stiffness matrix formulation follows in section 2.2 and the straight pipe element stiffness matrix formulation in section 2.3.

2.2 The Formulation of a Finite Curved Pipe Element Stiffness Matrix

The basis of the formulation of the stiffness matrix for the curved pipe element was that of DAVIS, HENSHELL and WARBURTON [2]; the same matrix was implemented into PAFEC 70. The element stiffness matrix was based on the integration of the exact differential equations of an infinitesimal element in static equilibrium. The stiffness matrix was formed for a local co-ordinate system as shown in fig [2.1]. It was then transformed into the local co-ordinate system shown in fig [2.2]. This transformation was carried out so that the pipe element co-ordinate system would be compatible with the other structural elements in the finite element program.

The general solution procedure [3] of the curved beam element stiffness matrix was to obtain the stress/strain relationships and three equilibrium conditions and then to find their general solution. Primarily, the difference between a straight beam and a curved beam is that the strain distribution across an arbitrary cross section is not linear but hyperbolic. The displacement across the section is linear but because the outer fibres are longer than the inner fibres the strains are hyperbolic, as will be shown later.

Consider a curved member as shown in fig [2.3]. The outer fibres are a distance r_0 from the centre of curvature O, the inner fibres are at a distance r_i and the distance from O to the centroidal axis is $\bar{r}$. The solution to this problem is based on the assumption that sections perpendicular to the axis of the beam remain plane after a bending moment M is applied. This is diagrammatically represented by the line ef in relation to an element of the beam abcd. The element is defined by the central angle ϕ.

Although the linear displacement assumption is the same as for straight beams, and, from Hooke's Law, the normal stress $\sigma = E\varepsilon$, a difficulty is encountered. The initial length gh depends on the distance r from the centre of curvature. Thus although the total displacement of beam fibres, described by small angle γ , follows a

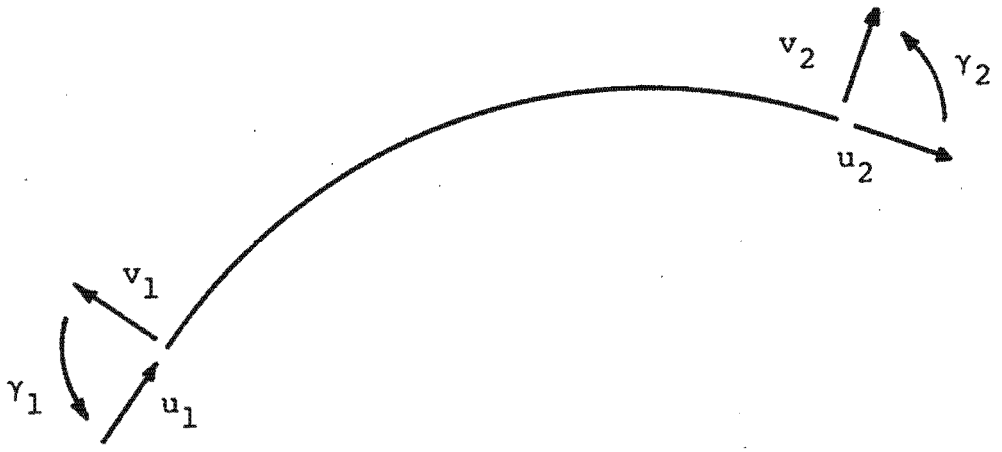

Figure 2.1 Initial Local Co-ordinate System

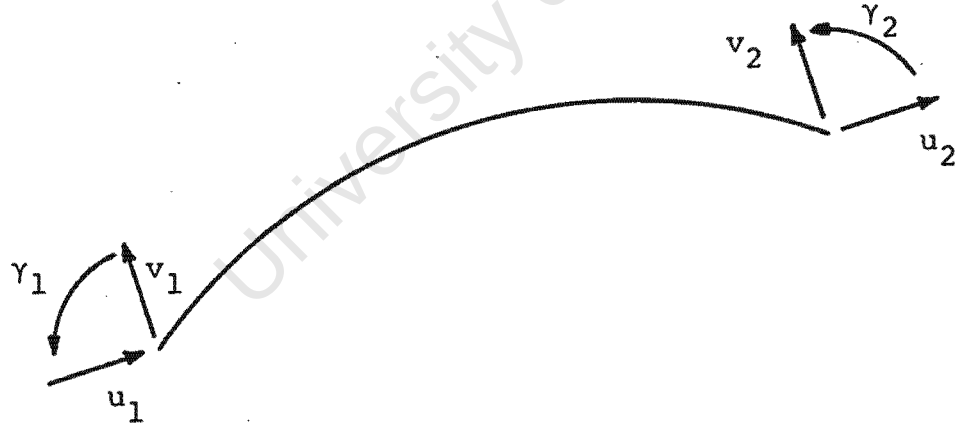

Figure 2.2 Final Local Co-ordinate System

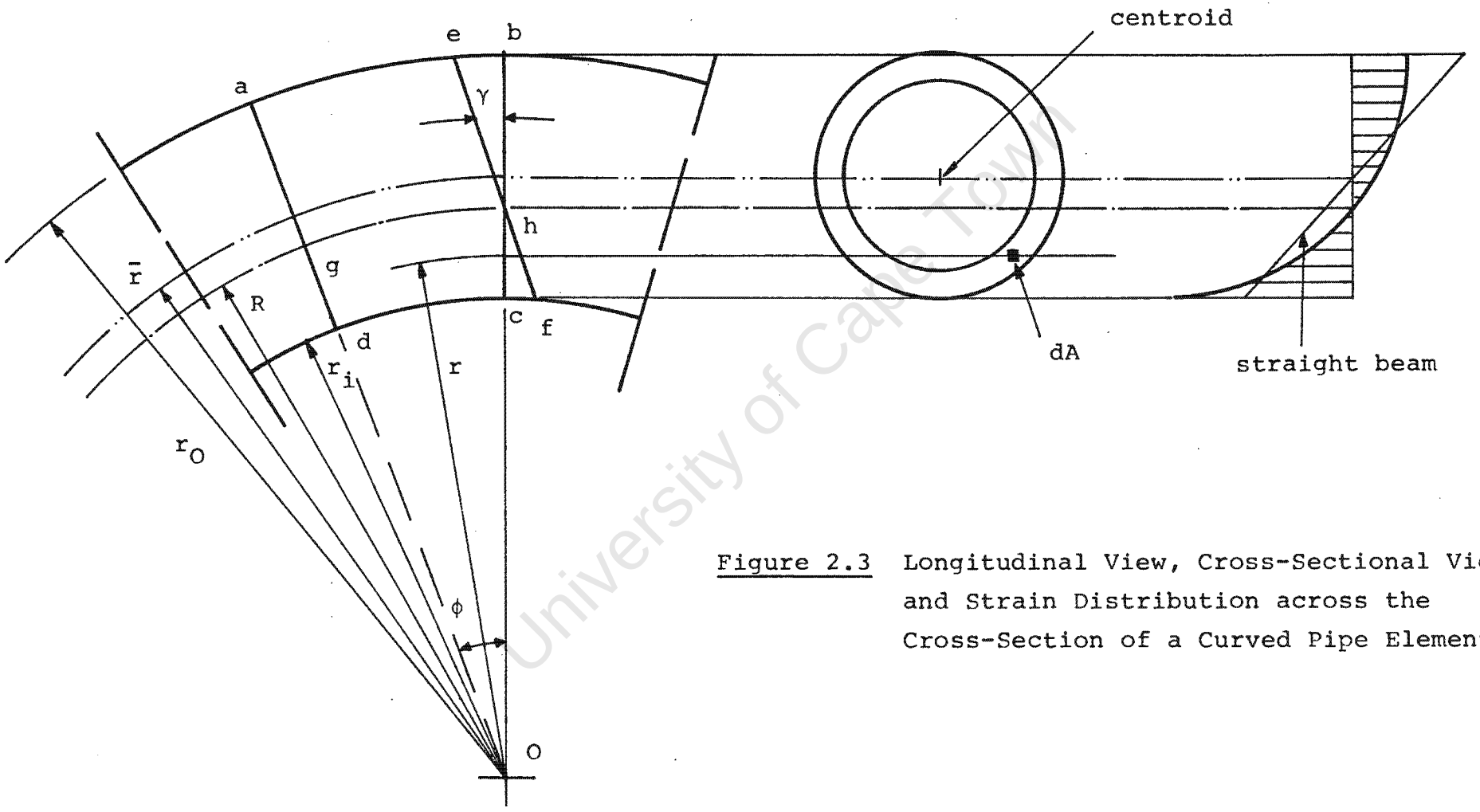

Figure 2.3 Longitudinal View, Cross-Sectional View and Strain Distribution across the Cross-Section of a Curved Pipe Element.

linear law, the strains do not. The elongation of a generic fibre gh is $(R - r)\gamma$, where R is the distance from O to the neutral axis, as yet unknown, and its initial length is $r\phi$. The strain of any arbitrary fibre is $(R - r)\gamma/r\phi$ and the normal stress $\sigma = E\varepsilon$ on an element dA of the cross sectional area is

$$\sigma = E\varepsilon = E(R-r).\frac{\gamma}{r\phi} \quad . \qquad (2.1)$$

Therefore rearranging terms we see that

$$\frac{\sigma r}{(R-r)} = E\frac{\gamma}{\phi} \quad . \qquad (2.2)$$

Equation (2.1) gives the normal stress acting on an element of area of the cross section of the curved beam. The location of the neutral axis follows from the condition that the total net axial force acting across the cross section of the element is equal to zero. Therefore, upon integrating the stresses over the cross sectional area,

$$\int_A \sigma \, dA = \int_A \frac{E(R-r)\gamma}{r\phi} \, dA = 0. \qquad (2.3)$$

However since E,R, ϕ and γ are independant of r at any section of a stressed beam, they may be taken outside the integral sign and a solution for R obtained. Thus,

$$E\frac{\gamma}{\phi}\int_A \frac{R-r}{r} \, dA = E\frac{\gamma}{\phi}\left(R\int_A \frac{dA}{r} - \int_A dA\right) = 0. \qquad (2.4)$$

Therefore,

$$R = \frac{A}{\int_A \frac{dA}{r}} \quad , \qquad (2.5)$$

which for convenience may be written as,

$$R = \frac{A}{A_m} \quad ,$$

where A_m is a function of the cross sectional shape of the beam. For

the particular case that has been dealt with in this thesis, namely a pipe section, A_m is given explicitly in terms of $\bar{r}, r_{pi}$ and r_{po} . The values $\bar{r}, r_{pi}$ and r_{po} are the distance from the centre of curvature of the bend, the pipe inner wall radius and the pipe outer wall radius respectively as shown in fig [2.4] and obtained from ref. [6]. Thus for a pipe section,

$$A_m = 2\pi[(\bar{r}^2 - r_{pi}^2)^{1/2} - (\bar{r}^2 - r_{po}^2)^{1/2}] \quad , \qquad (2.6)$$

and thus

$$R = \frac{(r_{po}^2 - r_{pi}^2)}{2[(\bar{r}^2 - r_{pi}^2)^{1/2} - (\bar{r}^2 - r_{po}^2)^{1/2}]} . \qquad (2.7)$$

Now that the radius at which zero axial strain is known, it is now possible to obtain the differential equations necessary to find a general solution.

Note that the neutral axis so found does not coincide with the centroidal axis. This differs from the situation for straight elastic beams.

Now that the radius R, the position of the neutral axis, is known, the equation for the stress distribution is obtained by equating the external moment to the internal moment, obtained from the stresses in equation (2.1). The integration of the stresses times their respective lever arms is made about the z-axis which is normal to the plane of the figure shown in fig [2.1]. Thus

$$M = \int_A \sigma \, dA(R-r) = \int_A \frac{E(R-r)^2 \gamma}{r\phi} \, dA \ .$$

The terms E, R, ϕ and γ are independent of r at the section, therefore using equation (2.2), the following is obtained,

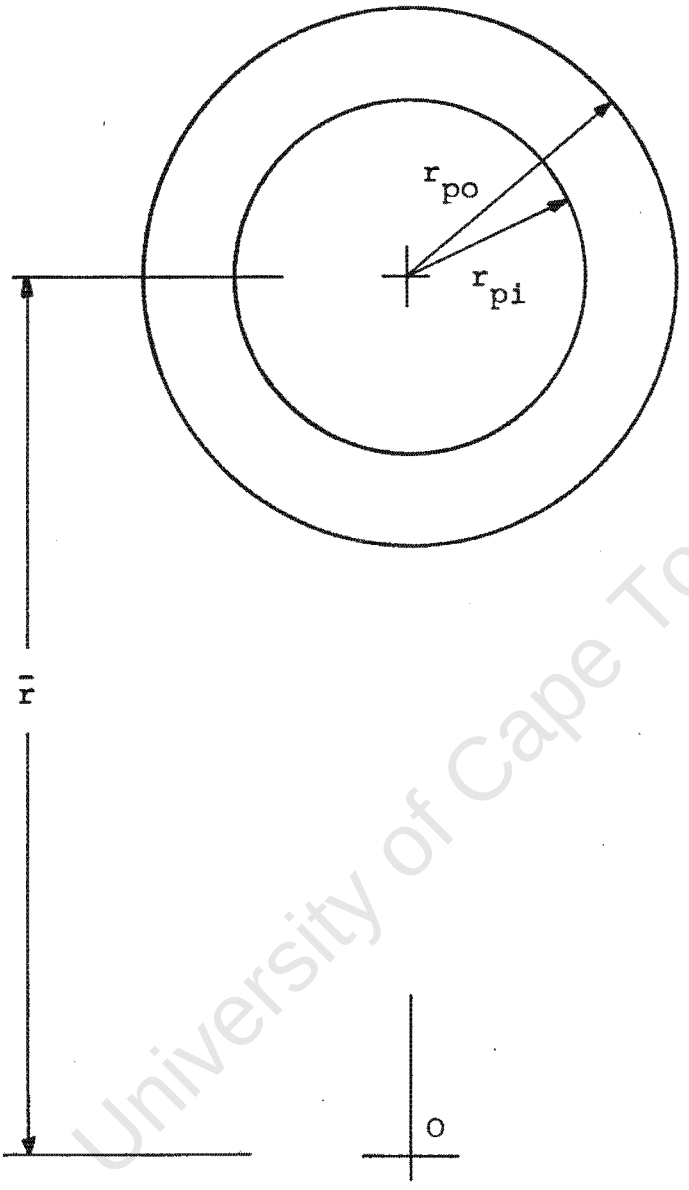

Figure 2.4 Cross-Section of Curved Pipe

$$M = \frac{E\gamma}{\phi}\int_A \frac{(R-r)^2}{r}\,dA = \frac{\sigma r}{(R-r)}\int_A \frac{(R-r)^2}{r}\,dA \ .$$

Using equation (2.4), it follows that

$$M = \frac{\sigma r}{(R-r)}\left[\int_A \frac{R(R-r)}{r}\,dA - \int_A \frac{r(R-r)}{r}\,dA\right]$$

$$= \frac{\sigma r}{(R-r)}\left[-R\int_A dA + \int_A r\,dA\right] \ .$$

The first integral is A and the second, by definition is $\bar{r}A$. Hence

$$M = \frac{\sigma r}{(R-r)}(\bar{r}A - RA) \ , \qquad (2.8)$$

whence the normal stress acting on a curved beam at distance r from the centre of curvature is

$$\sigma = \frac{M(R-r)}{rA(\bar{r}-R)} \ . \qquad (2.9)$$

Using equations (2.1) and (2.8) one obtains,

$$M = EA\frac{\gamma}{\phi}(\bar{r}-R) \qquad (2.10)$$

Fig [2.5] shows the displaced configuration of an element. From this it can be seen that,

$$\frac{\gamma}{\phi} = \frac{R^*}{R}$$

for small displacements i.e. $R \gg R^*$.

Therefore,

$$M = EAR^{*}\left(\frac{\bar{r}-R}{R}\right) \qquad (2.11)$$

As is also shown in fig [2.5] the total relative rotation is

$$\beta = \phi - \gamma ,$$

where

$$\gamma = \frac{1}{R}\left(\frac{dv}{d\phi}\right) ,$$

$$\phi = \frac{u}{R+v} .$$

Since $R \gg v$, we may put

$$\phi = \frac{u}{R} .$$

Therefore

$$\beta = -\frac{1}{R}\left(\frac{dv}{d\phi} - u\right) . \qquad (2.12)$$

From the geometry of deformation,

$$R^{*} = R\frac{d\beta}{d\phi} ,$$

$$= -R\frac{d}{d\phi}\left[\frac{1}{R}\left(\frac{dv}{d\phi} - u\right)\right] . \qquad (2.13)$$

Substituting (2.13) into (2.11),

$$M = -EA\left(\frac{\bar{r}-R}{R}\right)\left[\frac{d^{2}v}{d\phi^{2}} - \frac{du}{d\phi}\right]$$

$$= C_{1}\left[\frac{d^{2}v}{d\phi^{2}} - \frac{du}{d\phi}\right] . \qquad (2.14)$$

For thin walled sections and where $R \gg r_{po}, r_{pi}$ the constant C_{1}

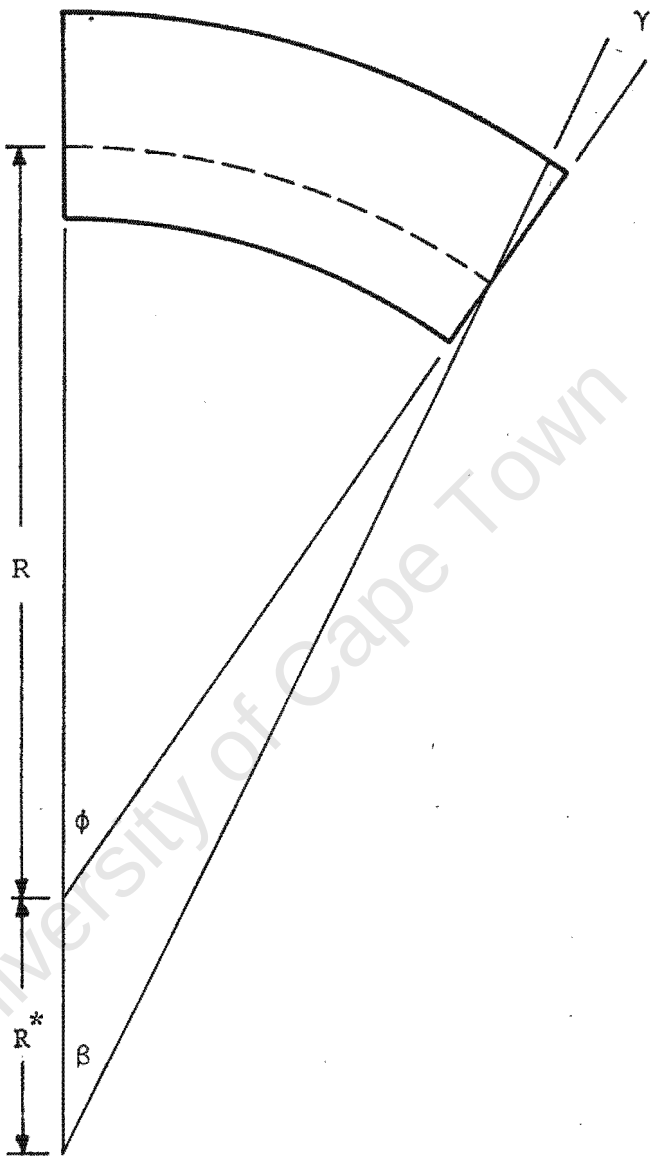

Figure 2.5 Displaced Configuration of a Curved Pipe Element under Pure Bending

converges to

$$C_1 = \frac{EI}{\bar{r}^2} \quad . \tag{2.15}$$

This makes the calculations somewhat easier as C_1 is no longer a complicated function of cross sectional shape but simply the second moment of area of the cross section about which bending occurs, the I value. The corresponding relationship between axial force and displacements is

$$F_u = \frac{EA}{\bar{r}} \left(\frac{du}{d\phi} + v \right)$$

$$= C_2 \left(\frac{du}{d\phi} + v \right) \quad . \tag{2.16}$$

From fig [2.6] the three equilibrium equations can be deduced. They are

$$\frac{dM}{d\phi} = RF_v \quad , \tag{2.17}$$

$$\frac{dF_u}{d\phi} = F_v \quad , \tag{2.18}$$

$$\frac{dF_v}{d\phi} = -F_u \quad . \tag{2.19}$$

Equations (2.14), (2.16), (2.17), (2.18) and (2.19) are the five differential equations necessary to find the general solution of the system. The five equations equations contain three displacement variables, u, v and γ, as well as three force variables, F_u, F_v and M. Four of the equations are first order differential equations and (2.14) is a second order differential equation leading to six constants of integration, α_1 to α_6. Solving these five equations one obtains two distinct equations relating diplacements and forces respectively to the constants of integration. Thus,

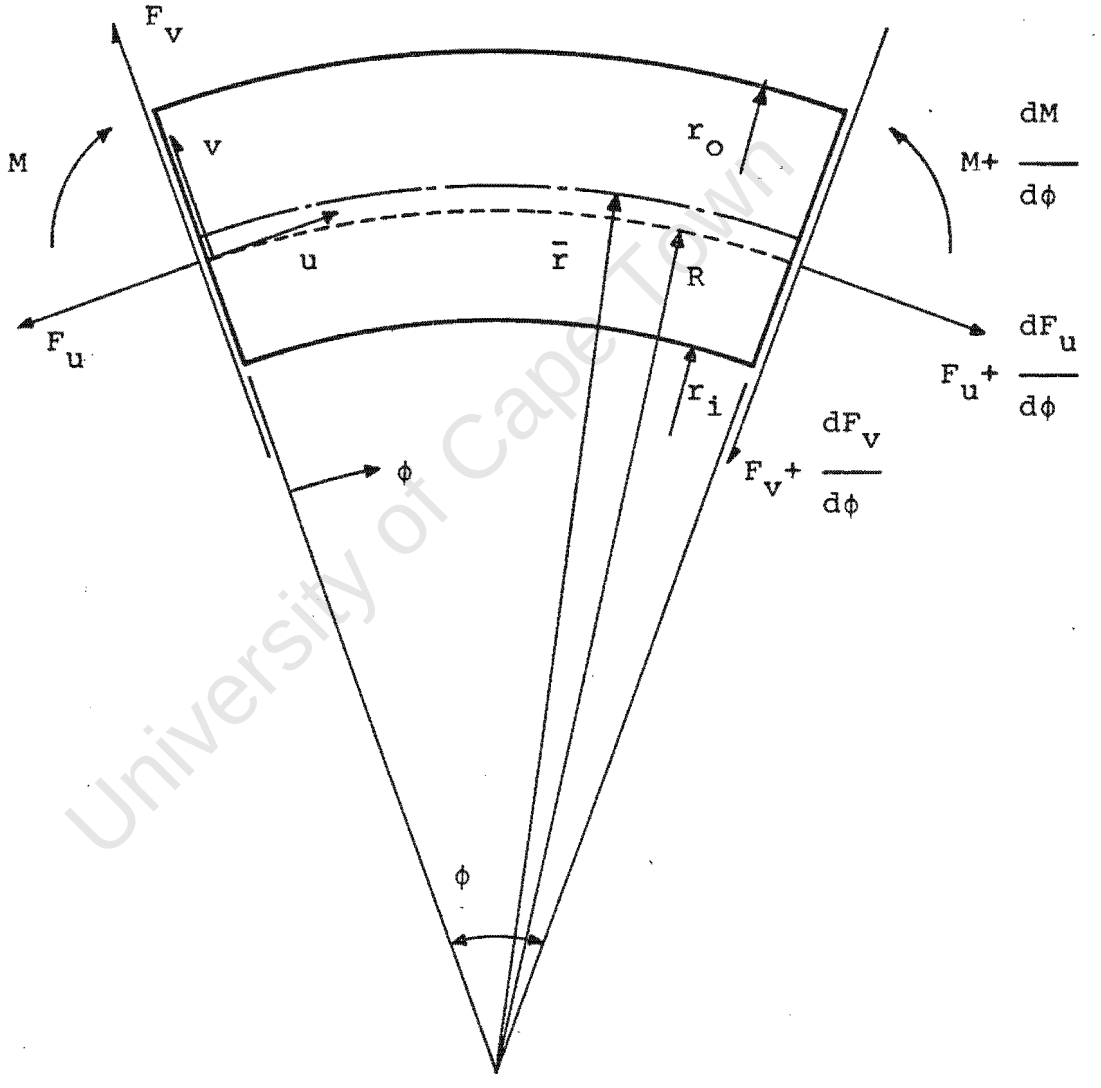

Figure 2.6 Forces and Displacements on an Infinitesimal Curved Pipe Element.

$$\begin{Bmatrix} u \\ v \\ \gamma \end{Bmatrix} = \begin{bmatrix} 1 & -\phi & \cos\phi & -\sin\phi & \phi\cos\phi & \phi\sin\phi \\ 0 & 1 & \sin\phi & \cos\phi & (\phi\sin\phi + C_3\cos\phi) & (C_3\sin\phi - \phi\cos\phi) \\ -\frac{1}{r_0} & \frac{\phi}{r_0} & 0 & 0 & C_4\frac{\sin\phi}{r_0} & -C_4\frac{\cos\phi}{r_0} \end{bmatrix} \begin{Bmatrix} \alpha_1 \\ \alpha_2 \\ \alpha_3 \\ \alpha_4 \\ \alpha_5 \\ \alpha_6 \end{Bmatrix}$$

and, (2.20)

$$\begin{Bmatrix} F_u \\ F_v \\ M \end{Bmatrix} = \begin{bmatrix} 0 & 0 & 0 & 0 & C_6\cos\phi & C_6\sin\phi \\ 0 & 0 & 0 & 0 & -C_6\sin\phi & C_6\cos\phi \\ 0 & C_1 & 0 & 0 & C_5\cos\phi & C_5\sin\phi \end{bmatrix} \begin{Bmatrix} \alpha_1 \\ \alpha_2 \\ \alpha_3 \\ \alpha_4 \\ \alpha_5 \\ \alpha_6 \end{Bmatrix}$$

(2.21)

where α_i are constants of integration.

The stiffness matrix [K] can now be found directly for the global directions.

The solutions to the differential equations (2.20) and (2.21) can now be applied to the finite element with the convention for the generalised forces and displacements shown in fig [2.7]. The forces and displacements of the infinitesimal element are described with reference to the local co-ordinate system given in fig. [2.1] and these forces must be resolved at the ends of the element into the directions shown in fig [2.7] to make the element compatible with

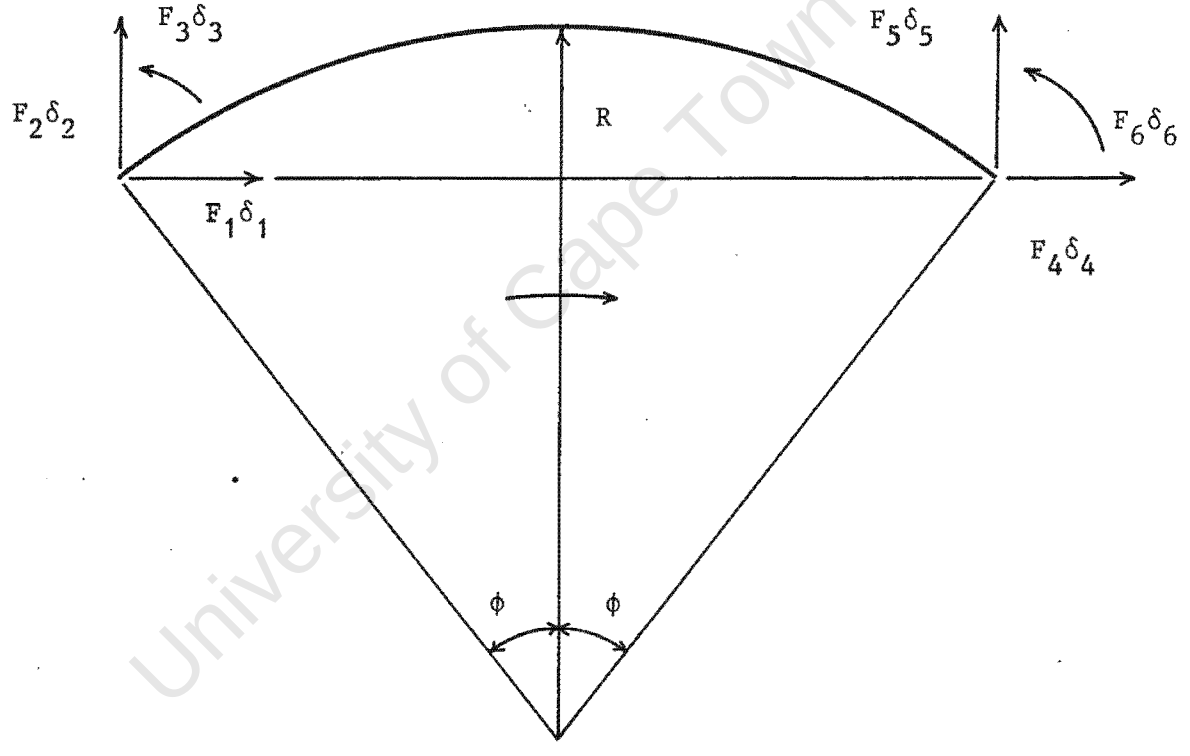

Figure 2.7 Convention of Generalised Forces and Displacements.

most computer programs.

The displacement vector $\{\delta\}$ shall now be defined as

$$\{\delta\} = \begin{Bmatrix} u \\ v \\ \gamma \end{Bmatrix}$$

and the force vector $\{F\}$ as

$$\{F\} = \begin{Bmatrix} F_u \\ F_v \\ M \end{Bmatrix} .$$

The relationship given in equations (2.20) and (2.21) can now be written as

$$\{\delta\} = [X]\{\alpha\} \qquad (2.22)$$

and

$$\{F\} = [Y]\{\alpha\} . \qquad (2.23)$$

To obtain displacements and forces in a different co-ordinate system the original displacement vector and force vector must be transformed by a transformation matrix [T]. Thus defining the new co-ordinate system displacement vector as $\{\hat{\delta}\}$ and the force vector as $\{\hat{F}\}$, the following relations hold true that

$$\{\hat{\delta}\} = [T]\{\delta\} \qquad (2.24)$$

$$\{\hat{F}\} = [T]\{F\} . \qquad (2.25)$$

Relating $\{\hat{\delta}\}$ and $\{\hat{F}\}$ through the transformation matrix [T], the constants of integration α and the matrices [X] and [Y], the equation

$$\{\hat{F}\} = [T][Y][[T][X]]^{-1}\{\hat{\delta}\} \qquad (2.26)$$

is obtained.

Substituting [T][Y] as [B] and [T][X] as [A] the simplified form of equation (2.26) is

$$\{\hat{F}\} = [B][A]^{-1}\{\hat{\delta}\} \qquad (2.27)$$

Which can be expressed as,

$$\{\hat{F}\} = [K]\{\hat{\delta}\}$$

where [K] is the element stiffness matrix for in-plane stiffness of a curved beam. The matrix [K] is symmetrical about the leading diagonal even though [A] and [B] are unsymmetrical matrices.

The constants C_1 and C_2, which appear in equation (2.14) and (2.16), together with constants C_3 to C_6, which are used in (2.20) and (2.21), are given below,

$$C_1 = \frac{EI}{\bar{r}^2} \qquad (2.28)$$

$$C_2 = \frac{EA}{\bar{r}^2} \qquad (2.29)$$

$$C_3 = \frac{\bar{r}C_2 - C_1}{-\bar{r}C_2 - C_1} \qquad (2.30)$$

$$C_4 = 1 - C_3 \qquad (2.31)$$

$$C_5 = C_1C_4 \qquad (2.32)$$

$$C_6 = C_2(1+C_3) \qquad (2.33)$$

The matrices [A] and [B] which together make up the stiffness matrix [K] are respectively,

$$[A] = \begin{bmatrix} \cos\phi & \phi\cos\phi-\sin\phi & 1 & 0 & -\phi-C_4\sin\phi\cos\phi & C_4\sin^2\phi \\ \sin\phi & \phi\sin\phi+\cos\phi & 0 & 1 & C_4\cos^2\phi & \phi-C_4\sin\phi\cos\phi \\ -1/R & -\phi/R & 0 & 0 & -C_5\sin\phi/R & -C_5\cos\phi/R \\ \cos\phi & \sin\phi-\phi\cos\phi & 1 & 0 & \phi+C_4\sin\phi\cos\phi & C_4\sin^2\phi \\ -\sin\phi & \phi\sin\phi+\cos\phi & 0 & 1 & C_4\cos^2\phi & -\phi+C_4\sin\phi\cos\phi \\ -1/R & \phi/R & 0 & 0 & C_5\sin\phi/R & -C_5\cos\phi/R \end{bmatrix} \quad (2.34)$$

and,

$$[B] = \begin{bmatrix} 0 & 0 & 0 & 0 & -C_7 & 0 \\ 0 & 0 & 0 & 0 & 0 & C_7 \\ 0 & -C_1 & 0 & 0 & -C_6\cos\phi & C_6\sin\phi \\ 0 & 0 & 0 & 0 & C_7 & 0 \\ 0 & 0 & 0 & 0 & 0 & -C_7 \\ 0 & C_1 & 0 & 0 & C_6\cos\phi & C_6\sin\phi \end{bmatrix} \quad (2.35)$$

Since $K = [B].[A]^{-1}$, to find [K] the constants C_1 to C_6, the value of ϕ from the co-ordinates of the end points of the curve and the known values of A (cross sectional area of pipe), I (second moment of area), E (Youngs Modulus) and $\bar{r}$ (the radius from the centre of a curvature of the bend to the centroid of the pipeline) have to be calculated.

2.3 Accuracy and Limitations of the Curved Pipe Element

The element derived in the previous section did not include the effects of shear deformation. This will lead to an inaccuracy in the displacements obtained from the analyses. As well as this, various simplifications were made to make the element easier to implement and use in a finite element program.

The first simplification, that of neglect of shear deformation, was introduced because the effect of shear is small compared to bending and axial effects for the particular pipeline problems under consideration and the extra computations required for a minor increase in accuracy are not justified.

The second simplification was that of assuming that the radius of the bend R was large in relation to the in plane radial displacement of the pipe, v. Fig [2.8] shows the actual deformation of a pipe element. In the formulation the angle β, the total rotation of the cross section relative to the left hand side face, was given by

$$\beta = -\frac{1}{R}\left(\frac{dv}{d\phi} - u\right) \quad . \qquad (2.36)$$

However, as can be seen from fig [2.8], β should be written as

$$\beta = -\frac{1}{R}\left(\frac{dv}{d\phi}\right) + \left(\frac{u}{R+v}\right) \quad . \qquad (2.37)$$

This complicates the equation and hence, since $R \gg v$, the equation (2.36) was used instead of (2.37).

The third and final simplification of the element was that the constant C_1 was, for thin walled pipes or for pipe bend radii much larger than the pipe wall outer radius, written as,

$$C_1 = \frac{EI}{r^2} \quad . \qquad (2.38)$$

This simplified the computations since the previous expression

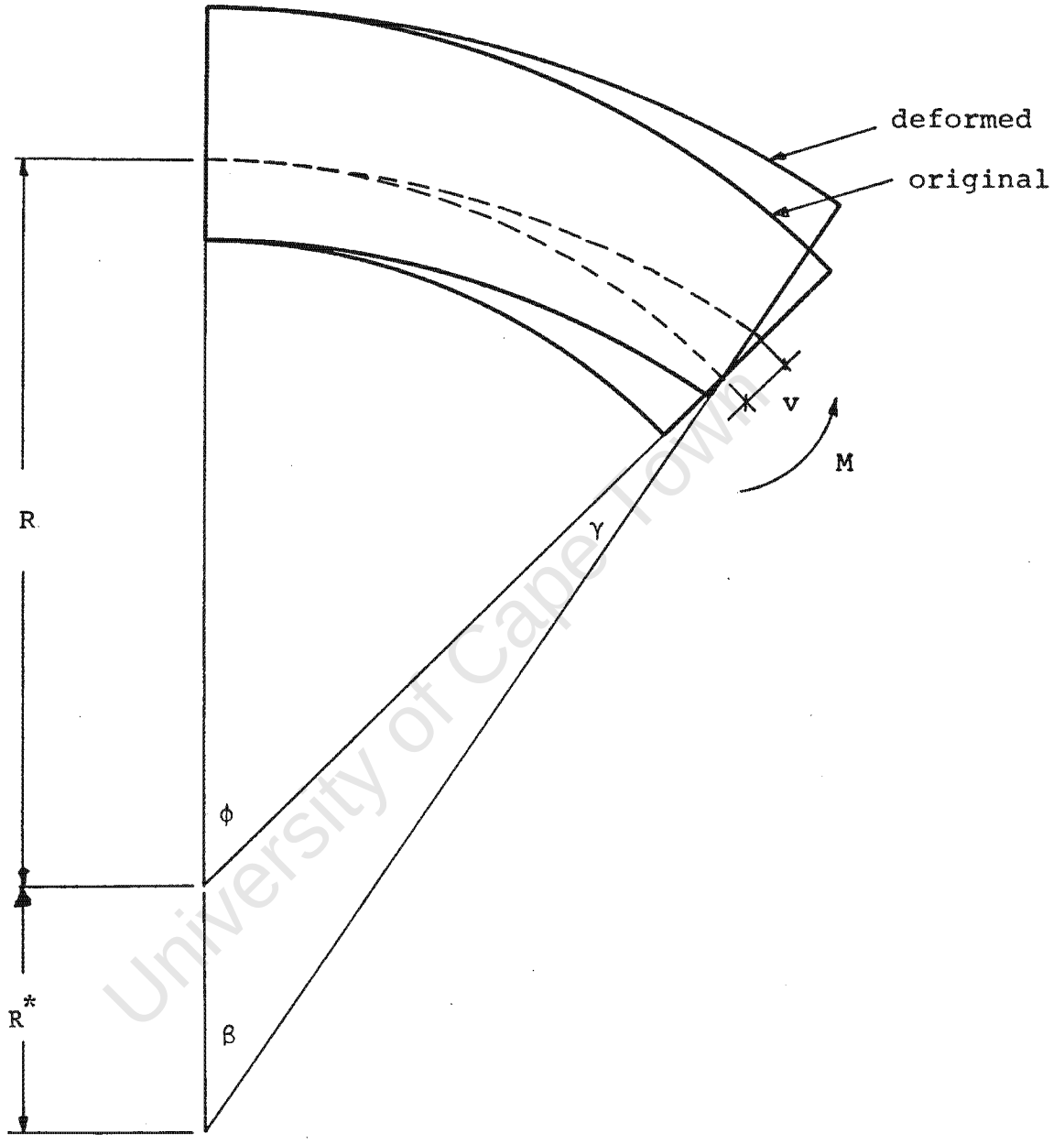

Figure 2.8 Actual Deformation Pattern of a Curved Beam under Pure Bending Moment.

for C_1,

$$C_1 = -EA\left(\frac{\bar{r}-R}{R}\right) \qquad (2.39)$$

was dependent on R which was in turn dependent on the cross sectional area.

Due to the above simplifications and approximations, the prime limitation placed on the element usage, is that the element should never subtend an angle of more than 45° or less than 5°. These values were found by running certain test analyses and checking the results against analytical solutions. Furthermore the limitation is stipulated in the PAFEC-70 User's Manual [12].

2.4 The Formulation of a Finite Straight Pipe Element Stiffness Matrix

The basic assumption [4] in straight pipe-bending analyses, excluding shear deformations, is that a normal to the midsurface (neutral axis) of the pipe remains straight during deformation and that the angular rotation is equal to the slope of the beam mid-surface. This kinematic assumption, illustrated in fig [2.9] leads to the well-known pipe-bending governing differential equation in which the transverse displacement, w, is the only variable. Therefore using straight pipe elements formulated with this theory, displacement continuity between elements requires that w and dw/dx be continuous.

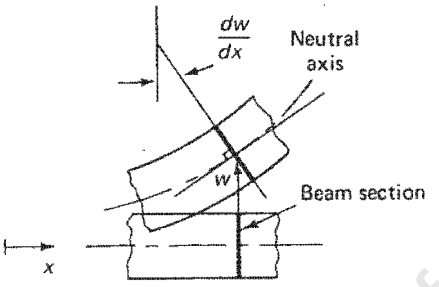

Deformation of cross-section

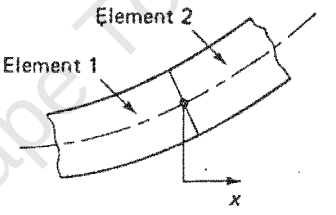

Boundary conditions between beam elements

$$w\Big|_{x^{-0}} = w\Big|_{x^{+0}} \; ; \; \frac{dw}{dx}\Big|_{x^{-0}} = \frac{dw}{dx}\Big|_{x^{+0}}$$

Figure 2.9 Beam Deformations excluding Shear Effect

The stiffness matrix of a thin uniform beam fig [2.10] shall now be derived [5] starting from the interpolation formula for the deflection w. The element is loaded only at the nodes, the two ends; it takes a cubic deflected shape. This follows from the equation

$$d^4w/dx^4 = 0 \ ,$$

so that

$$w = a_1x^3 + a_2x^2 + a_3x + a_4 \ ,$$

where $a_1,\ldots,a_4$ are constants of integration defined by the boundary conditions.

It is much more convenient to introduce the boundary conditions via the shape functions N_i (Table 2.1), so that

$$w = w_a N_1 + \Theta_A N_2 + w_B N_3 + \Theta_B N_4 \qquad (2.40)$$

where $\Theta_A = dw/dx$ at node A, for example. Thus the slopes are additional nodal variables.

shape functions	x = 0		x = ℓ		graph
	N	dN/dx	N	dN/dx	
$N_1=1-3(x/\ell)^2+2(x/\ell)^3$	1	0	0	0	
$N_2=x(1-(x/\ell))^2$	0	1	0	0	
$N_3=3(x/\ell)^2-2(x/\ell)^3$	0	0	1	0	
$N_4=(x-\ell)(x/\ell)^2$	0	0	0	1	

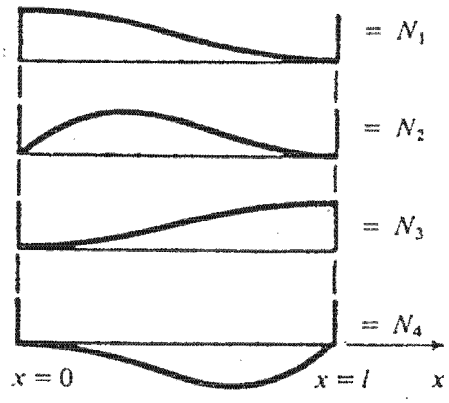

Table 2.1 Shape Functions

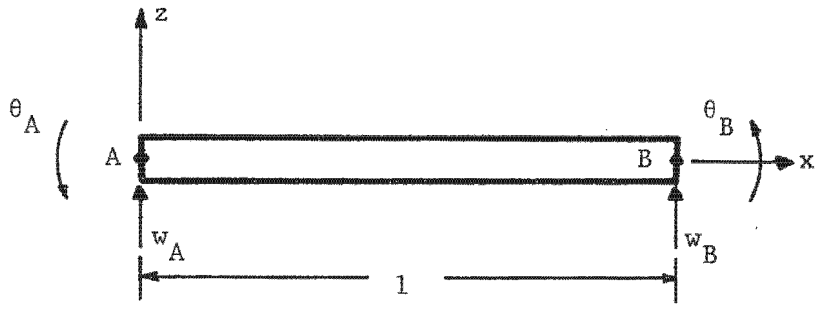

Fig 2.10 Beam Element

For the beam element the strain energy is $\int \frac{1}{2} EI\ (\kappa)^2\ dx$, where EI is the bending modulus, and κ is the curvature.

$$\kappa = \frac{d^2w}{dx^2} = w_A\frac{d^2N_1}{dx^2} + \theta_A\frac{d^2N_2}{dx^2} + w_B\frac{d^2N_3}{dx^2} + \theta_B\frac{d^2N_4}{dx^2}$$

$$= [w_A, \theta_A, w_B, \theta_B] \cdot \begin{bmatrix} -\frac{6}{l^2} + \frac{12x}{l^3} \\ -\frac{4}{l} + \frac{6x}{l^2} \\ +\frac{6}{l^2} - \frac{12x}{l^3} \\ -\frac{2}{l} + \frac{6x}{l^2} \end{bmatrix}$$

$$= \begin{bmatrix} -\frac{6}{l^2} + \frac{12x}{l^3} & -\frac{4}{l} + \frac{6x}{l^2} & \frac{6}{l^2} - \frac{12x}{l^3} & -\frac{2}{l} + \frac{6x}{l^2} \end{bmatrix} \begin{bmatrix} w_A \\ \theta_A \\ w_B \\ \theta_B \end{bmatrix} \qquad (2.41)$$

Thus putting $l = 1$ the strain energy is expanded to:

$$\text{Strain energy} = \tfrac{1}{2} \int_0^1 [w_A, \theta_A, w_B, \theta_B] \cdot \begin{bmatrix} -6 + 12x \\ -4 + 6x \\ 6 - 12x \\ -2 + 6x \end{bmatrix} x$$

$$EI\ [-6+12x\ ,\ -4+6x\ ,\ 6-12x\ ,\ -2+6x] \begin{bmatrix} w_A \\ \theta_A \\ w_B \\ \theta_B \end{bmatrix} dx \qquad (2.42)$$

Using $\{\delta\}$ for the vector of deflection, we observe that we can take

$\{\delta\}$ outside the integral, because the nodal w_i and θ_i are variables in the structural problem, but not in the integration. As before, we recall the strain energy, $S = \frac{1}{2}\,\delta^T K \delta$ so that

$$K = \int_0^1 \begin{bmatrix} -6+12x \\ -4+6x \\ 6-12x \\ -2+6x \end{bmatrix} EI \; [-6+12x \quad -4+6x \quad 6-12x \quad -2+6x] \; dx \qquad (2.43)$$

Integrating a matrix is not difficult, because each term integrates as a scalar. After integration the stiffness matrix K as shown below is found.

$$K = \frac{EI}{l^3} \begin{bmatrix} 12 & 6l & -12 & 6l \\ 6l & 4l^2 & -6l & 2l^2 \\ -12 & -6l & 12 & -6l \\ 6l & 2l^2 & -6l & 4l^2 \end{bmatrix} \qquad (2.44)$$

This stiffness matrix does not include the effect of axial deformations in the pipe. Adding in the axial effect term, the total stiffness matrix for a straight pipe element with a co-ordinate system as shown in fig. [2.11], together with the displacement and load vector, is

$$\begin{bmatrix} \frac{AE}{l} & 0 & 0 & -\frac{AE}{l} & 0 & 0 \\ 0 & \frac{12EI}{l^3} & \frac{6EI}{l^2} & 0 & \frac{-12EI}{l^3} & \frac{6EI}{l^2} \\ 0 & \frac{6EI}{l^2} & \frac{4EI}{l} & 0 & \frac{-6EI}{l^2} & \frac{2EI}{l} \\ \frac{-AE}{l} & 0 & 0 & \frac{AE}{l} & 0 & 0 \\ 0 & \frac{-12EI}{l^3} & \frac{-6EI}{l^2} & 0 & \frac{12EI}{l^3} & \frac{-6EI}{l^2} \\ 0 & \frac{6EI}{l^2} & \frac{2EI}{l} & 0 & \frac{-6EI}{l^2} & \frac{4EI}{l} \end{bmatrix} \begin{Bmatrix} \delta_1 \\ \delta_2 \\ \delta_3 \\ \delta_4 \\ \delta_5 \\ \delta_6 \end{Bmatrix} = \begin{Bmatrix} F_1 \\ F_2 \\ F_3 \\ F_4 \\ F_5 \\ F_6 \end{Bmatrix} \qquad (2.45)$$

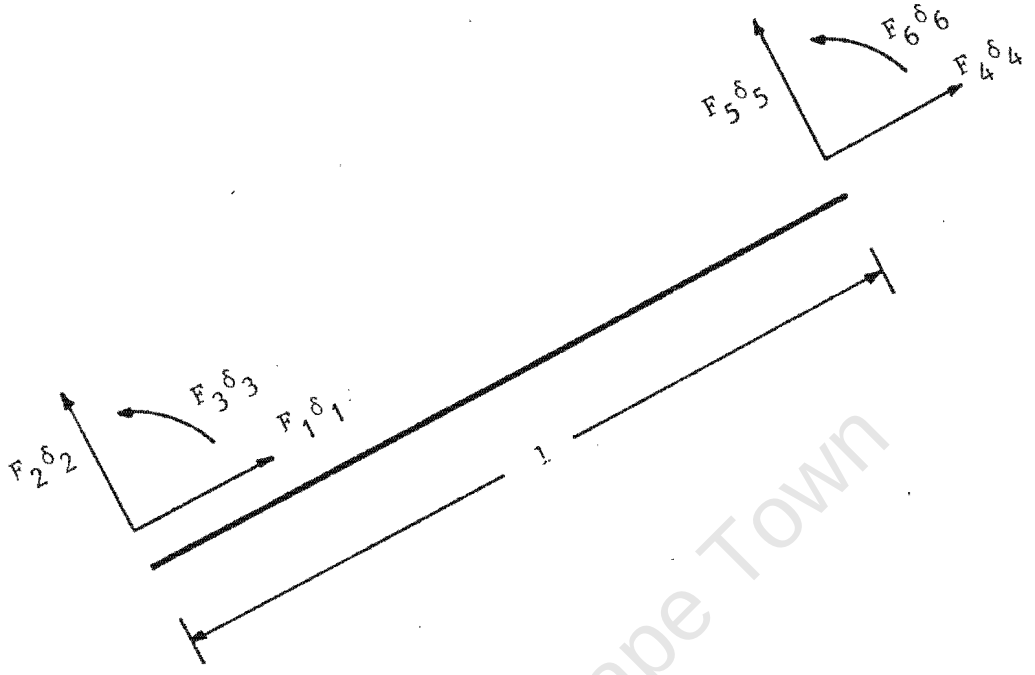

Figure 2.11 Straight Pipe Local Co-ordinate System

2.5 NOSTRUM - A Nonlinear Structural Mechanics Finite Element Program

NOSTRUM is a two dimensional finite element program for the nonlinear incremental analysis of plane continua and structures. Both physical and geometric nonlinearity, the latter using an updated Langrangian formulation, have been incorporated and several constitutive models are available. The program is capable of carrying out static and dynamic analyses, the latter includes both time history and modal analyses.

The structural finite element library comprises a 2-noded truss element, an Hermitian beam element, a spring element, a sliding spring element and a curved pipe element. All these elements have been formulated for small displacement, small strain plane problems. The truss and special spring element are the only structural elements in the library capable of elastic-plastic behaviour, with either isotropic or kinematic hardening. The other elements are only suitable for elastic analysis. A post-processing program (NOSTRUM*PLTTR) is now available to plot various outputted results as well as to evaluate certain maximum and minimum values that many occur over an analysis. To implement the pipe element into NOSTRUM was straightforward, because the framework of the program was such that all that was required was to add three subroutines to the program and adapting input routines, to calculate the element stiffness matrix for a particular bend element and to calculate the force residuals. The implementation of the element is given briefly in the next section.

2.6 Implementation of Curved Pipe into NOSTRUM

All dynamic analyses, including seismic analyses, involve solving the second-order differential equation of motion,

$$[M]\{\ddot{u}\} + [C]\{\dot{u}\} + [K]\{u\} = \{F\} \quad .$$

To solve this equation, the first thing to be set up are the mass matrix [M], the damping matrix [C] and the stiffness matrix [K]. These are all functions of the geometrical and material properties of the structure being considered. With the three matrices [M], [C] and [K] evaluated, either an acceleration-time, a displacement-time history record or a loading history can be input and the remaining variables evaluated by some numerical integration scheme, such as NEWMARK [8] discussed in section 3.2.

The flow chart of the method of analysis in NOSTRUM is

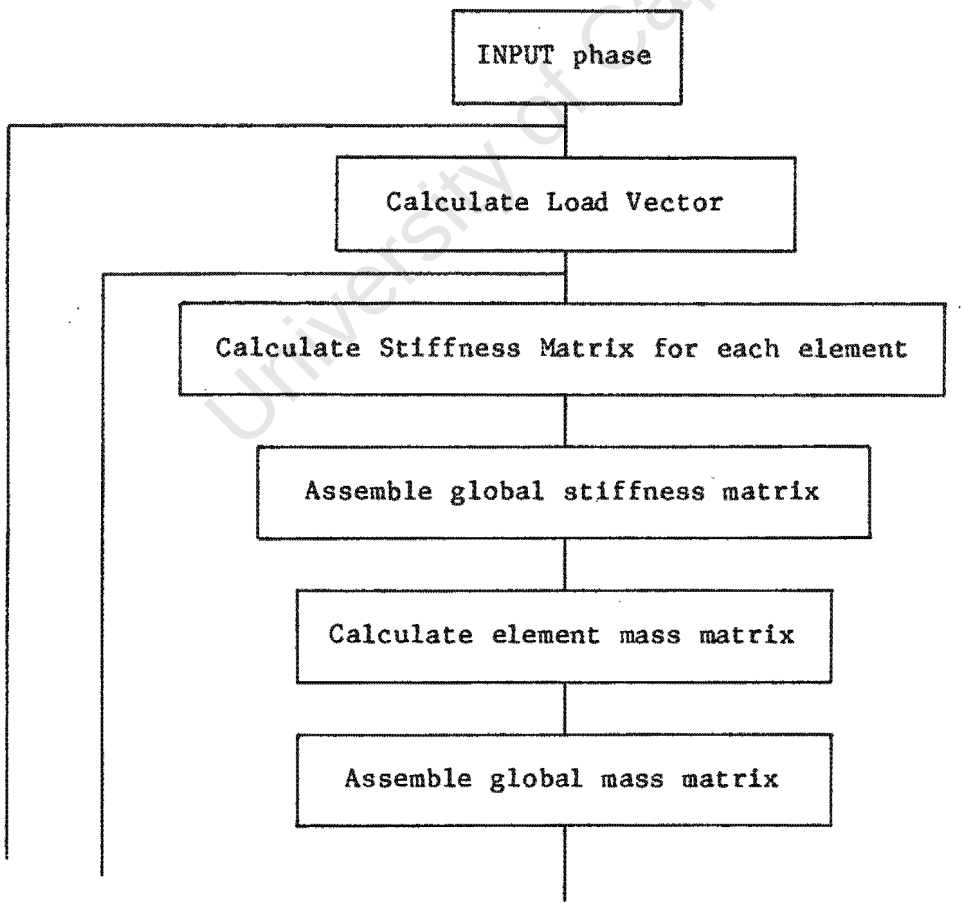

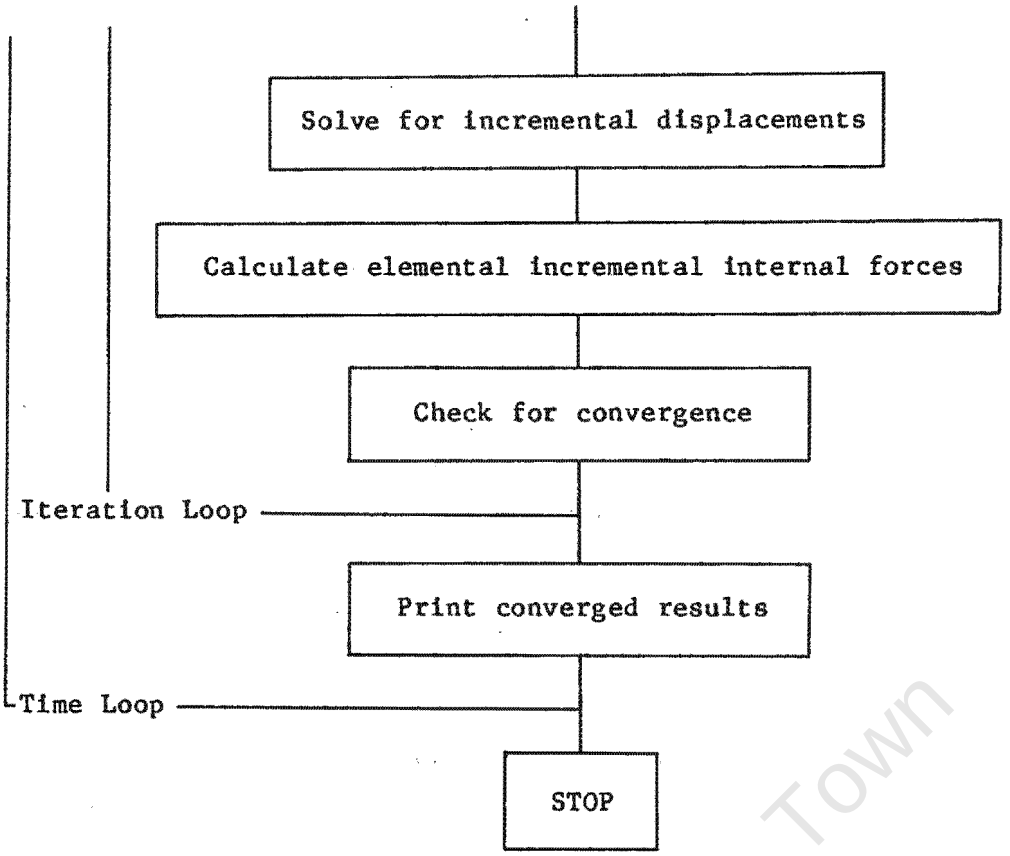

The stiffness matrix for the straight and curved pipe element was inserted into the program so that at each convergence loop iteration an updated stiffness matrix could be calculated.

The mass matrix for both elements was a lumped mass matrix, with half the mass of the pipeline placed at each node.

The method of calculating the force residuals, necessary for the convergence check, had to be derived and implemented for the curved element.

CHAPTER THREE

3. Seismic Analysis Theory

In order to carry out seismic analyses, some particular method of dynamic analysis must be chosen beforehand, as this will have bearing on the accuracy of the results. The first method which could be used is the response spectrum approach where the natural frequencies, the eigenvalues, and the non-dimensional modal shapes, the eigenvectors are found for the system. The second is a direct integration method, where the equation of motion

$$[M]\{\ddot{u}\} + [C]\{\dot{u}\} + [K]\{u\} = \{F\}$$

is solved without prior transformation. The two approaches will be discussed in this chapter, starting with the response spectrum approach and followed by a direct integration technique.

3.1 Modal Superposition with a Response Spectrum

The procedure involved in the response spectrum approach is to select a certain number of natural frequencies and corresponding mode shapes for a structure, to read off values of displacement, velocity and acceleration from a response spectrum for a single degree of freedom system, and to find participation factors which will produce maximum values of displacement, velocity and acceleration for each mode of the multi-degree of freedom structure. The following sections will explain the general procedure followed in this method of analysis from the derivation of a response spectrum to the combination of the separate modal effects.

3.1.1 Response Spectrum

An earthquake record can be represented in various ways. It can be an acceleration- , a velocity - or a displacement- time record. Fig [3.1] shows the accelerograph together with the integrated velocity and displacement time history plots for El Centro Earthquake of 1940. To put these plots into a useable form, a single degree of freedom damped linear structure is initially considered as shown in fig [3.2]. The structure is regarded as unloaded but subject to a base motion $x_0(t)$. The absolute displacement of the mass is $x(t)$. The relative displacement of the mass with respect to the base is therefore

$$u(t) = x(t) - x_0(t) \qquad (3.1)$$

The equation of motion is then,

$$m\ddot{u} + c\dot{u} + ku = -m\ddot{x}_0, \qquad (3.2)$$

which is rewritten as

$$\ddot{u} + 2\zeta\omega_0\dot{u} + \omega_0^2 u = -\ddot{x}_0, \qquad (3.3)$$

where ω_0 is the natural circular frequency and ζ is the degree of critical damping.

For a particular earthquake and for a particular frequency and damping of the one degree of freedom structure equation (3.3) can be solved numerically to find u_{max}, the absolute maximum relative displacement, which is referred to as D. This value of D corresponds to the maximum strain in the spring; thus the maximum force in the spring is kD. The displacement u_{max} occurs when $\dot{u}_{max} = 0$; therefore when $u = u_{max}$, $\dot{u} = 0$, $C\dot{u} = 0$ so therefore the force in the dashpot is zero. Therefore the force acting on the mass is kD, the force in the spring, and hence the maximum absolute acceleration $\ddot{x}_{max}$ is given by

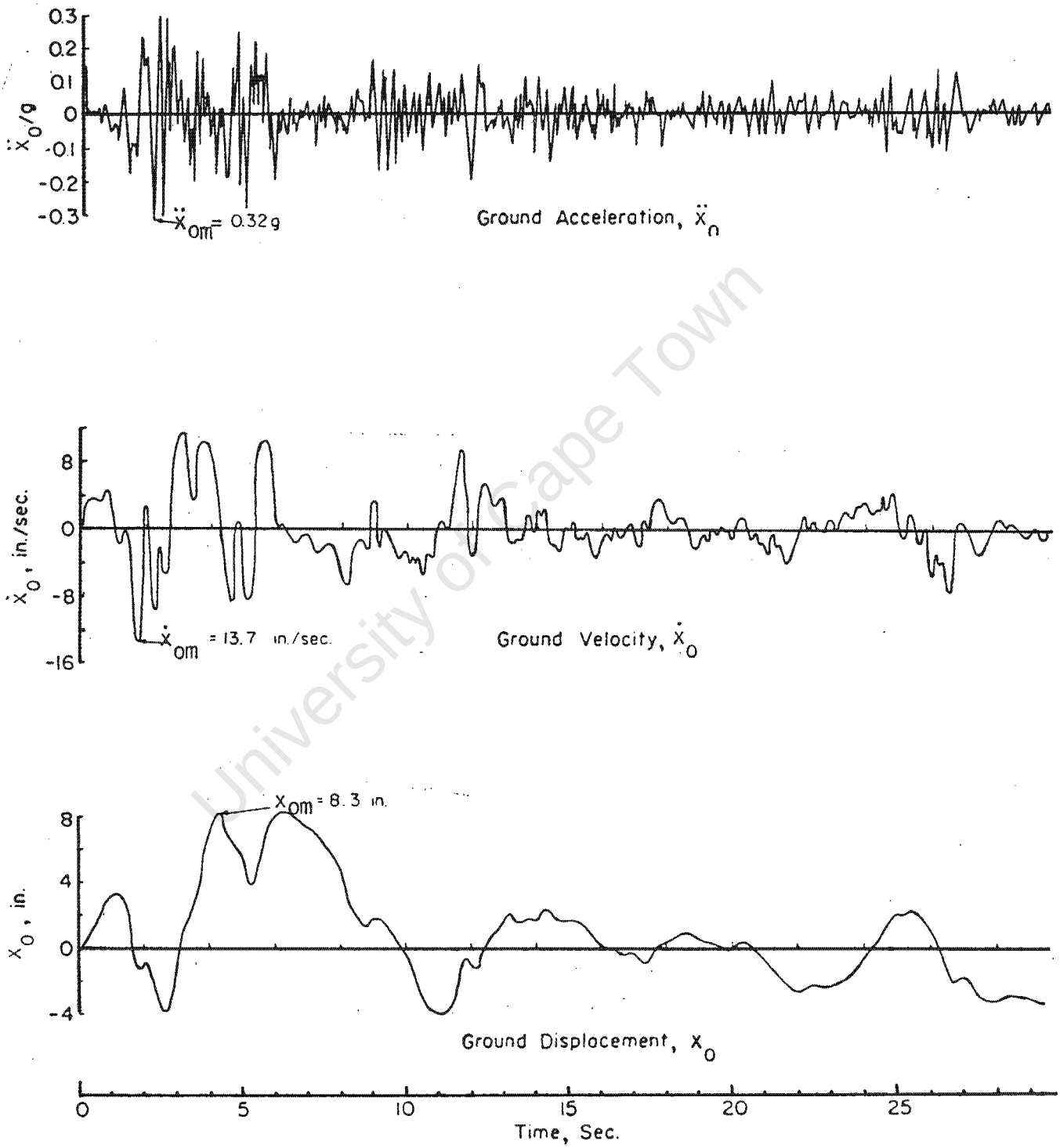

Figure 3.1 El Centro Earthquake of May 18, 1940 Accelerograph of the N-S Component with Integrated Velocity and Displacement Records.

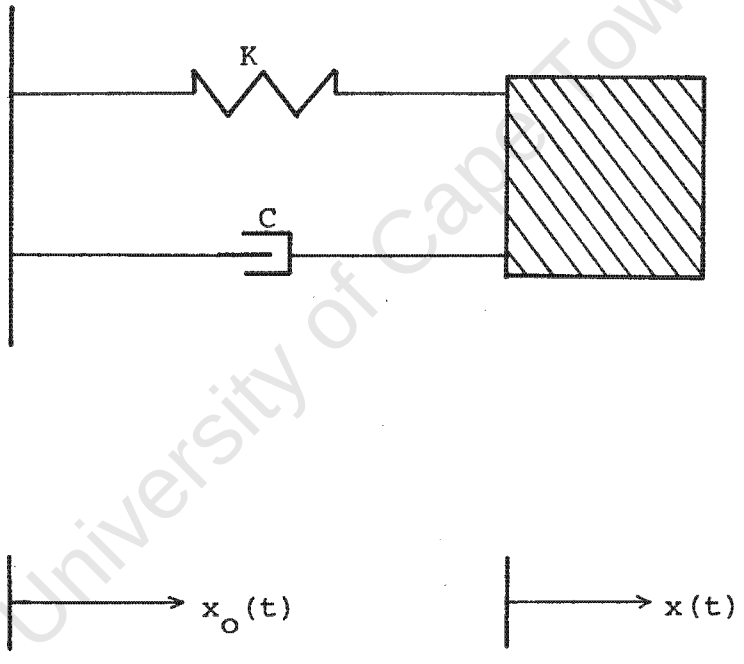

Figure 3.2 Single Degree of Freedom Model

$$m\ddot{x}_{max} = kD \qquad (3.4)$$

Putting

$$\ddot{x}_{max} = Ag \qquad (3.5)$$

where g is the acceleration due to gravity and A is a gravity multiplier, the following expression is otained;

$$Ag = \frac{k}{m} D = \omega_0^2 D \quad . \qquad (3.6)$$

The pseudovelocity V may now be introduced and defined. We put

$$\tfrac{1}{2} kD^2 = \tfrac{1}{2} mV^2 \qquad (3.7)$$

where V is the maximum pseudovelocity. The term V is the maximum relative velocity $\dot{u}$ and not the maximum absolute velocity $\dot{x}$. The pseudovelocity V is close to the maximum absolute velocity for high frequencies but significantly different for low frequencies of the one degree of freedom structure.

From equation (3.7) we see that

$$V = \left(\frac{k}{m}\right)^{1/2} D = \omega_0 D \quad , \qquad (3.8)$$

and hence from (3.6)

$$Ag = \omega_0 V = \omega_0^2 D \quad . \qquad (3.9)$$

These three values A, V and D are related by ω_0, the natural circular frequency. Thus any single degree of freedom structure can be defined by ω_0 and ζ and its response to a particular earthquake can be determined from the response spectrum. By doing this it can be seen that

$$D = D(\omega_0, \zeta) \ , \ V = V(\omega_0, \zeta) \ , \ A = A(\omega_0, \zeta) \qquad (3.10)$$

Thus a response spectrum is a plot of D,V and A against ω_0, the natural frequency, for fixed values of ζ ,the degree of critical damping, which ranges from zero upwards (eg. ζ = 0, 0.05, 0.10, 0.20 etc), for a particular earthquake. The values D, V and A can be plotted separately against ω_0 but because of the simple ratio between them, as shown in equation (3.10), all three quantities can be plotted on a tripartite plot; fig [3.3], a deformation spectrum for elastic systems subjected to the El Centro Earthquake, illustrates this relationship.

At very low and very high frequencies the spectra for the various damping ratios converge. At low frequencies the mass is relatively heavy with a weak spring and hence the mass stays stationary as the ground moves. At high frequencies, the spring is stiff and the mass is relatively small and hence the mass motion and maximum acceleration are approximately equal to the ground motion and acceleration respectively. This asymtotic behaviour is prevalent in all response spectra; therefore a characteristic of an earthquake is governed by its variation in between these two extremes.

For any single degree of freedom system it is now possible, knowing the natural frequency of the system, to estimate the maximum deflections of the structure. However all complex structures are multi-degree of freedom systems and hence a multiplication factor for each mode must be found that relates the displacement, acceleration and velocity read from the response spectrum for a single degree of freedom system to the actual values for a multi-degree of freedom system. These multiplication factors are called participation factors and their derivation follows in section 3.1.2.

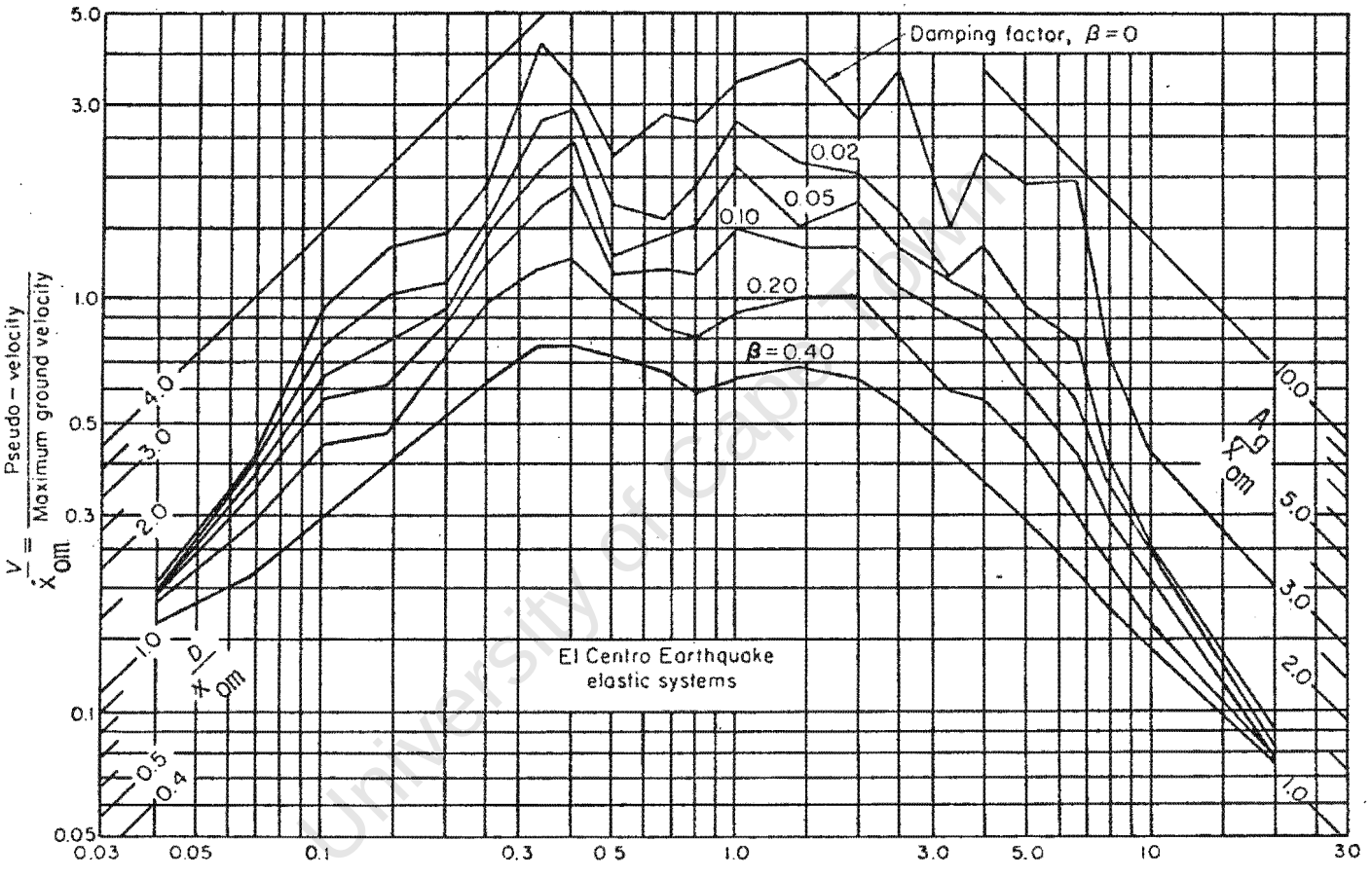

Figure 3.3 Elastic Response Spectrum of El Centro Earthquake of 1940.

3.1.2 Participation Factors for Multi-Degree of Freedom Systems

The method to predict the response of a multi-degree of freedom structure from the response of a single degree of freedom system is shown below for the structure behaving elastically under the earthquake imput. Having set up the response spectrum (see 3.1.1), in order now to analyse a multi-degree of freedom system the eigenvalues and corresponding eigenvectors of the system need to be found, so that the equations of motion can be written in uncoupled form The equation of motion

$$[M]\{\ddot{u}\} + [C]\{\dot{u}\} + [K]\{u\} = \{F\} \qquad (3.11)$$

is transformed through the relation

$$\{u\} = \sum_{j=1}^{N} \xi_j \{u_j\} \qquad (3.12)$$

where ξ_j are the mode amplitudes and $\{u_j\}$ are the eigenvectors, the dimensionless mode shapes. Substituting (3.11) into (3.12), premultiplying by one mode shape vector and using the orthogonality result, equation (3.11) becomes

$$\ddot{\xi}_j + 2\zeta_j\omega_j\dot{\xi}_j + \omega_j^2\xi_j = \frac{\{u_j\}^T\{F\}}{\{u_j\}^T[M]\{u_j\}} \qquad (3.13)$$

$$j = 1,2,.....,N$$

The above equation (3.13) is the transformed equation of motion in terms of ζ_j, ω_j and ξ_j of which the first two are known; ξ_j is the unknown quantity.

Each mode acts independently so that for the j^{th} mode we enter the response spectrum with j^{th} frequency.

$$f_j = \frac{\omega_j}{2\pi}$$

and read off D, the maximum displacement. Now one needs a participation factor to multiply D by to get ξ_j^{max}, the mode amplitude.

We know that the response spectrum was derived from solutions of equation (3.3)

$$\ddot{u} + 2\zeta\omega_0\dot{u} + \omega_0^2 u = -\ddot{x}_0 \qquad (3.14)$$

where x_0 is the ground motion. For the multi-degree of freedom system an imposed vertical or horizontal ground motion leads to a forcing function in equation (3.11) of the form

$$\{F\} = -[m]\{A\}\ddot{x}_0 \quad , \qquad (3.15)$$

where $\{A\}$ is a column matrix whose i^{th} element A_i is such that

$$\ddot{u}_i = A_i\ddot{x}_0 \quad , \qquad (3.16)$$

where $\ddot{u}_i$ is the acceleration of the i^{th} nodal point if the structure is rigid. Substituting (3.15) into (3.13), we have

$$\ddot{\xi}_j + 2\zeta_j\omega_j\dot{\xi}_j + \omega_j^2\xi_j = -\frac{\{u_j\}^T[M]\{A\}}{\{u_j\}^T[M]\{u_j\}}\ddot{x}_0 \quad . \qquad (3.17)$$

Comparing (3.14) and (3.12) the j^{th} mode of the multi-degree of freedom system responds to an input acceleration of

$$\frac{\{u_j\}^T[M]\{A\}}{\{u_j\}^T[M]\{u_j\}} \qquad (3.18)$$

times the actual ground acceleration. This value of (3.18) is the

participation factor by which D is multiplied to give the value of ξ_j^{max}, the maximum mode amplitude. Similarly the value of $\ddot{\xi}_j^{max}$, is found by multiplying the participation factor by the maximum acceleration read off the response spectrum. The actual maximum displacements and accelerations of the j^{th} mode are then ξ_j^{max} and $\ddot{\xi}_j^{max}$ respectively multiplied by the dimensionless j^{th} mode shape, namely

$$\{u\}^{max} = \xi_j^{max}\{u_j\} \tag{3.19}$$

$$\{\ddot{u}\}^{max} = \ddot{\xi}_j^{max}\{u_j\} \tag{3.20}$$

In this way the elastic response spectrum applicable for single degree of freedom systems has been extended for multi-degree of freedom purposes. Following the above procedure one obtains maximum displacements and accelerations at every point in the structure for every natural frequency. These peak displacement, velocity and acceleration values for each mode do not occur at the same time in the structure and therefore a mathematical averaging routine must be introduced.

3.1.3 Combination of Modal Displacements and Accelerations

For each frequency, the maximum response of the structure has been computed. A direct superposition of these maximum values will give a conservative estimate of the actual maximum of the quantity under consideration. This is so because it is extremely unlikely that maxima will occur in each mode at exactly the same time. The maximum value of a quantity composed of contributions from several modes cannot be calculated precisely from the information given in the response spectrum. An empirical averaging procedure must be adopted, and that usually chosen is the root mean square (RMS) method.Let Q(t) be a quantity made up of modal contribution $Q_1(t)$, $Q_2(t)$,.....,$Q_n(t)$ Hence

$$Q(t) = Q_1(t) + Q_2\ (t) +.....+ Q_n(t) \qquad (3.21)$$

If Q_{max} is the maximum valueof Q(t), and Q_{1max}, Q_{2max}...Q_{nmax}, the maxima of the constituent modes, the RMS method estimates

$$Q_{max} = (Q^2_{1max} + Q^2_{2max} +....+ Q^2_{nmax})^{1/2} \qquad (3.22)$$

Thus at every point in the structure there is a final maximum value of displacement, velocity and acceleration for that particular earthquake.

The accuracy of the mode superposition method depends on the number of modes used in the analysis and on the RMS averaging procedure. However, it is a very inexpensive method of seismic analysis compared with the method of direct integration.

3.2 Direct Integration using Newmark's [8] method

In dynamic problems, both linear and nonlinear, the solution algorithm integrates forward in time. There are two distinct groups of algorithms which do this, the explicit and implicit algorithms.

Explicit algorithms do not require any iterations within a time step. The mass matrix [M] has to be inverted, which is simple in the particular case when [M] is a diagonal lumped mass matrix. Explicit algorithms are conditionally stable and hence the time steps must be small to ensure accuracy and stability.

Implicit algorithms are unconditionally stable and hence larger time steps can be chosen, but iterations are required within each time step. Moreover, a matrix inversion of the same kind as the static method is required for each time step, and for each iteration if the matrix is updated. The dynamic implicit algorithm is similar to a static equilibrium, but where the tangent stiffness matrix [K] is replaced by an updated matrix $[K^*]$.

NOSTRUM [9] uses an explicit-implicit algorithm developed by Hughes [7] which caters for the interaction of materials with different properties. The finite element mesh is divided into two groups, the implicit and explicit group, which are treated separately in the algorithm. The implicit part uses the Newmark method in predictor-corrector form, whilst the explicit method is also in a predictor-corrector form without the option of equilibrium iterations. If all the elements are implicit, or all explicit, then the method reduces to a direct implicit or explicit algorithm.

Both algorithms start with the predictor phase. Assuming that the conditions at the end of the previous step u_t, $\dot{u}_t$ and $\ddot{u}_t$ are known, we define

$$u^*_{t+\Delta t} = u_t + \Delta t \dot{u}_t + \Delta t^2 \frac{(1-2\beta)}{2} \ddot{u}_t \qquad (3.23)$$

$$\dot{u}^{*}_{t+\Delta t} = \dot{u}_t + \Delta t(1-\gamma)\ddot{u}_t \qquad (3.24)$$

where β and γ are the Newmark factors. Unless $\gamma = 1/2$, a spurious damping is introduced, proportional to the quantity $(\gamma - 1/2)$. If γ is zero then negative damping occurs, causing a self excited vibration arising solely from the numerical procedure. If γ is greater than $1/2$, positive damping occurs even though no damping may be specified. To ensure that the method is unconditionally stable, it is necessary to make

$$\beta = 0.25(\gamma - 1/2)^2 \qquad (3.25)$$

Thus following the trapezoidal rule, for example, we set $\beta = 0.25$, $\gamma = 0.5$. For the first iteration we set either

$$u^{0}_{t+\Delta t} = u^{*}_{t+\Delta t} \qquad (3.26)$$

$$\dot{u}^{0}_{t+\Delta t} = \dot{u}^{*}_{t+\Delta t}$$

$$\ddot{u}^{0}_{t+\Delta t} = 0$$

or

$$u^{0}_{t+\Delta t} = u_t \qquad (3.27)$$

$$\dot{u}^{0}_{t+\Delta t} = \dot{u}_t$$

$$\ddot{u}^{0}_{t+\Delta t} = (u^{0}_{t+\Delta t} - u^{*}_{t+\Delta t})/(\Delta t^2 \beta)$$

Equations (3.26) are used for mixed implicit/ explicit integration while equations (3.27) are used for purely implicit integration. Elastic-plastic problems of the type which we are concerned with are

usually integrated implicitly.

The initial residual force is then

$$\psi^0 = R_{t+\Delta t} - \{[M]\ddot{u}_{t+\Delta t} + [C]\dot{u}_{t+\Delta t} + F^0_{t+\Delta t}\} \qquad (3.28)$$

where $R_{t+\Delta t}$ is the total load vector at $t = t + \Delta t$,
$F^0_{t+\Delta t}$ is the initial internal force at time $t = t+\Delta t$ and
$F^0_{t+\Delta t}$ is computed from $u^0_{t+\Delta t}$.

In the explicit method the effective stiffness matrix is

$$[K^*] = \frac{1}{\Delta t^2 \beta}[M] \ , \qquad (3.29)$$

and the equations

$$[K^*]\Delta u^0 = \psi^0 \qquad \text{are solved.}$$

The corrector phase is then entered, putting

$$u_{t+\Delta t} = u^0_{t+\Delta t} + \Delta u^0 \ , \qquad (3.30)$$

$$\ddot{u}_{t+\Delta t} = (u^0_{t+\Delta t} - u^*_{t+\Delta t})/(\Delta t^2 \beta) \ , \qquad (3.31)$$

$$\dot{u}_{t+\Delta t} = \dot{u}^0_{t+\Delta t} + \Delta t \gamma \ddot{u}_{t+\Delta t} \ . \qquad (3.32)$$

In the implicit method the effective stiffness is

$$[K^*] = \frac{1}{\Delta t^2 \beta}[M] + \frac{\gamma}{\Delta t \beta}[C] + [K] \qquad (3.33)$$

where [K] is calculated at the start of every iteration (ie. full Newton Raphson) or [K] is calculated at the beginning of every load step (ie. modified Newton Raphson).

We solve equations

$$[K^*]^i_{t+\Delta t}\Delta u^i = \psi^i \quad , \tag{3.34}$$

where i indicates that equilibrium iterations are now permitted (i = 0 on the first iteration) The residual ψ^i is now

$$\psi^i = R_{t+\Delta t} - \{[M]\ddot{u}_{t+\Delta t} + [C]_{t+\Delta t}\dot{u}^i_{t+\Delta t} + F^i_{t+\Delta t}\} \tag{3.35}$$

The corrector equations are also of the form of equations (3.30-3.31) with,

$$u^{i+1}_{t+\Delta t} = u^i_{t+\Delta t} + \Delta u^i \tag{3.36}$$

$$\ddot{u}^{i+1}_{t+\Delta t} = (u^{i+1}_{t+\Delta t} - u^*_{t+\Delta t})/(\Delta t^2\beta) \tag{3.37}$$

$$\dot{u}^{i+1}_{t+\Delta t} = \dot{u}^i_{t+\Delta t} + \Delta t\gamma\ddot{u}^{i+1}_{t+\Delta t} \quad . \tag{3.38}$$

The iterations continue until an acceptable accuracy is reached.

CHAPTER FOUR

4. Simulation of Pipelines using NOSTRUM

In carrying out seismic analyses, as discussed in Chapter 3, a response spectrum approach or a direct integration approach can be used. In either method a particular structure is subjected to a particular design ground motion, which produces certain pipe support reactions which may not be representative of an actual earthquake that may occur during the life of the structure. In order to define a standardised earthquake record, a smoothing curve is drawn through a number of response spectra, termed a design spectrum, as shown in fig [4.1]. This act of smoothing the curve often cuts off the peaks in the spectrum and less conservative results could occur using this method, resulting in possible yielding of pipe supports in the course of an earthquake. During the lifetime of the plant the pipelines could be subjected to an earthquake which is of a greater intensity than the pipe was designed to withstand. Effectively the pipe supports would underdesigned for that particular earthquake.

The consequences of this underdesigning may become apparent in one or both of two ways. Firstly the pipe stresses may become too high or secondly, the other pipe supports may yield considerably leading ultimately to the first condition; either way the pipe is unserviceable. The purpose of this thesis was to subject various pipelines to various earthquakes and to examine the consequences if a pipe support was underdesigned and hence yielded under peak loads.

In the following sections, the pipe layouts and strategy of analyses will be discussed.

Figure 4.1 Design Spectrum

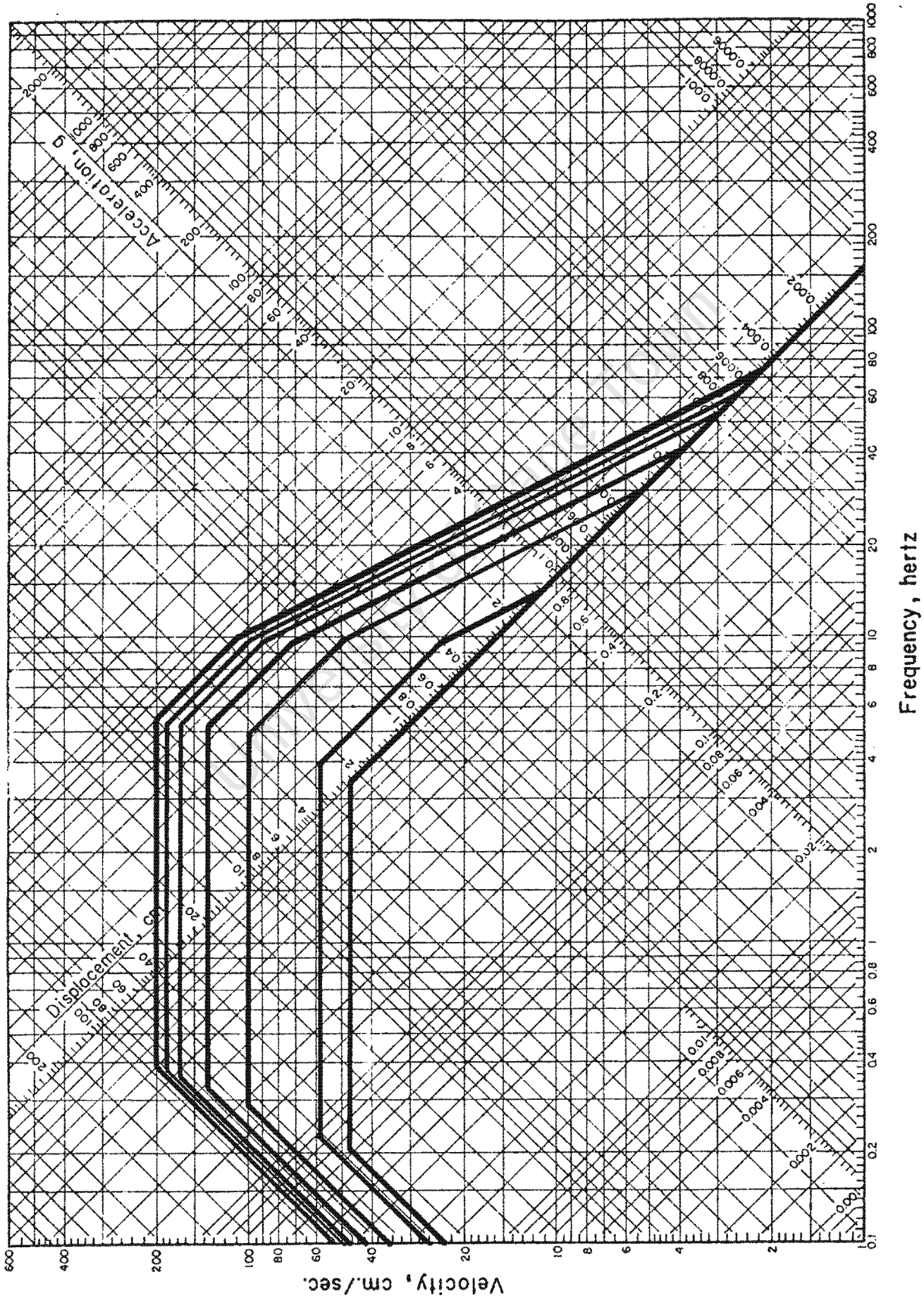

4.1 Pipeline One

Fig [4.2] shows pipeline one, simply supported at each end with a hangar support six metres along from the left hand side of the beam.

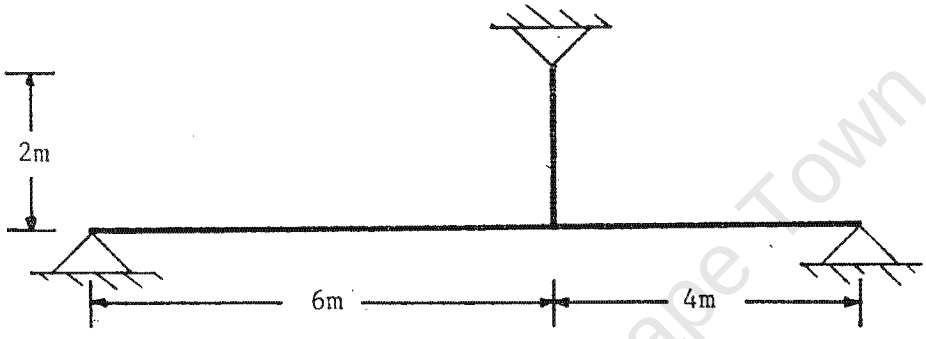

Figure 4.2 Pipeline One Configuration

The pipeline was ten metres in length, 406mm outer wall diameter, wall thickness varying from one to fifteen millimetres and a mass per unit length ranging from 220 to 450kg/m. This mass included the steel wall, the internal fluid and the external cladding. There was assumed to be no internal pressure. The hangar chosen was a 12mm diameter steel rod with a Young's Modulus of 200GPa. The yield stress of the bar was however allowed to change depending on the analysis at hand, in order to simulate a yielding support.

The aim of these analyses was to find the behaviour or response of the structure when the hangar was allowed to progressively yield. Initially an elastic analysis was done on the system subjecting it to

an earthquake. The mass of the pipeline was lumped at the nodes, and an earthquake record scaled to 0.3g maximum ground acceleration was used as the vertical ground acceleration.

Direct integration was used in all the analyses so that a high degree of accuracy could be obtained. Once a peak hangar force had been found for a particular earthquake the peak stress σ_y could be found. Six more analyses were then done with an elastic-plastic hangar where the yield stress was σ_y, $0.8\sigma_y$, $0.6\sigma_y$, $0.4\ \sigma_y$, $0.2\sigma_y$ and finally $0.0\sigma_y$. The last case was that of a simply supported beam with no internal support. The forces, moments and displacements were recorded for all nodes during the analyses.

A frequency analysis was done on the elastic systems when the hangar was an elastic support and when the support was removed entirely. The results of these frequency analyses are given in Chapter 5. These frequencies were used to check against the corresponding response spectrum that the structure was behaving as expected.

The entire process was repeated for various earthquake records, so that general trends could be seen for any general earthquake. The earthquakes chosen for pipeline one were:

1. SSE1 - An artificially generated earthquake record.

2. Imperial Valley Earthquake - October 15, 1979 Station 952

3. San Fernando Earthquake - February 9, 1971 Station 128

4. Coyote Lake Earthquake - August 6, 1979 Station 1408

5. Parkfield Earthquake - June 27, 1966 Station 014

All the peak accelerations were scaled to 0.3g; however not all the records used were vertical records. Imperial Valley, San Fernando and Coyote Lake Earthquakes were all horizontal records with their

peak accelerations scaled to 0.3g. SSE1 and Parkfield were vertical acceleration-time records with their peak accelerations also scaled to 0.3g. The response spectra for the earthquakes are given in Appendix B.

Once trends were obtained for the different earthquakes, the frequency of the same structure was changed to examine the effect. The pipe wall thickness was reduced from its original 0.0048m to 0.001 m; this reduced the natural frequency of the structure. Another wall thickness chosen was 0.015 m, where the frequency was higher.

4.2 First Mode Approximation Single Degree of Freedom Systems

Fig [4.3] illustrates a single degree of freedom model.It consists of two elastic springs with stiffnesses k_1 and k_2, where the latter spring is in series with a plastic element, P. The fundamental circular frequencies were found for the multi-degree of freedom systems firstly when the internal hangar support was fully elastic, ω, and secondly when the hangar was removed, ω_1, namely when the yield stress in the hangar was reduced to zero. When the plastic element was rigid the fundamental frequency of the single degree of freedom system was ω, the same as that of the multi-degree of freedom system with an internal elastic hangar support. When the plastic element was totally released, the single degree of freedom system had the same fundamental frequency as the multi-degree of freedom system without an internal hangar support, ω_1 . The choice of the stiffness values k_1 and k_2 was made so that

$$\omega = \left(\frac{k_1+k_2}{m} \right)^{1/2}$$

and

$$\omega_1 = \left(\frac{k_1}{m} \right)^{1/2} .$$

Inverting the equations the stiffnesses k_1 and k_2 are found explicitly;

$$k_1 = \omega_1^2 m$$

and

$$k_2 = \omega^2 m - \omega_1^2 m \quad .$$

With these values of k_1 and k_2 the fundamental frequency of the multi-degree of freedom system was the same as that single degree of freedom system.

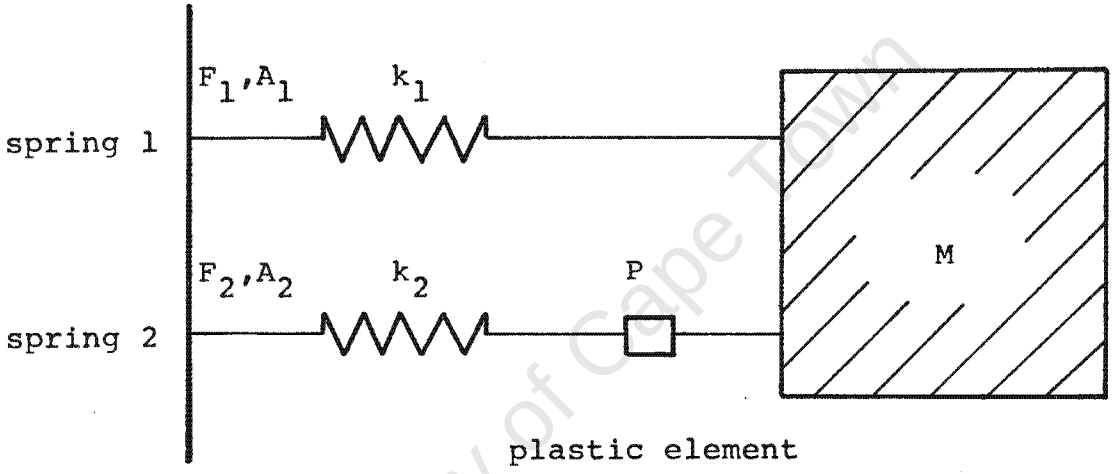

Figure 4.3 Single degree of Freedom Model

The single degree of freedom systems were subjected to the same earthquake records as those of the multi-degree of freedom systems. For any one particular pipe model and for a particular earthquake record the maximum force in the plastic spring as shown in fig [4.3], F_2, was found during the response when the plastic element was rigid. Dividing by the cross-sectional area of the spring the maximum yield stress σ_{Y2} was evaluated. As in the case of the multi-degree of freedom system the plastic element yield stress was then reduced from 1.0 to 0.0 times its maximum value. The results of the single degree of freedom system are given in Appendix A.

4.3 Pipeline 2

Fig. [4.4] shows pipeline 2, a pipeline ten metres long, three metres deep with a 12mm diameter steel rod hangar.

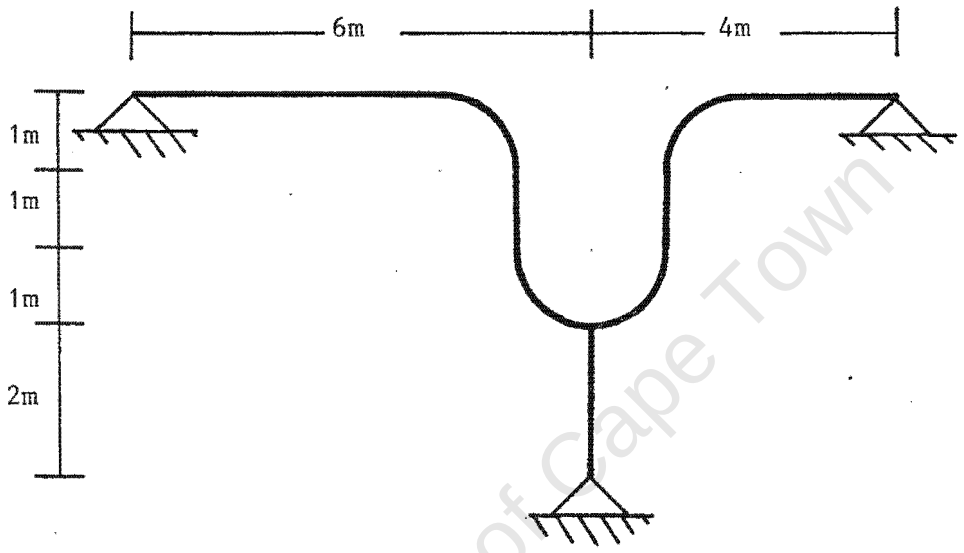

Figure 4.4 Pipeline Two Configuration

This time, since the lumped mass at the nodes were not in one direction , horizontal acceleration was used as well as vertical acceleration. The horizontal records were scaled to 0.3 g and the corresponding vertical records to 0.2g. The records used were:

1. SSE1 - Horizontal and Vertical

2. Imperial Valley Earthquake - October 15, 1979 Station 952
   Horizontal and Vertical

3. San Fernando Earthquake - February 9, 1971 Station 128
   Horizontal and Vertical

4. Coyote Lake Earthquake - August 6, 1979 Station 1408
   Horizontal and Vertical

5. Parkfield Earthquake - June 27, 1966 Station 014
   Horizontal and Vertical.

In this second pipeline, the curved beam element was used on the bends but owing to the limitations imposed on the element, six elements were used for each 90° bend. The procedure of analysis was the same as for pipeline one except that for this case only two different thicknesses were chosen; that of 0.001m and 0.0048m. This was done because an increase in thickness to 0.015m would have made the pipe a thick pipe, which was not acceptable, as the element was formulated for thin beam theory. The horizontal ground accelerations used for pipeline two were scaled to 0.3g peak ground acceleration while the vertical ground accelerations used were scaled to 0.2g peak ground acceleration, two-thirds that of the horizontal peak acceleration.

CHAPTER FIVE

5. Results

The results of all the analyses are tabulated and presented graphically in Appendix A. An explanation of the graphs and tables are included in the appendix.

Five pipelines were analysed with only two variations in pipeline configuration. Three pipe wall thicknesses were chosen for pipeline one configuration and two thicknesses for pipeline two. These pipeline configurations are shown in figures [4.2] and [4.4]. The natural frequencies of the pipelines with and without the internal hangar support are given in Table 5.1. Four frequencies were found for pipeline one because there were four degrees of freedom and eight were found for pipeline two, not because there were eight degrees of freedom but because the higher frequencies were outside the range of the earthquake excitation.

5.1 Time History Analyses

The time history analyses of the pipelines produced various trends which are given in point form below.

1. The hanger axial force decreased linearly in most of the analyses. In a few of the analyses deviations from the linear behaviour occured. This was attributed to the fact that the model contained a small strain hardening term. Thus as the hangar increasingly yielded the force that could be taken by the hangar increased. The force in the hanger always decreased as the yield stress diminished and always remained higher than the adjacent end shear forces until at least a 50% reduction in peak axial hanger yield stress had been reached. The peak axial hanger force for all degrees of yielding, varied greatly from earthquake to earthquake for the same pipeline, even though the

Pipeline		Frequency (Hz) With Support	Without Support
Pipeline One	f_1	11.07	3.43
t=0.001m	f_2	21.77	13.65
	f_3	33.93	30.22
	f_4	56.05	49.76
Pipeline One	f_1	16.66	6.33
t=0.0048m	f_2	28.90	25.25
	f_3	57.18	55.90
	f_4	94.07	92.05
Pipeline One	f_1	16.81	8.79
t=0.015m	f_2	36.53	35.09
	f_3	78.26	77.68
	f_4	128.8	127.9
Pipeline Two	f_1	1.42	0.42
t=0.001m	f_2	4.94	1.44
	f_3	8.28	8.24
	f_4	10.94	10.94
	f_5	24.54	11.93
	f_6	30.78	24.57
	f_7	237.9	237.9
	f_8	238.1	238.1
Pipeline Two	f_1	5.62	1.62
t=0.0048m	f_2	10.03	5.74
	f_3	27.20	27.09
	f_4	40.38	40.37
	f_5	52.48	47.80
	f_6	57.42	57.11
	f_7	444.5	444.5
	f_8	446.3	446.3

Table 5.1 Natural Frequencies

maximum accelerations for all the earthquakes were scaled to 0.3g. Thus in carrying out an earthquake analysis, emphasis should be placed on the selection of a representative acceleration record. From the tables it is shown that the peak deflection of the point on the pipe where the hangar is attached initially does not change dramatically, although at approximately 80% reduction in peak yield stress the deflections tend to increase dramatically. When the support was totally removed the hanger deflection in all cases rose above any previous peak displacement. The removal of the hanger support led to deflections which were too large for serviceability in most cases.

2. In pipeline one, the left hand end shear force was always greater than the right hand shear force. Both end shear forces for pipeline one always converged to the same value when the internal support was removed. Without the hanger the structure was symmetrical and hence this behaviour was expected. In pipeline two, the right hand shear force was most often higher than the left hand shear force. When the hangar was removed the two end shear forces were not similar because the structure was unsymmetrical.

3. Although the peak forces occured at different stages in the response, the sum of the peak forces in the vertical direction followed the same pattern as the sum of the peak forces for the single degree of freedom first mode approximation system. Appendix A shows this relationship.

4. The shear forces at the ends of the pipeline usually decrease slightly until at least 60 %, and often 80 %, reduction in hanger yield stress.

5. The sum of the maximum forces is defined as the maximum shear force at the left hand support over the response added to the maximum shear force at the right hand support over the response

added to the maximum axial force in the hangar over the response.

5.2 Single degree of freedom, first mode approximation results

The results for the single degree of freedom model showed similar trends to those for the pipelines. As before, the trends are given in point form below. Figure [4.3] contains the salient nomenclature.

1. The force, F_2, in the lower spring decreased linearly as the yield stress was linearly reduced.

2. The force, F_1, in the upper spring decreased until a reduction in peak yield stress reached approximately 60% whereafter it either increased or decreased depending on the analysis.

3. The sum of the maximum forces for the single degree of freedom system is defined as the maximum force in spring 1 over the response plus the maximum force in spring 2 over the response.

5.3 Limitations of Analyses

The analyses carried out were specific rather than general. Thus before any predictions or conclusions can be reached it is necessary to examine the limitations under which these conclusions can be drawn. Various limitations that we feel may influence the overall findings are given below.

1. Only vertical behaviour was studied. Horizontal accelerations were imposed on the structures but their effect was not examined. Thus axial hanger and end shear forces as well as vertical hanger displacement were recorded as only vertical accelerations would have only increased the axial effects in the pipe and had no effect in the pipe moments. In the case of pipeline 2, horizontal accelerations affected the pipe moments because the expansion loop in the pipeline lay out of the x-axis.

2. The parameter of pipe diameter was fixed.

3. The parameters of pipe hangar type and position were fixed.

4. A kinematic hardening model was used with a very small strain hardening parameter thus making the behaviour effectively elastic-perfectly plastic.

5. No damping was included in the elastic analyses; this may accentuate the effect of energy absorbing restrainers.

6. Only in-phase shaking was considered i.e. the supports were subjected to the same earthquake record simultaneously.

7. General trends were examined and hence, although minor deviations in some analyses occured, these were considered to be exceptions to the general trends.

5.4 Discussion of Results

The main objective of this thesis was to ascertain whether the yielding of an internal hangar support, brought about by an earthquake occuring with a greater intensity than the pipe was designed for, would lead to the danger of adjacent supports failing. Trends for the multi-degree of freedom pipeline and trends for the single degree of freedom pipeline model as the yield stress decreased were found. A parameter linking the two approaches was sought so that predictions for the multi-degree of freedom system could be made from results of the first mode single degree of freedom analyses. One particular parameter which was similar in both approaches for the cases which were studied was the ratio of the sum of the maximum forces over the response, as defined in 5.1 and 5.2. This parameter followed the same trend in both models. Further investigation showed that the sum of the maximum reactions over the response was, for the cases considered, approximately equal in most cases to the maximum of the sum of the reactions.

Fig. [5.1] is a graph of the percentage reduction in hangar yield stress versus a force ratio. The force ratio is the sum of the maximum vertical reactions divided by the sum of the maximum vertical reactions when the hangar is elastic. The graph consists of two envelopes. The one is enclosed by a set of dotted lines, the other by solid lines. The solid lines indicate the range over which the sum of the maximum vertical reactions for the multi-degree of freedom pipelines varied as the yield stress decreased. Similarly, the dotted lines indicate the range over wich the sum of the two maximum spring forces, F_1 and F_2, varied as the yield stress of the plastic element decreased.

This graph shows that for both the single and multi-degree of freedom systems the force ratio initially decreases as the yield stress is reduced. This behaviour continues until approximately 60% reduction in yield stress is reached, whereupon, depending on the structure and the earthquake, the force ratio may increase or decrease with further

yielding.

Furthermore the results show that the force ratios for the single and multi-degree of freedom systems follow each other closely for all percentage reductions in yield stress for each analysis involving a particular pipeline and a particular earthquake. This is an indication that the pipelines considered behaved predominantly in their first mode. The first mode approximation is however slightly

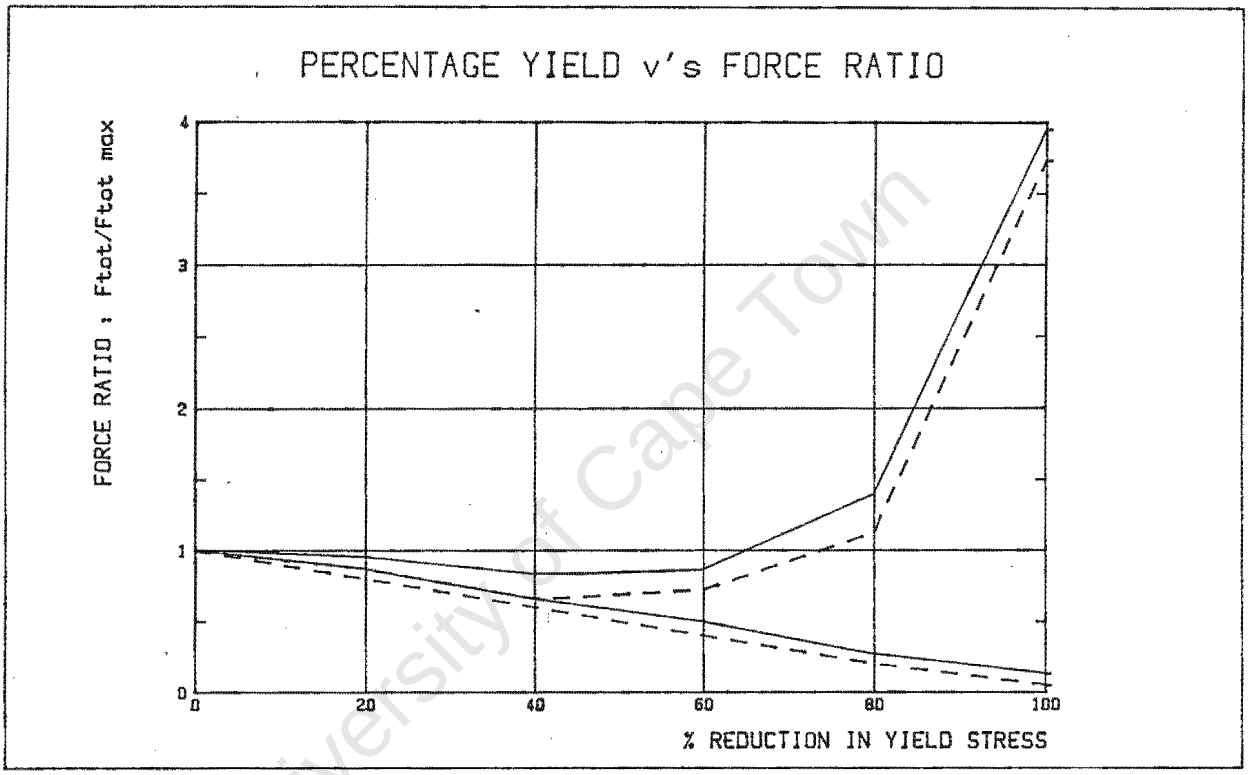

Figure 5.1 Percentage yield v's Force Ratio

unconservative. The results suggest that a simplified design procedure can be adopted to estimate the change in the sum of the maximum reactions over the response when an internal support yields. Firstly a response spectrum analysis should be carried out on the pipeline with and without the internal support. A single degree of freedom first mode approximation model should then be set up in the manner described in section 4.2. In attempting to predict the basic trends it is sufficient to carry out time history analyses with 0%, 50%, 85% and 100% reduction in yield stress in the plastic

element. This implies that only two inelastic analyses are required, as the 0% analysis is elastic and is used to determine the yield value and the 100% analysis is also elastic. Linear interpolation between these four points will produce a plot which gives the overall trends with sufficient accuracy and reliability.

REFERENCES

1. POWELL, G.H. and ROW, D.G. "Effect of Energy Absorbing Supports on Seismic Pipe Stresses", Transaction of the 5th International Conference on Structural Mechanics in Reactor Technology,1979.

2. DAVIS, R., HENSHELL, R.D., WARBURTON G.B. "Constant Curvature Beam Finite Elements for In-plane Vibration", Journal of Sound and Vibration (1972). 25 (4), Pgs 561 - 576.

3. POPOV, E.P. "Introduction to mechanics of Solids", Macdonald, London, England, 1968.

4. BATHE, K.J., "Finite Element Procedures in Engineering Analysis", Prentice - Hall, Inc., Englewood Cliffs, New Jersey.

5. IRONS, B.M. and AHMAD, s. "Techniques of Finite Elements", Ellis Horwood, Chichester, England, 1979.

6. BORESI, A.P. SIDEBOTTOM, O.M., SEELY, F.B. and SMITH, J.O., "Advanced Mechanics of Materials", 3rd edition, John Wiley and Sons, New York, U.S.A.

7. HUGHES, T.J.R., PISTER, K.S. and TAYLOR, R.L. "Implicit-Explicit Finite Element in Nonlinear Transient Analysis", Computer Methods in Applied Mechanics and Engineering Volume 17/18, 1979, Pgs. 159 - 188.

8. ASCE Proceedings, Engineering Mechanics Division Journal, Volume 85, EM, 1959, July Pgs 67 - 94.

9. DUFFETT, G.A., GRIFFIN, T.B., MARTIN, J.B., MERCER, C.D., REDDY, B.D., RESENDE, L.N. "Nostrum - a finite element program for nonlinear structural mechanics", Nonlinear Structural Mechanics Research Unit, U.C.T., S.A. Technical Report 18 B, November 1983.

10. MARTIN, J.B. "Structural Dynamics",Notes for postgraduate course in the Department of Civil Engineering, University of Cape Town, South Africa.

11. NOSTRUM users manual.

12. PAFEC 70 users manual

APPENDIX A

In this appendix, the detailed results in the form of tables and graphs are given for both the multi-degree and single degree of freedom pipelines respectively.

Multi-Degree of Freedom Results

The actual pipelines set up are the multi-degree of freedom systems. Each table contains the results for a different pipeline. The pipelines that were analysed were pipeline one and pipeline two (see Chapter 4). Three wall thicknesses were used in pipeline one, 0.001m, 0.0048m and 0.015m respectively. Two wall thicknesses were used in pipeline two, 0.001m and 0.0048m. Therefore there are five separate tables of results.

Each pipeline was analysed with five different earthquake records.

They were

1. SSE1 - Safe Shutdown Earthquake 1
2. I952 - Imperial Valley Earthquake
3. S128 - San Fernando Earthquake
4. C1408 - Coyote Lake Earthquake
5. P014 - Parkfield Earthquake

The internal pipe support was allowed to progressively yield from no yield condition be a zero yield stress, where the effect of the support was zero. Thus the yield stress went from a 0% reduction to a 100% reduction in yield stress. Thus in the left hand column on the tables the earthquake type and percentage yield of the internal hanger support is given. The second column contains the maximum

absolute shear force in Newtons at the left hand node, always node number one. The third column contains the maximum absolute shear force in Newtons at the right hand side of the pipe, either node 6 in the case of pipeline one or node 30 in the case of pipeline 2. The third column contains the maximum absolute axial force in Newtons in the hanger support and the fourth contains the maximum absolute deflection in millimeters of the hanger support.

The graphs are aranged in groups of earthquake records. The solid lines always refer to the left hand shear force at node one, the dotted line to the right hand shear force at node 6 in the case of pipeline one or node 30 in the case of pipeline 2.

The dot dash line shows the linear decrease in the hanger axial force as the yield stress in the hanger is decreased to zero. The horizontal ordinate in the graphs refers to the percentage reduction in the yield stress in the hanger. As an example, if the maximum stress recorded in an elastic analysis on the pipeline were 100 MPa then the yield stress of the hanger support would start off at 100 MPa and reduce progressively to 80 MPa, 60 MPa, 40 Mpa, 20 MPa and finally 0 MPa where the support is non existent.

Single Degree of Freedom Results

The single degree of freedom systems contained only two springs acting on a single mass, as described in Chapter 4. Therefore the results tabulated are as given as follows. In column one, the earthquake type and percentage reduction in yield stress is shown. Referring to fig [4.3] in column two, the upper spring force, F_1, is given in Newtons as described in Chapter 4. In column three, the lower spring force, F_2, in Newtons is given and once again, column four gives the deflection of the lumped mass in millimetres.

The graphs show two lines, a dotted and a solid line. The dotted line refers to the maximum absolute lower spring force and the solid line to the maximum absolute upper spring force.

PIPELINE ONE WALL THICKNESS = 0.001m MULTI DEGREE OF FREEDOM

ANALYSIS	FS1 (N)	FS6 (N)	FN7 (N)	DELTA mm
SSE1-0	1899.3	1948.0	6322.3	00.56
SSE1-20	1899.3	1653.1	5055.8	00.67
SSE1-40	1961.7	1411.7	3789.4	00.95
SSE1-60	1784.1	1132.3	2522.8	00.94
SSE1-80	1204.3	724.53	1781.3	01.33
SSE1-100	5612.8	5606.1	31.38	34.25
I952-0	1199.6	647.95	3080.8	00.27
I952-20	1168.8	684.49	2464.8	00.55
I952-40	1196.8	841.54	1849.5	01.74
I952-60	1555.0	1093.9	1236.3	03.89
I952-80	951.02	837.84	1640.6	03.57
I952-100	3594.7	3590.3	19.947	21.77
S128-0	2059.8	886.41	4019.6	00.36
S128-20	1988.8	853.71	3216.6	00.38
S128-40	1536.8	735.47	2412.7	00.54
S128-60	1076.4	668.34	1610.7	01.50
S128-80	1423.5	1287.3	2302.7	05.95
S128-100	3143.3	3139.6	17.623	19.24
C1408-0	6909.0	4638.2	16480.	01.46
C1408-20	6533.2	3951.8	13184.	01.63
C1408-40	5744.9	3015.5	9887.6	01.29
C1408-60	4492.5	2550.2	6593.1	02.34
C1408-80	3016.1	1885.4	3297.6	02.29
C1408-100	2828.5	2823.2	15.760	17.20
P014-0	1776.5	1389.1	5063.4	00.45
P014-20	1747.4	1389.1	4050.3	00.51
P014-40	1534.0	1386.1	3038.2	00.61
P014-60	1318.3	1281.9	2026.5	01.10
P014-80	1134.6	775.35	1740.1	02.29
P014-100	4771.0	4765.3	26.808	29.26

PIPELINE ONE WALL THICKNESS = 0.0048m MULTI DEGREE OF FREEDOM

ANALYSIS	FS1 (N)	FS6 (N)	FN7 (N)	DELTA mm
I952-0	1546.3	265.44	4362.3	00.39
I952-20	1462.9	547.06	3489.3	00.47
I952-40	1317.7	983.13	2617.6	00.77
I952-60	1804.8	1494.4	1746.4	01.50
I952-80	3192.1	2631.6	1351.6	03.43
I952-100	8445.7	8443.5	10.060	10.98
S128-0	1599.5	288.99	4088.6	00.36
S128-20	1389.1	344.64	3270.9	00.38
S128-40	1113.1	532.38	2453.3	00.41
S128-60	1809.3	1460.3	1636.9	01.70
S128-80	3073.8	2745.3	2428.0	03.44
S128-100	11639.	11636.	13.880	15.15
C1408-0	8032.0	1491.8	18650.	01.65
C1408-20	7386.9	1732.1	14918.	01.88
C1408-40	5972.9	1490.3	11192.	01.79
C1408-60	3718.0	1072.6	7462.0	01.49
C1408-80	2363.9	1502.9	3731.1	01.51
C1408-100	10124.	10121.	12.050	13.15
P014-0	4755.8	571.65	11762.	01.04
P014-20	4321.8	748.99	9412.3	01.00
P014-40	3550.5	910.54	7058.8	00.83
P014-60	2500.5	857.44	4706.4	00.71
P014-80	1825.5	1737.4	2353.1	00.89
P014-100	15776.	15772.	18.830	20.56

PIPELINE ONE WALL THICKNESS = 0.015m MULTI DEGREE OF FREEDOM

ANALYSIS	FS1 (N)	FS6 (N)	FN7 (N)	DELTA mm
SSE1-0	12373.	4525.8	27.70.	02.39
SSE1-20	10470.	3930.5	21657.	02.06
SSE1-40	7892.7	3080.2	16242.	01.59
SSE1-60	5653.4	2439.2	10828.	01.13
SSE1-80	3499.1	1923.3	5527.4	00.71
SSE1-100	15614.	15612.	6.4300	07.02
I952-0	2784.9	1263.1	6171.8	00.55
I952-20	2475.5	1177.7	4938.0	00.51
I952-40	2325.0	1396.3	3703.1	00.57
I952-60	2460.2	2224.3	2469.6	00.87
I952-80	4108.9	3875.5	1235.3	01.64
I952-100	10624.	10623.	4.3544	04.75
S128-0	3195.2	1205.5	6976.0	00.62
S128-20	2731.8	1136.3	5580.4	00.56
S128-40	2388.8	1176.8	4186.0	00.50
S128-60	1872.6	1559.2	2790.4	00.53
S128-80	3752.7	3417.3	1396.8	01.38
S128-100	6364.6	6364.0	2.6070	02.85
C1408-0	18407.	6841.9	40323.	03.57
C1408-20	16390.	6972.2	32259.	03.42
C1408-40	13069.	5528.6	24195.	02.62
C1408-60	9276.6	4438.2	16130.	02.11
C1408-80	6184.3	2932.4	8065.9	01.48
C1408-100	10320.	10320.	4.3031	04.70
P014-0	10778.	4057.3	23487.	02.08
P014-20	9146.2	3675.8	18791.	01.90
P014-40	7730.3	3465.9	14093.	01.59
P014-60	6045.7	3128.7	9395.7	01.37
P014-80	3100.3	2252.1	4697.5	00.87
P014-100	23159.	23157.	9.4840	10.35

PIPELINE TWO WALL THICKNESS = 0.001m MULTI DEGREE OF FREEDOM

	(N)	(N)	(N)	mm
ANALYSIS	FS1	FS30	FN31	DELTA
SSE1-0	3391.0	4913.7	9754.9	00.86
SSE1-20	3251.6	4899.0	7805.3	00.97
SSE1-40	2984.2	4476.4	5854.0	01.68
SSE1-60	2337.4	3631.0	3902.9	01.34
SSE1-80	1975.3	2207.8	1953.1	02.44
SSE1-100	10950.	13296.	36.263	39.58
I952-0	2423.0	2892.9	21591.	01.91
I952-20	2275.3	2750.4	17273.	01.86
I952-40	1895.5	2356.8	12955.	01.42
I952-60	1361.0	2094.2	8636.6	01.11
I952-80	1229.4	2022.2	4318.8	01.10
I952-100	3279.3	3239.3	9.8152	10.71
S128-0	4079.5	4733.3	45205.	04.00
S128-20	3444.0	4327.2	36164.	03.71
S128-40	2971.5	3919.3	27123.	02.71
S128-60	2696.5	3525.4	18083.	02.13
S128-80	2189.2	2906.6	9042.1	01.73
S128-100	2785.6	3815.3	8.5090	09.29
C1408-0	2124.2	2703.8	14934.	01.32
C1408-20	2041.4	2680.3	11947.	01.21
C1408-40	1907.9	2515.3	8961.2	01.10
C1408-60	1715.7	2603.5	5974.3	00.91
C1408-80	1842.0	2473.6	2987.7	01.11
C1408-100	6194.9	8559.9	19.370	21.14
P014-0	1579.6	2449.9	11371.	01.01
P014-20	1569.0	2332.3	9096.8	00.98
P014-40	1541.8	2205.2	6822.5	00.98
P014-60	1200.6	1734.5	4549.2	00.80
P014-80	896.54	1323.7	2275.2	00.99
P014-100	4890.0	6030.0	19.522	21.31

PIPELINE TWO WALL THICKNESS = 0.0048m MULTI DEGREE OF FREEDOM

ANALYSIS	FS1 (N)	FS30 (N)	FN31 (N)	DELTA mm
SSE1-0	6100.4	6243.5	19240.	01.70
SSE1-20	5267.5	5425.4	15392.	01.62
SSE1-40	3910.4	5022.7	11544.	01.46
SSE1-60	2859.4	3708.9	7696.4	01.12
SSE1-80	1976.7	2739.1	3849.5	01.10
SSE1-100	16318.	16723.	13.269	14.48
I952-0	3159.9	5649.4	15810.	01.40
I952-20	2985.7	5258.1	12648.	01.34
I952-40	2516.5	4220.6	9486.3	01.10
I952-60	1845.2	3066.0	6324.2	00.83
I952-80	2149.1	2719.7	3162.8	01.13
I952-100	4526.3	6171.2	3.3630	03.67
S128-0	4198.2	8603.9	21098.	01.87
S128-20	3857.8	7338.6	16879.	01.74
S128-40	3354.7	6459.3	12659.	01.40
S128-60	2905.1	5740.4	8439.5	01.07
S128-80	2219.5	3560.7	4220.1	00.77
S128-100	13889.	15164.	11.652	12.72
C1408-0	3995.6	2252.0	16211.	01.43
C1408-20	3543.2	2209.3	12969.	01.38
C1408-40	2882.2	2371.6	9726.8	01.03
C1408-60	2215.3	2203.4	6484.7	00.99
C1408-80	1906.9	3296.5	3242.3	01.24
C1408-100	16829.	19598.	14.218	15.52
P014-0	3094.6	4260.3	10311.	00.91
P014-20	2783.9	4192.6	8249.0	00.94
P014-40	2313.5	3251.5	6186.9	00.88
P014-60	1982.5	2429.7	4124.9	00.88
P014-80	1617.7	1685.0	2062.6	01.00
P014-100	12172.	13438.	10.498	11.46

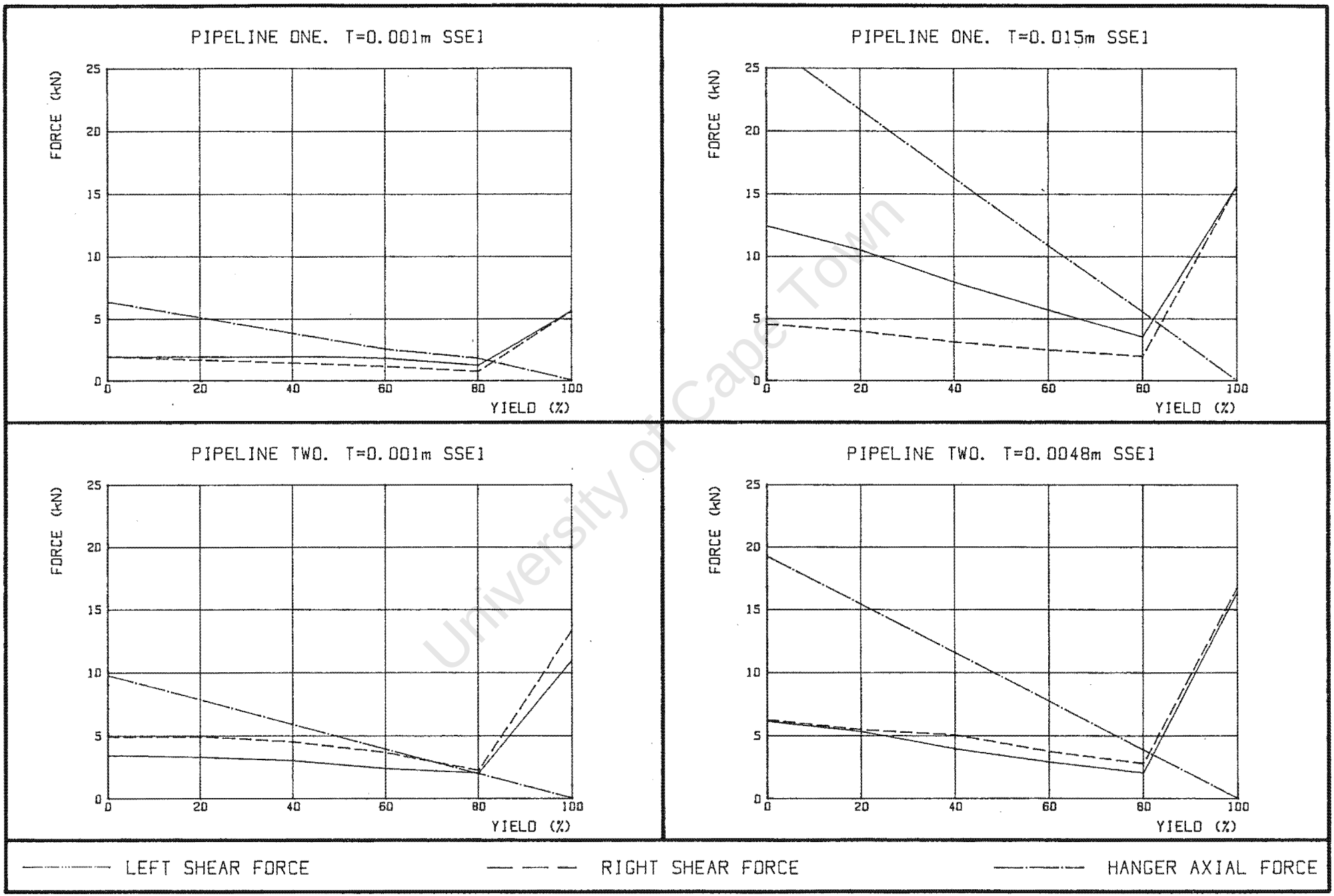

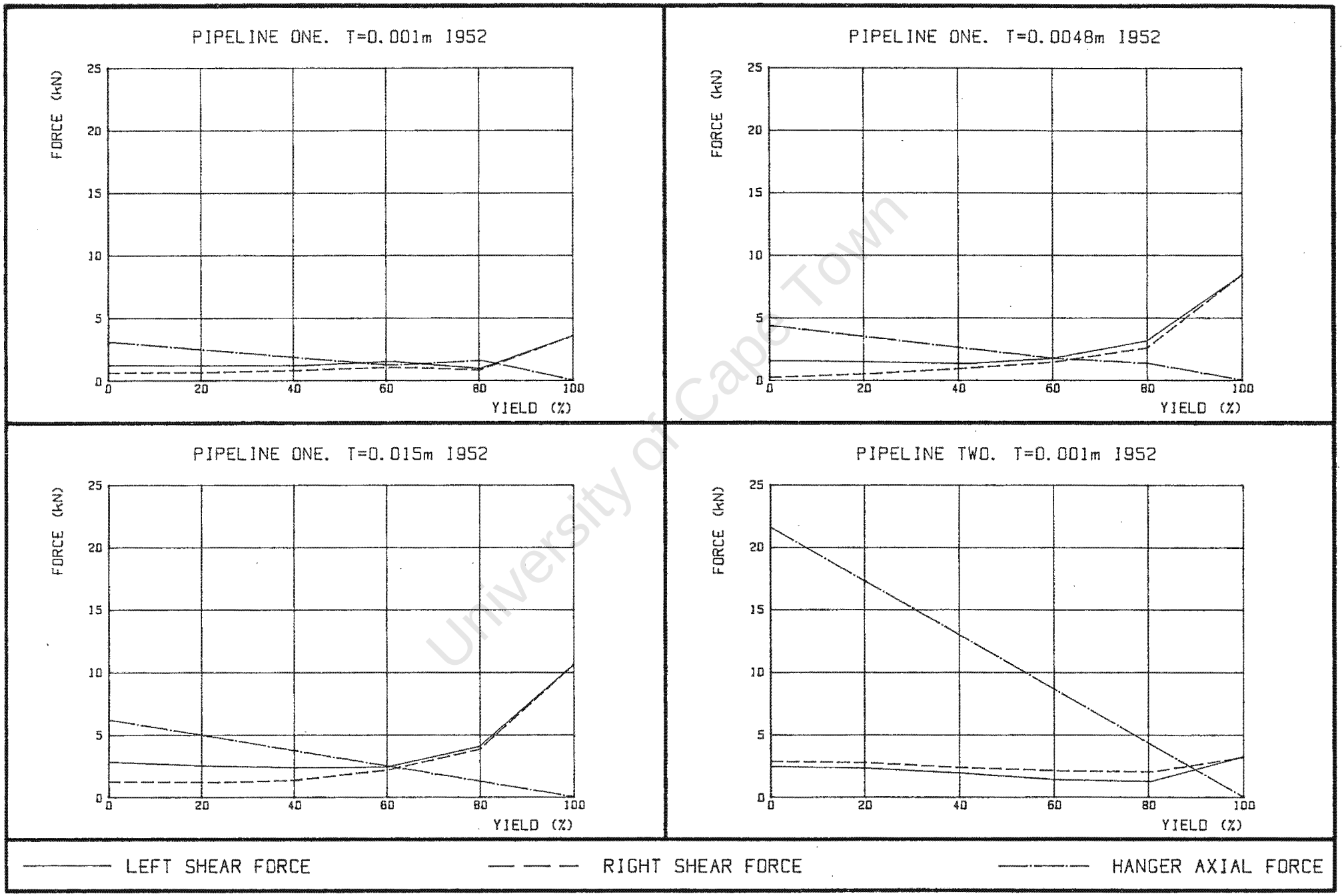

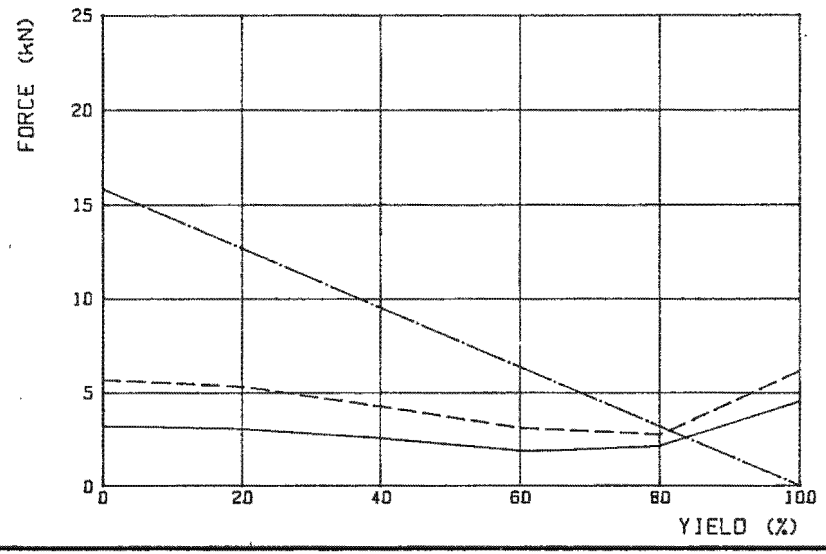

——— LEFT SHEAR FORCE — — — RIGHT SHEAR FORCE ———·——— HANGER AXIAL FORCE

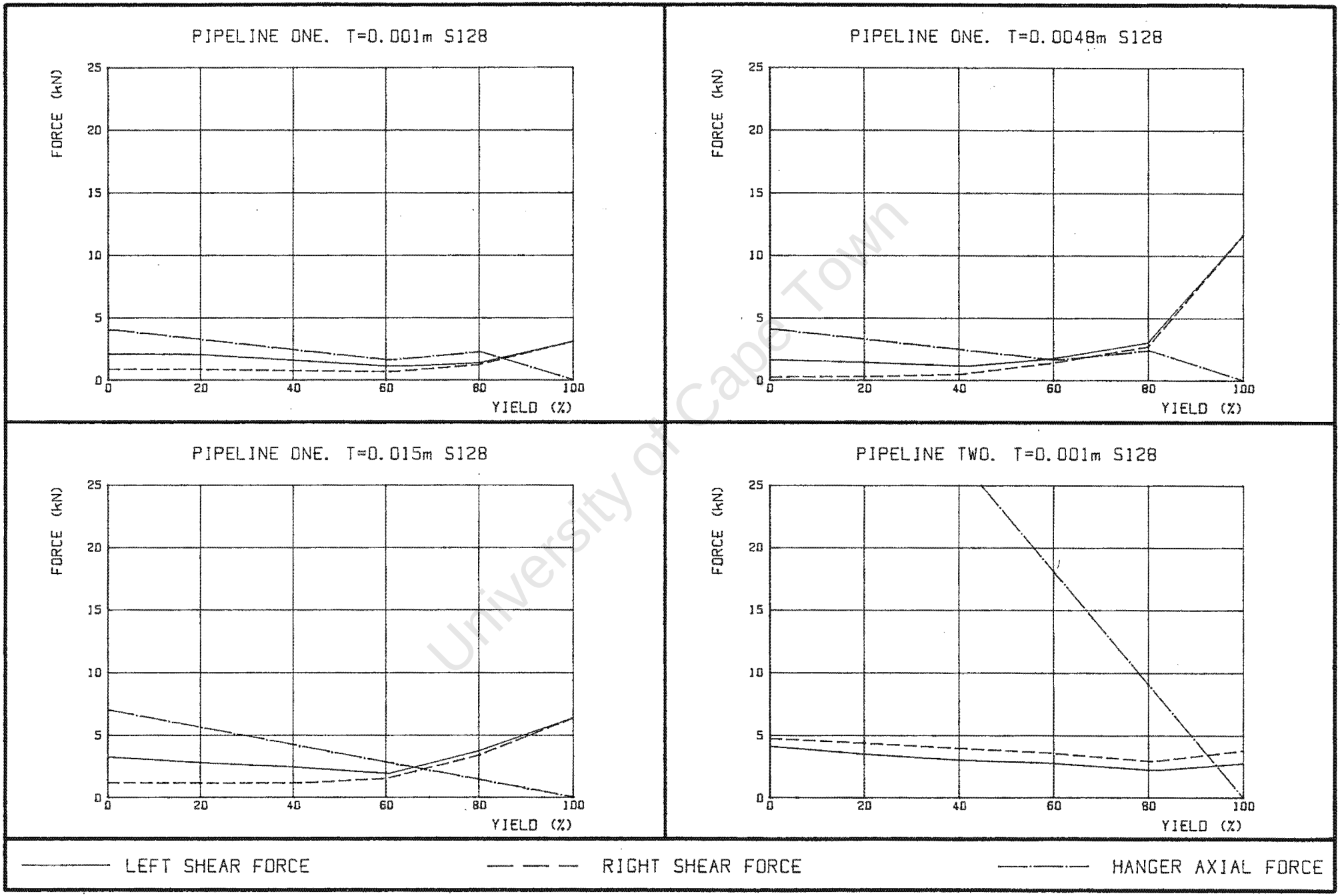

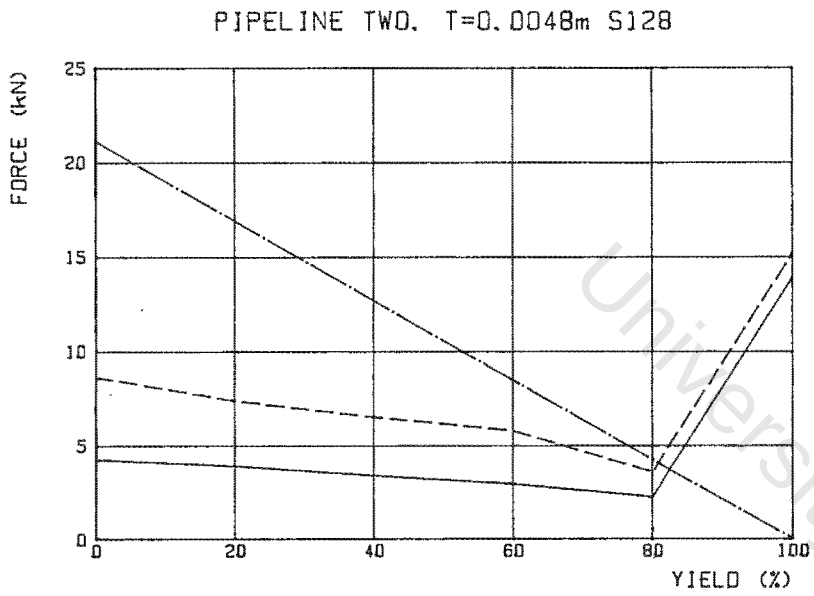

——— LEFT SHEAR FORCE — — — RIGHT SHEAR FORCE ———·——— HANGER AXIAL FORCE

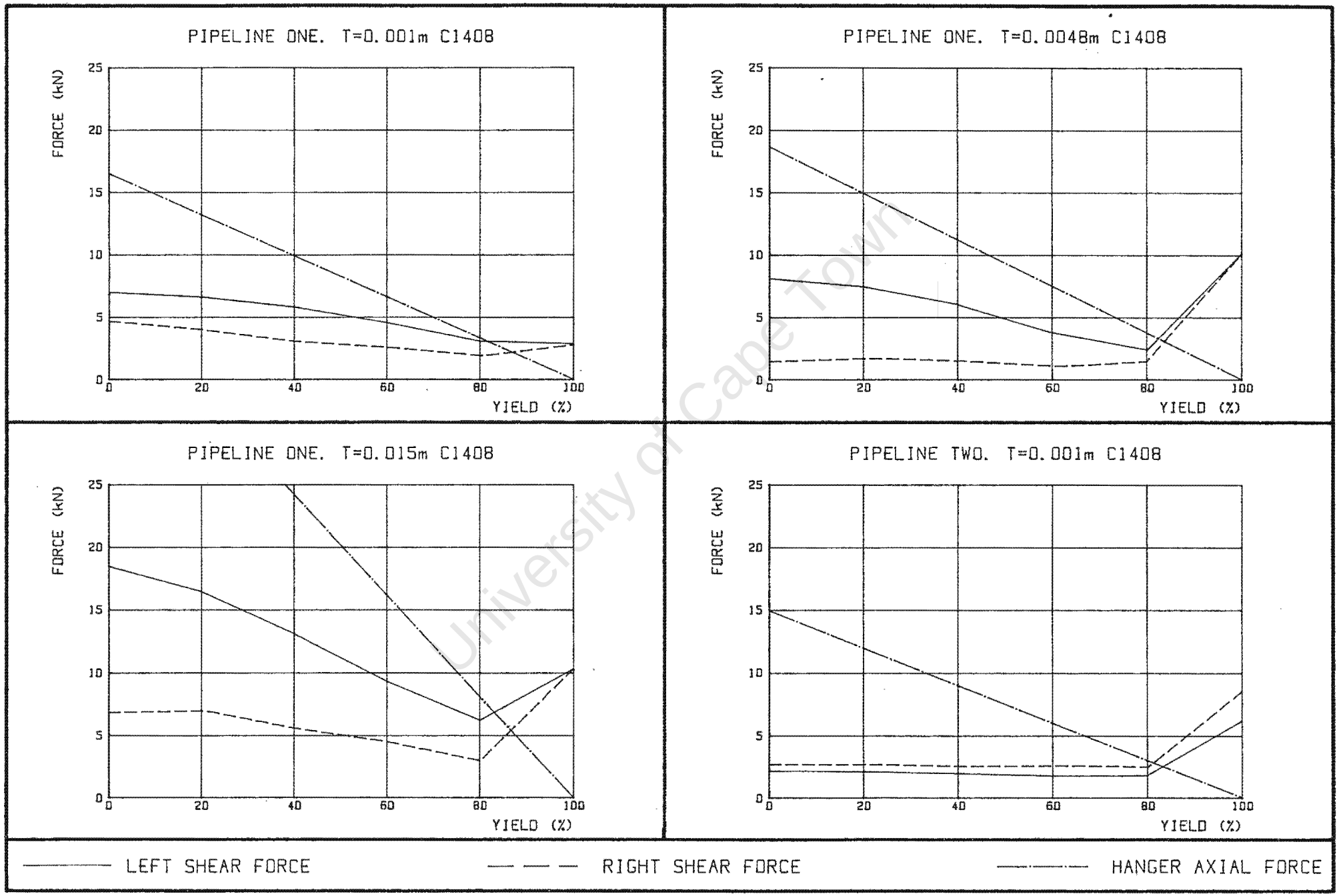

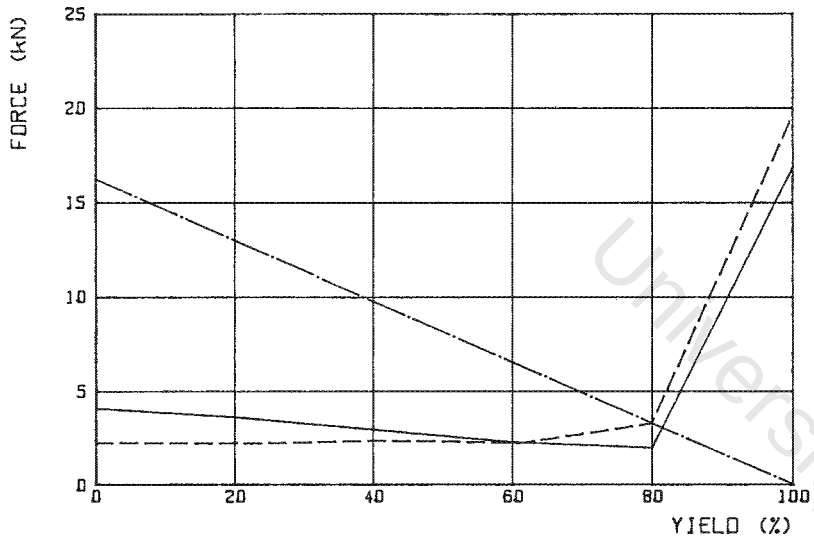

LEFT SHEAR FORCE — — — RIGHT SHEAR FORCE —·—·— HANGER AXIAL FORCE

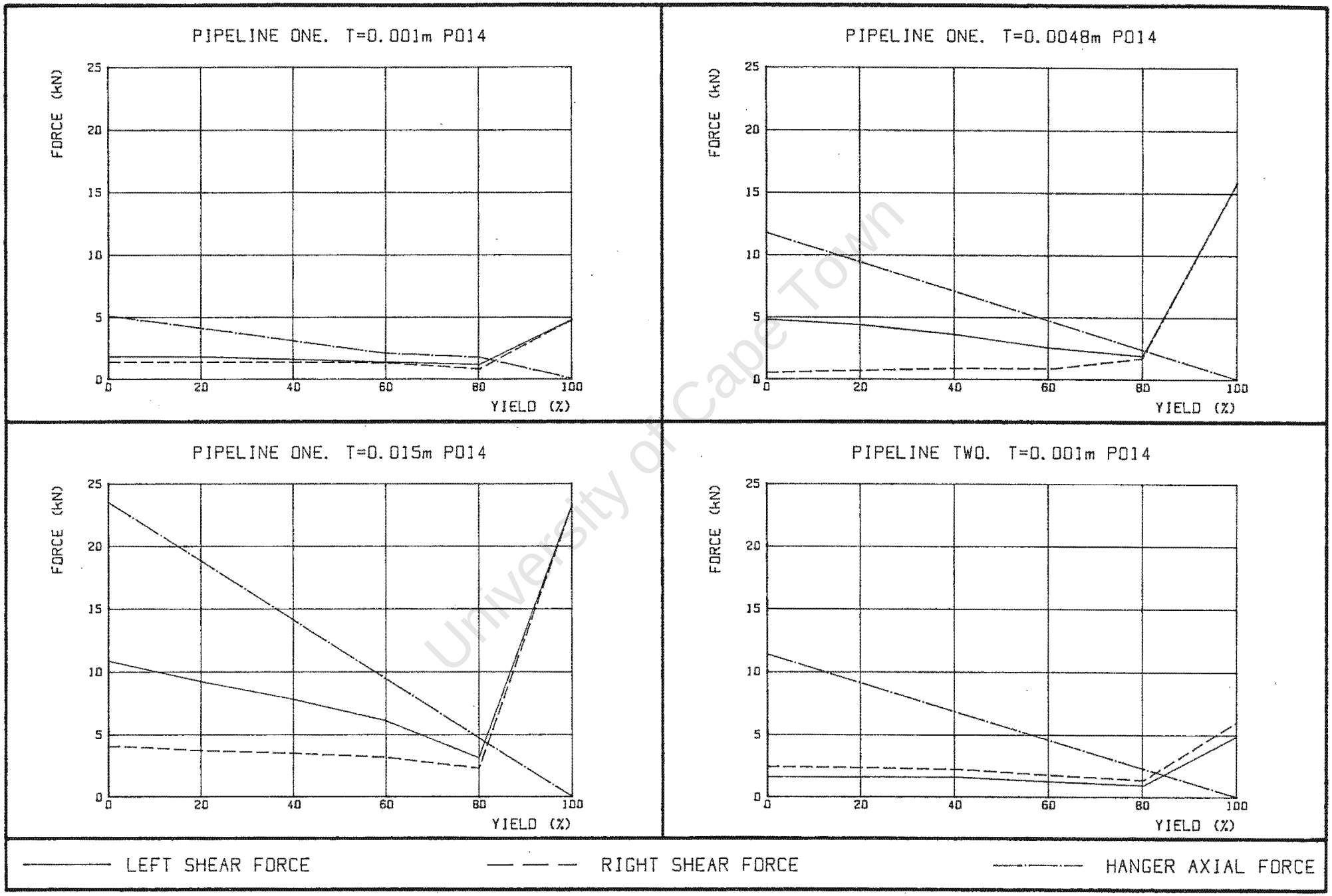

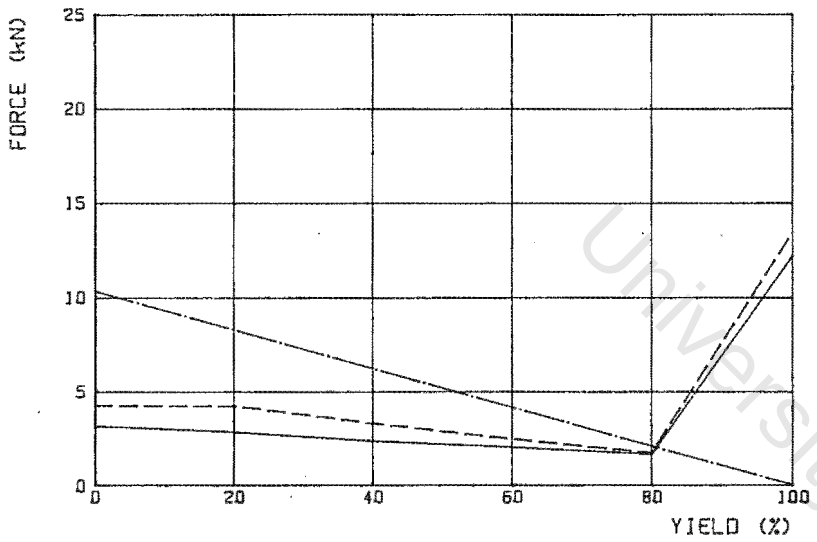

LEFT SHEAR FORCE — — — RIGHT SHEAR FORCE ——·—— HANGER AXIAL FORCE

PIPELINE ONE WALL THICKNESS = 0.001m SINGLE DEGREE OF FREEDOM

ANALYSIS	TOP FORCE (N)	BOTTOM FORCE (N)	DELTA mm
SSE1-0	1.0729	10.129	2.32
SSE1-20	0.9959	8.1032	2.15
SSE1-40	0.9217	6.0774	1.99
SSE1-60	0.8267	4.0516	1.78
SSE1-80	0.7865	2.0258	1.70
SSE1-100	13.591	0.0000	29.3
I952-0	0.6699	6.3245	1.45
I952-20	0.6236	5.0596	1.35
I952-40	0.7155	3.7947	1.54
I952-60	1.2537	2.5298	2.71
I952-80	2.1004	1.2649	4.53
I952-100	8.6226	0.0000	18.6
S128-0	1.1376	10.740	2.46
S128-20	0.9760	8.5920	2.11
S128-40	0.7924	6.4440	1.71
S128-60	0.6868	4.2960	1.48
S128-80	1.2509	2.1480	2.70
S128-100	7.6182	0.0000	16.4
C1408-0	3.8285	36.143	8.26
C1408-20	3.2653	28.914	7.05
C1408-40	2.9458	21.686	6.36
C1408-60	2.2988	14.457	4.96
C1408-80	1.3558	7.2286	2.93
C1408-100	6.3538	0.0000	13.7
P014-0	0.9796	9.2483	2.11
P014-20	0.8605	7.3986	1.86
P014-40	0.7552	5.5490	1.63
P014-60	0.6649	3.6993	1.43
P014-80	0.9547	1.8497	2.06
P014-100	11.566	0.0000	25.0

PIPELINE ONE WALL THICKNESS = 0.0048m SINGLE DEGREE OF FREEDOM

ANALYSIS	TOP FORCE (N)	BOTTOM FORCE (N)	DELTA mm
I952-0	0.8015	4.7504	0.51
I952-20	0.8849	3.8003	0.56
I952-40	1.1955	2.8502	0.76
I952-60	1.9503	1.9002	1.23
I952-80	4.2551	0.9501	2.69
I952-100	14.852	0.0000	9.39
S128-0	0.7935	4.7031	0.50
S128-20	0.7456	3.7625	0.47
S128-40	0.7058	2.8219	0.45
S128-60	1.5140	1.8812	0.96
S128-80	4.3891	1.8572	2.77
S128-100	20.471	0.0000	12.9
C1408-0	3.7963	22.501	2.40
C1408-20	3.8585	18.001	2.44
C1408-40	3.1828	13.501	2.01
C1408-60	2.5736	9.0000	1.63
C1408-80	1.6620	4.5000	1.05
C1408-100	17.759	0.0000	11.2
P014-0	2.4828	14.715	1.57
P014-20	2.2226	11.776	1.41
P014-40	1.7699	8.8318	1.12
P014-60	1.2650	5.8879	0.80
P014-80	1.2175	2.9439	0.77
P014-100	27.791	0.0000	17.6

PIPELINE ONE WALL THICKNESS = 0.015m SINGLE DEGREE OF FREEDOM

ANALYSIS	TOP FORCE (N)	BOTTOM FORCE (N)	DELTA mm
SSE1-0	7.1661	19.019	2.35
SSE1-20	6.1503	15.215	2.01
SSE1-40	4.8269	11.411	1.58
SSE1-60	3.3365	7.6076	1.09
SSE1-80	1.9982	3.8038	0.65
SSE1-100	18.297	0.0000	5.99
I952-0	1.6019	4.2513	0.52
I952-20	1.4469	3.4010	0.47
I952-40	1.5487	2.5508	0.51
I952-60	2.4055	1.7005	0.79
I952-80	4.3009	0.8503	1.41
I952-100	12.404	0.0000	4.06
S128-0	1.8272	4.8492	0.60
S128-20	1.6013	3.8794	0.52
S128-40	1.4451	2.9095	0.47
S128-60	1.4298	1.9397	0.47
S128-80	3.5270	0.9698	1.16
S128-100	7.4158	0.0000	2.43
C1408-0	10.576	28.069	3.46
C1408-20	9.8119	22.455	3.21
C1408-40	7.7919	16.841	2.55
C1408-60	5.7200	11.228	1.87
C1408-80	4.0848	5.6138	1.34
C1408-100	12.245	0.0000	4.01
P014-0	6.1450	16.309	2.01
P014-20	5.3952	13.047	1.77
P014-40	4.6241	9.7854	1.51
P014-60	3.8578	6.5236	1.26
P014-80	2.4348	3.2618	0.80
P014-100	27.035	0.0000	8.86

PIPELINE TWO WALL THICKNESS = 0.001m SINGLE DEGREE OF FREEDOM

ANALYSIS	TOP FORCE (N)	BOTTOM FORCE (N)	DELTA mm
SSE1-0	0.4463	4.6072	63.48
SSE1-20	0.4524	3.6858	64.35
SSE1-40	0.3400	2.7643	48.36
SSE1-60	0.2405	1.8429	34.20
SSE1-80	0.1879	0.9214	26.72
SSE1-100	0.8152	0.0000	116.0
I952-0	0.5885	6.0750	83.71
I952-20	0.5121	4.8600	72.83
I952-40	0.4148	3.6450	59.00
I952-60	0.3187	2.4300	45.33
I952-80	0.2587	1.2150	36.80
I952-100	2.3568	0.0000	335.2
S128-0	0.1755	1.8121	24.97
S128-20	0.1532	1.4497	21.78
S128-40	0.1347	1.0873	19.16
S128-60	0.1102	0.7248	15.67
S128-80	0.1149	0.3624	16.34
S128-100	0.1935	0.0000	27.53
C1408-0	0.2729	2.8170	38.82
C1408-20	0.2540	2.2536	36.12
C1408-40	0.2162	1.6902	30.75
C1408-60	0.1707	1.1268	24.28
C1408-80	0.1244	0.5634	17.70
C1408-100	0.5122	0.0000	72.85
P014-0	0.2218	2.2899	31.55
P014-20	0.2190	1.8319	31.15
P014-40	0.2497	1.3739	35.52
P014-60	0.2039	0.9160	29.00
P014-80	0.1879	0.4580	26.73
P014-100	0.5723	0.0000	81.40

PIPELINE TWO WALL THICKNESS = 0.0048m SINGLE DEGREE OF FREEDOM

ANALYSIS	TOP FORCE (N)	BOTTOM FORCE (N)	DELTA mm
SSE1-0	1.7638	19.453	17.0
SSE1-20	1.6365	15.562	15.8
SSE1-40	1.2660	11.672	12.2
SSE1-60	0.8824	7.7812	8.51
SSE1-80	0.5531	3.8906	5.33
SSE1-100	6.3566	0.0000	61.3
I952-0	0.8786	9.6894	8.47
I952-20	0.8853	7.7515	8.53
I952-40	0.7046	5.8136	6.79
I952-60	0.7560	3.8758	7.29
I952-80	0.9242	1.9379	9.81
I952-100	5.0703	0.0000	48.9
S128-0	2.5370	27.980	24.5
S128-20	2.1499	22.384	20.7
S128-40	1.6580	16.788	16.0
S128-60	1.2414	11.192	12.0
S128-80	1.0525	5.5960	10.2
S128-100	1.2798	0.0000	12.3
C1408-0	1.9277	21.260	18.6
C1408-20	1.7045	17.008	16.4
C1408-40	1.4068	12.756	13.6
C1408-60	1.1591	8.5040	11.2
C1408-80	0.9841	4.2520	9.49
C1408-100	2.8339	0.0000	27.3
P014-0	1.9379	21.372	18.7
P014-20	1.6974	17.098	16.4
P014-40	1.4688	12.823	14.2
P014-60	1.0428	8.5488	10.1
P014-80	0.7092	4.2744	6.84
P014-100	3.1452	0.0000	30.3

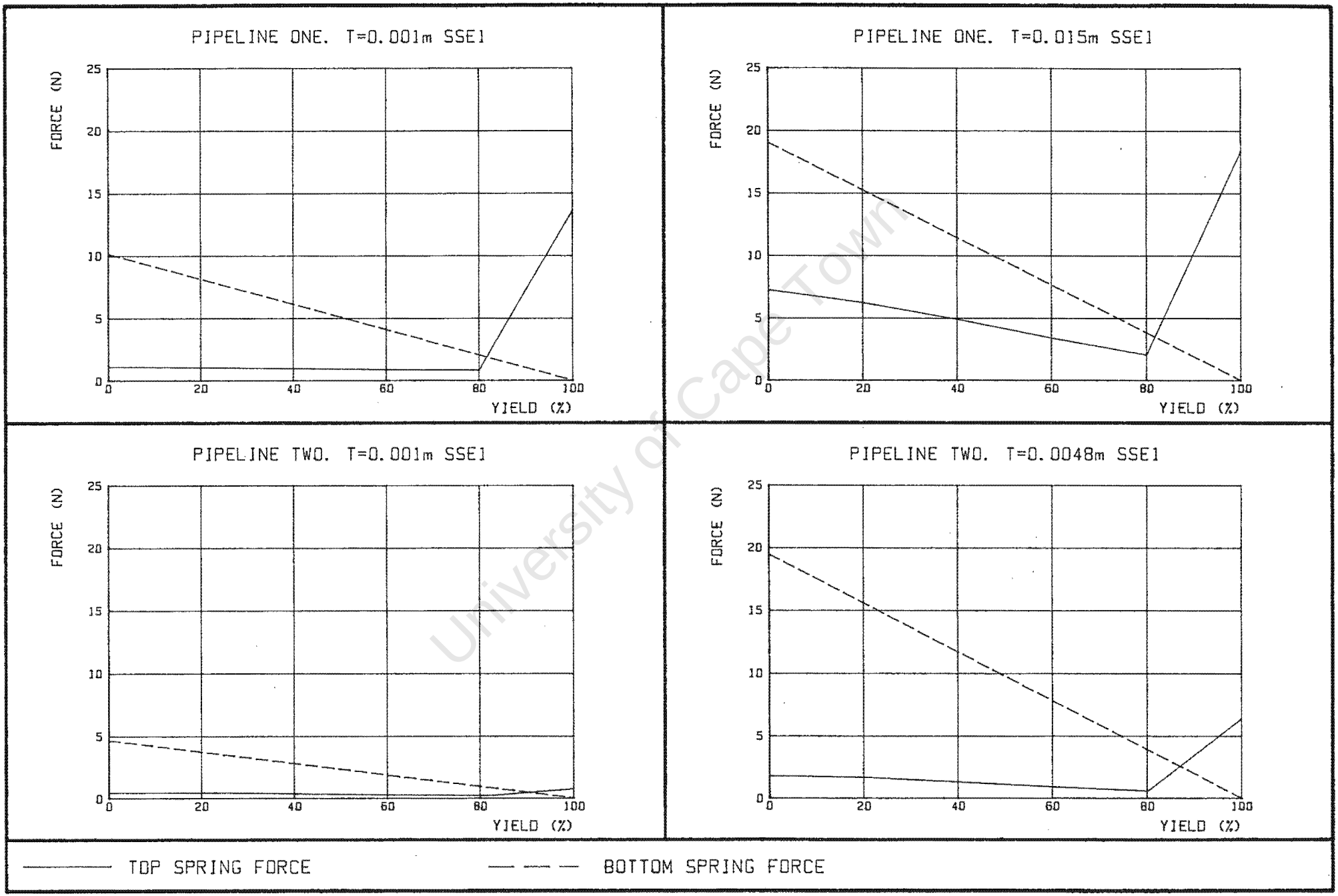

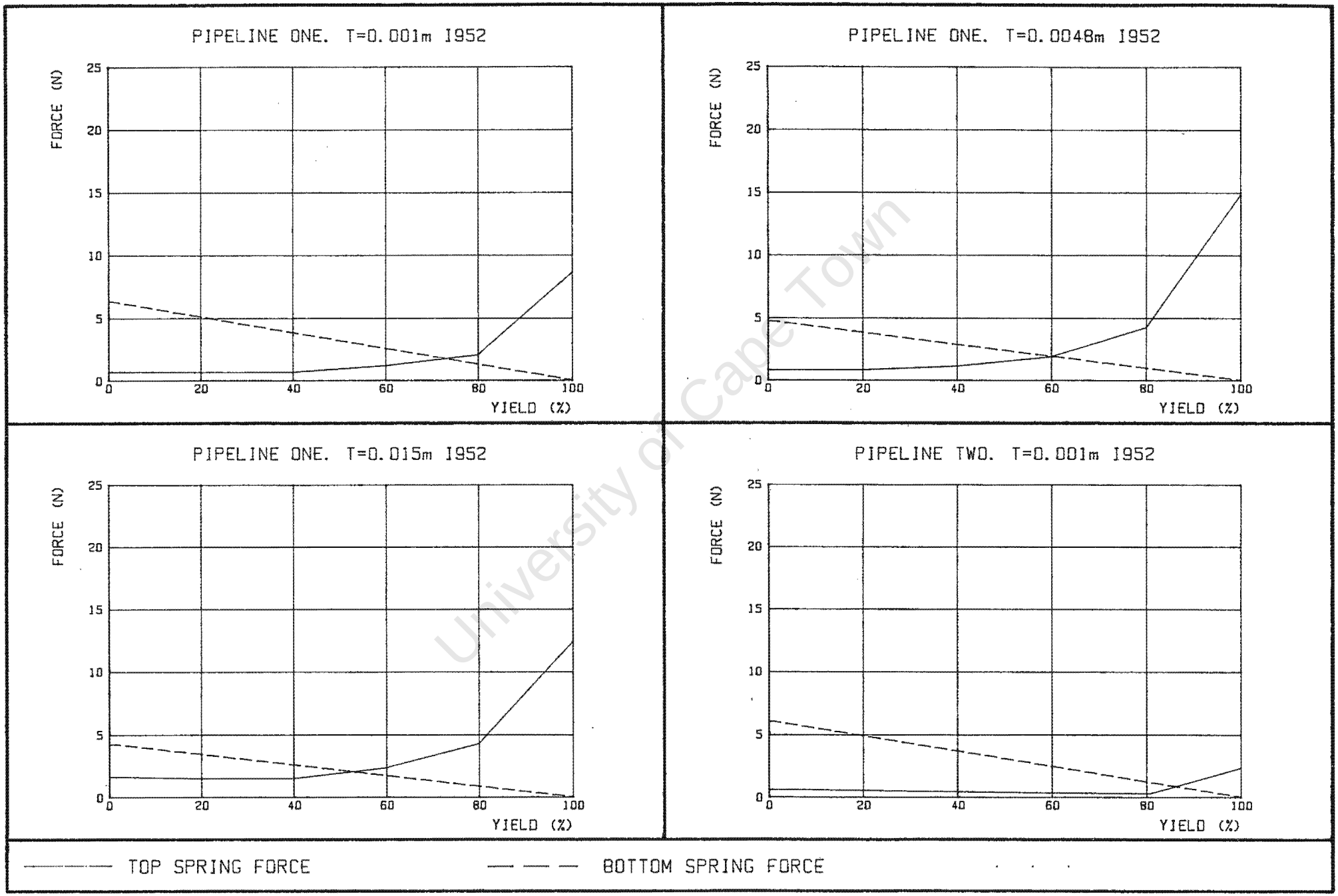

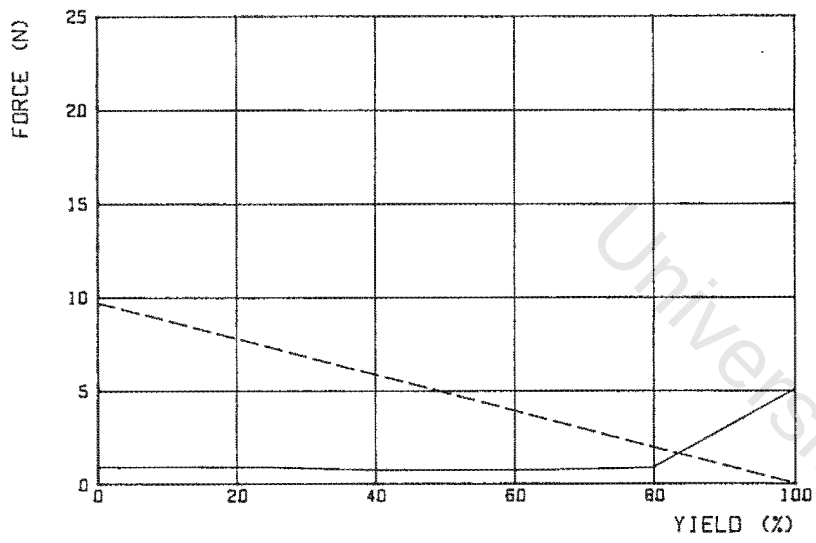

——— TOP SPRING FORCE — — — BOTTOM SPRING FORCE

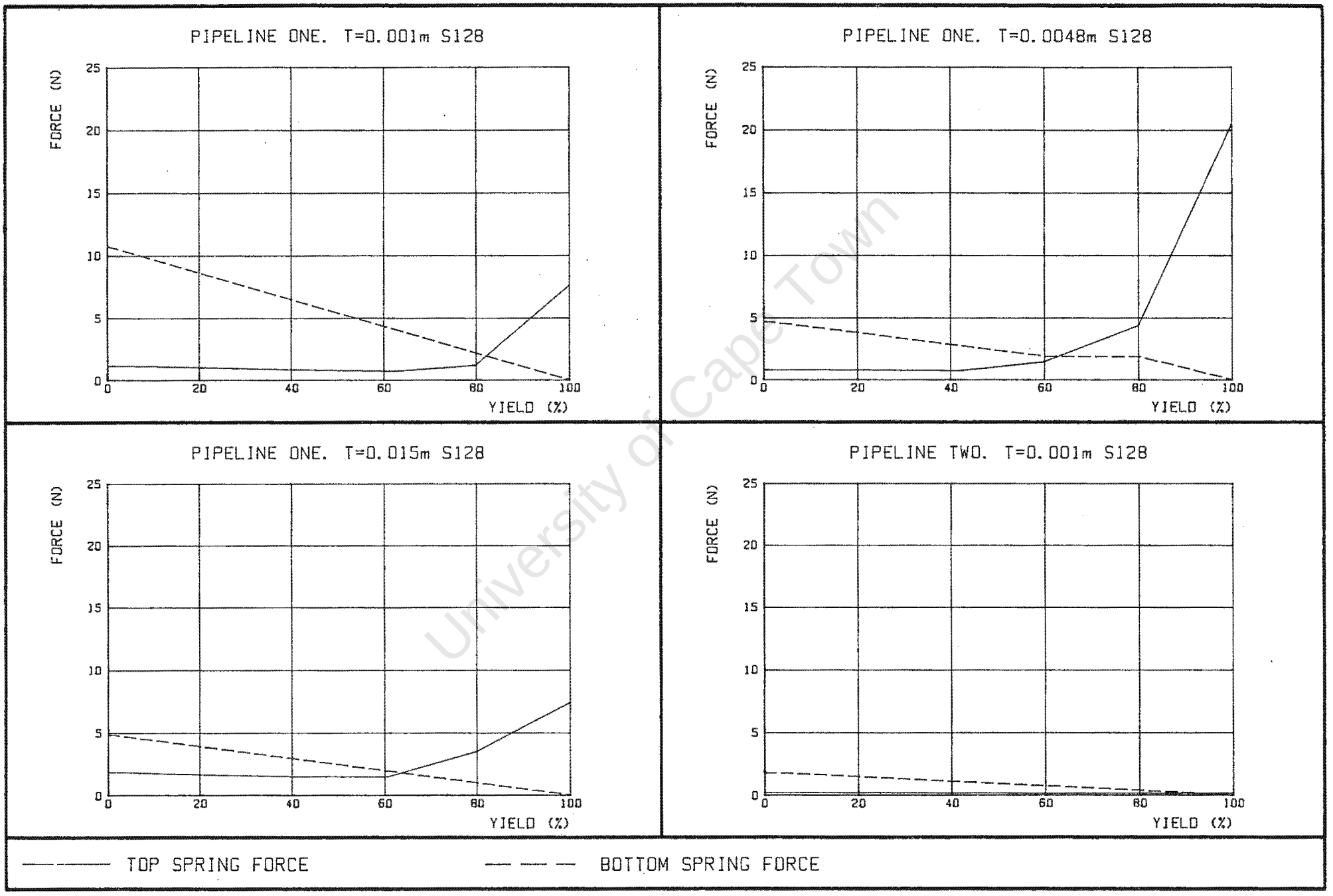

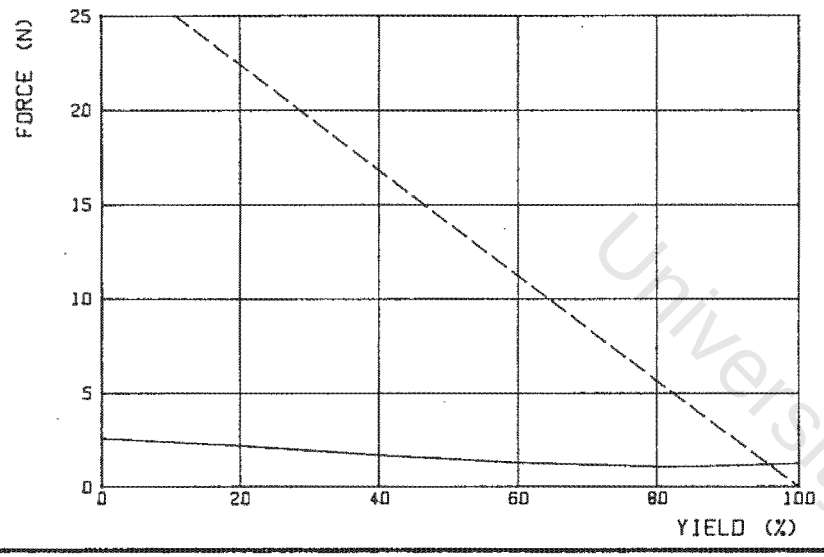

——— TOP SPRING FORCE — — — BOTTOM SPRING FORCE

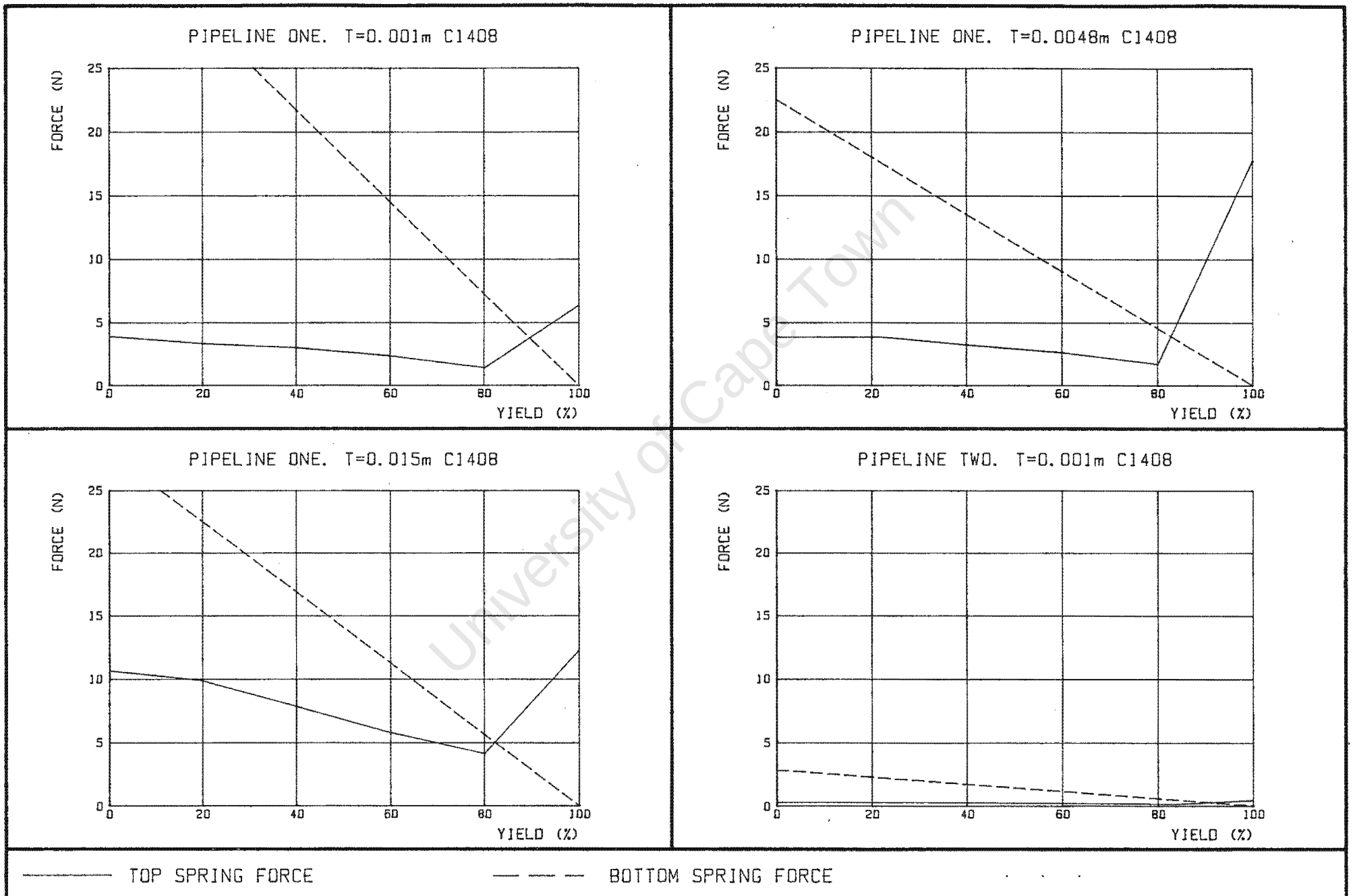

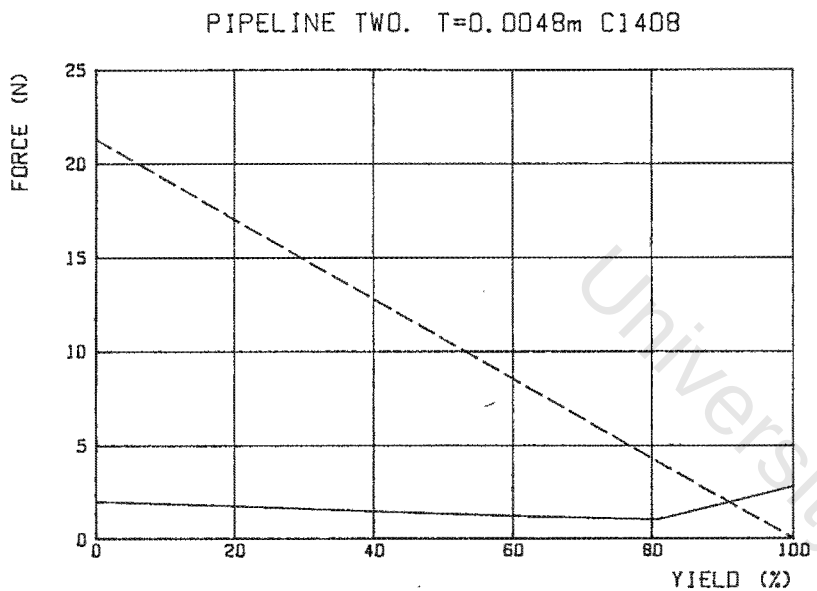

——— TOP SPRING FORCE — — — BOTTOM SPRING FORCE

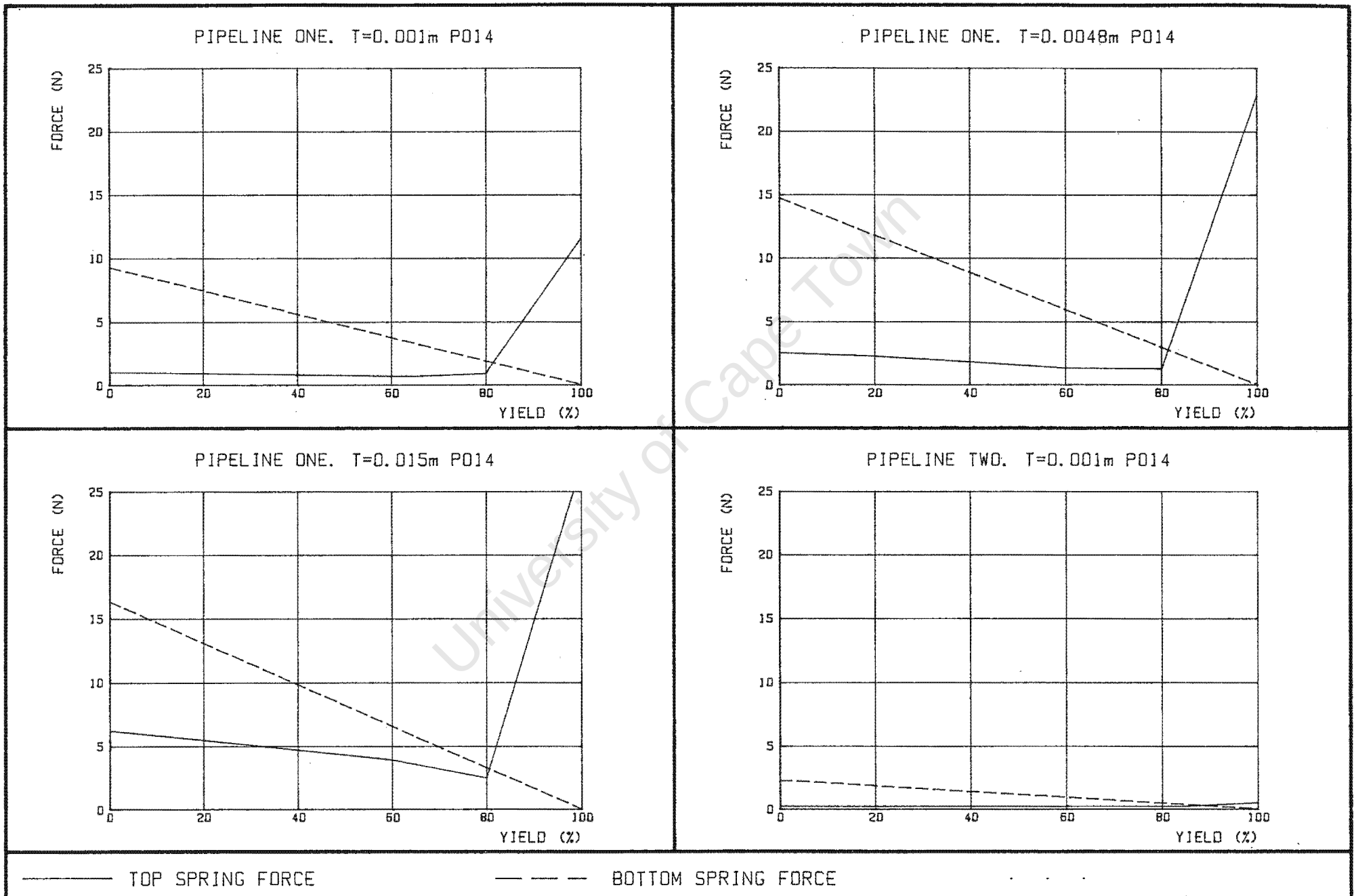

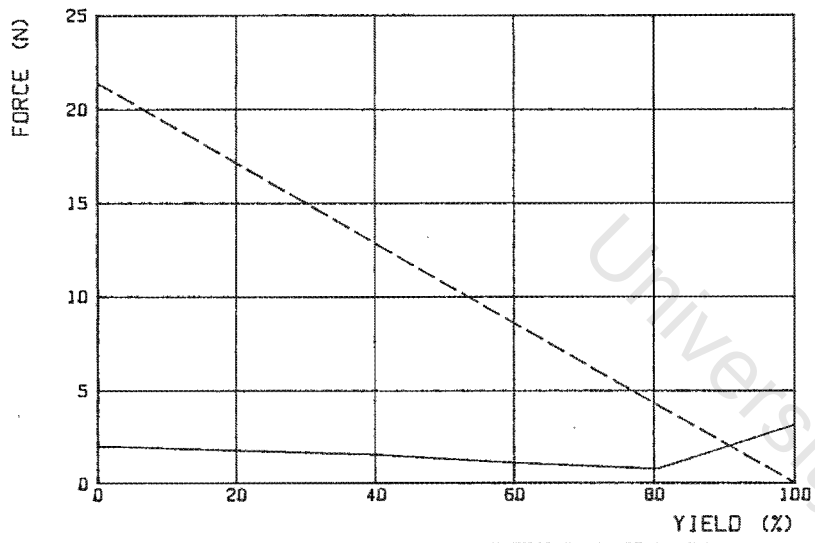

——— TOP SPRING FORCE — — — BOTTOM SPRING FORCE

APPENDIX B

In this appendix the accelerograms and the response spectra for the various earthquakes in both the horizontal and vertical directions that were used in the analyses are given. They are given in the following order, first the horizontal and vertical accelerograms followed by the horizontal and vertical response spectra.

1. SSE1- Horizontal Accelerogram
2. SSE1- Vertical Accelerogram
3. SSE1- Horizontal Response Spectrum
4. SSE1- Vertical Response Spectrum
5. Imperial Valley Station 952- Horizontal Accelerogram
6. Imperial Valley Station 952- Vertical Accelerogram
7. Imperial Valley Station 952- Horizontal Response Spectrum
8. Imperial Valley Station 952- Vertical Response Spectrum
9. San Fernando Station 128- Horizontal Accelerogram
10. San Fernando Station 128- Vertical Accelerogram
11. San Fernando Station 128- Horizontal Response Spectrum
12. San Fernando Station 128- Vertical Response Spectrum
13. Coyote Lake Station 1408- Horizontal Accelerogram
14. Coyote Lake Station 1408- Vertical Accelerogram
15. Coyote Lake Station 1408- Horizontal Response Spectrum
16. Coyote Lake Station 1408- Vertical Response Spectrum
17. Parkfield Station 014- Horizontal Accelerogram
18. Parkfield Station 014- Vertical Accelerogram
19. Parkfield Station 014- Horizontal Response Spectrum
20. Parkfield Station 014- Vertical Response Spectrum

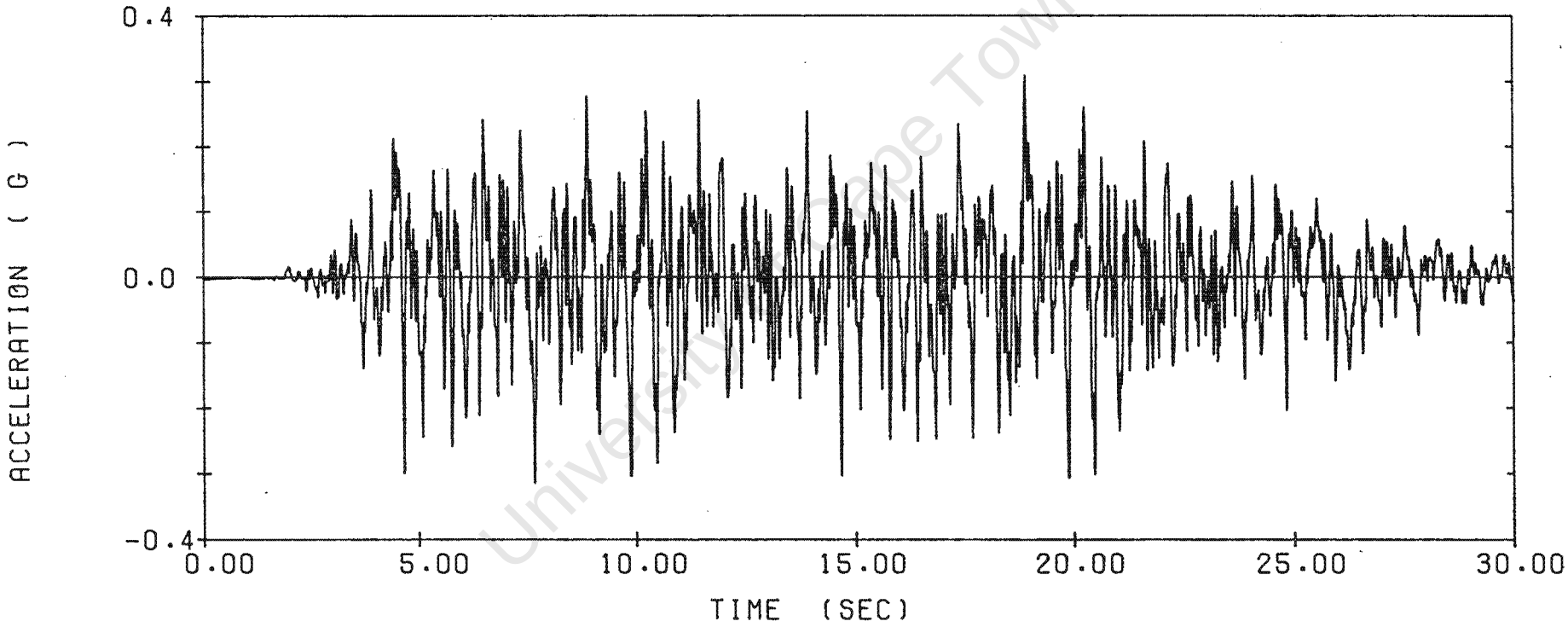

HØRIZØNTAL RECØRD SSE - 1

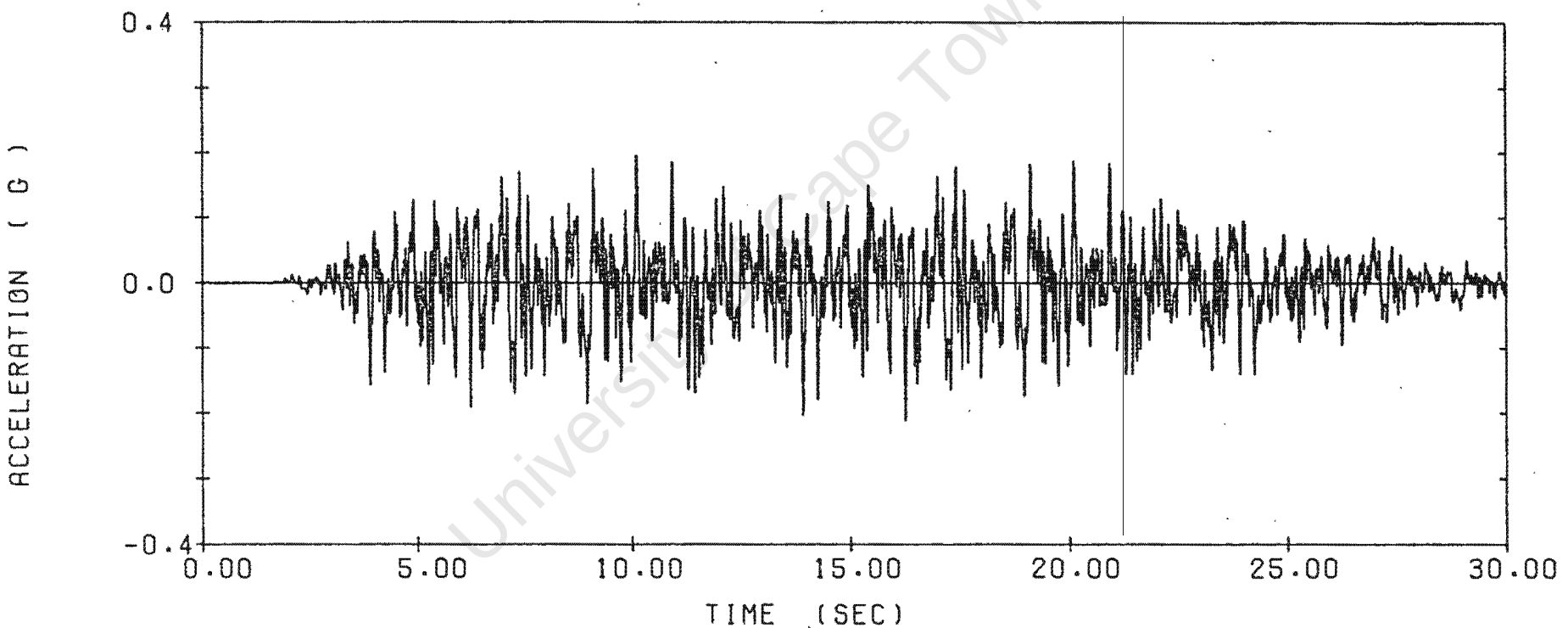

VERTICAL RECORD SSE - 1

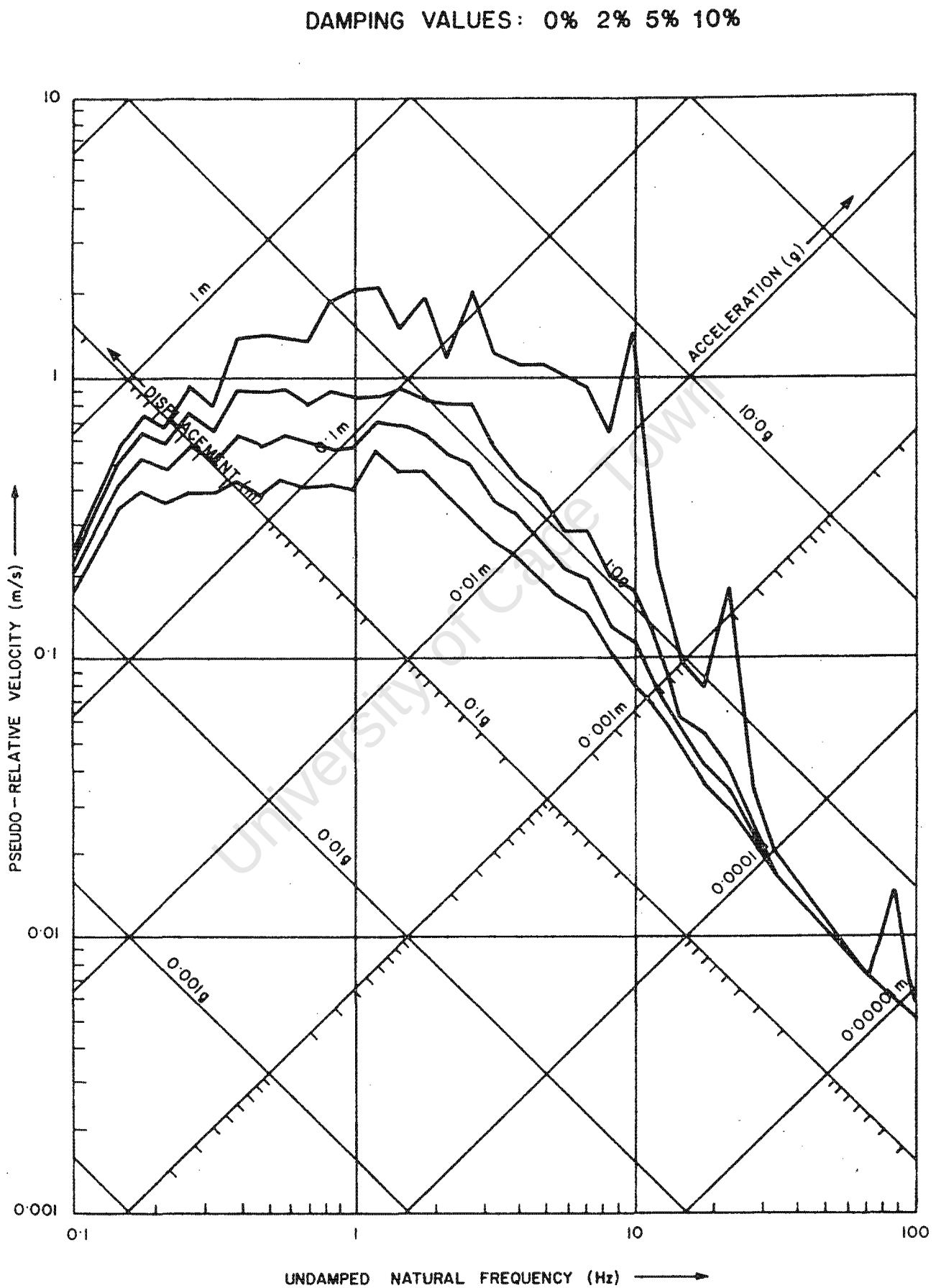

FIG. 4.5 : RESPONSE SPECTRA FOR HORIZONTAL HISTORY

DAMES & MOORE

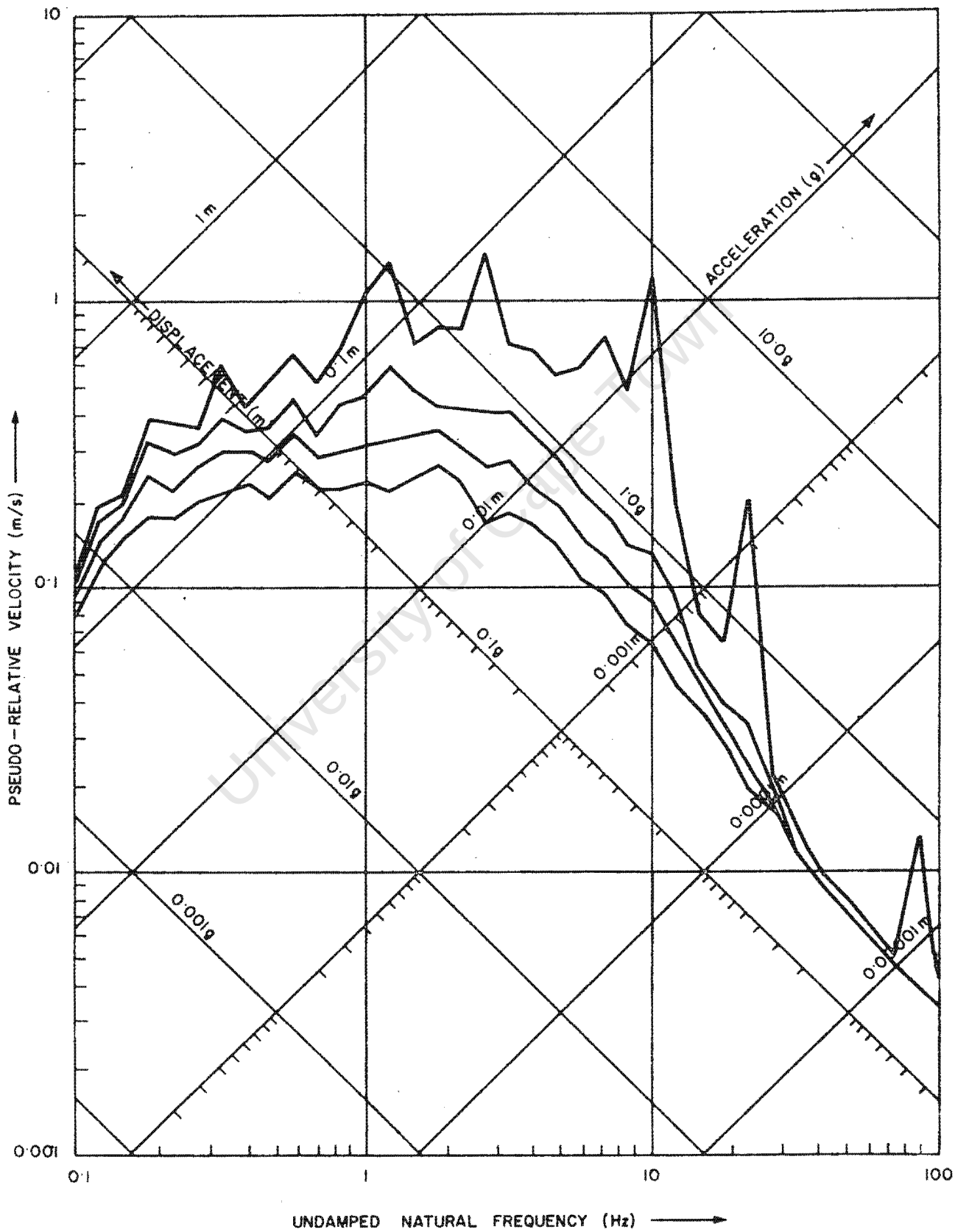

FIG. 4.6 : RESPONSE SPECTRA FOR VERTICAL HISTORY

DAMES & MOORE

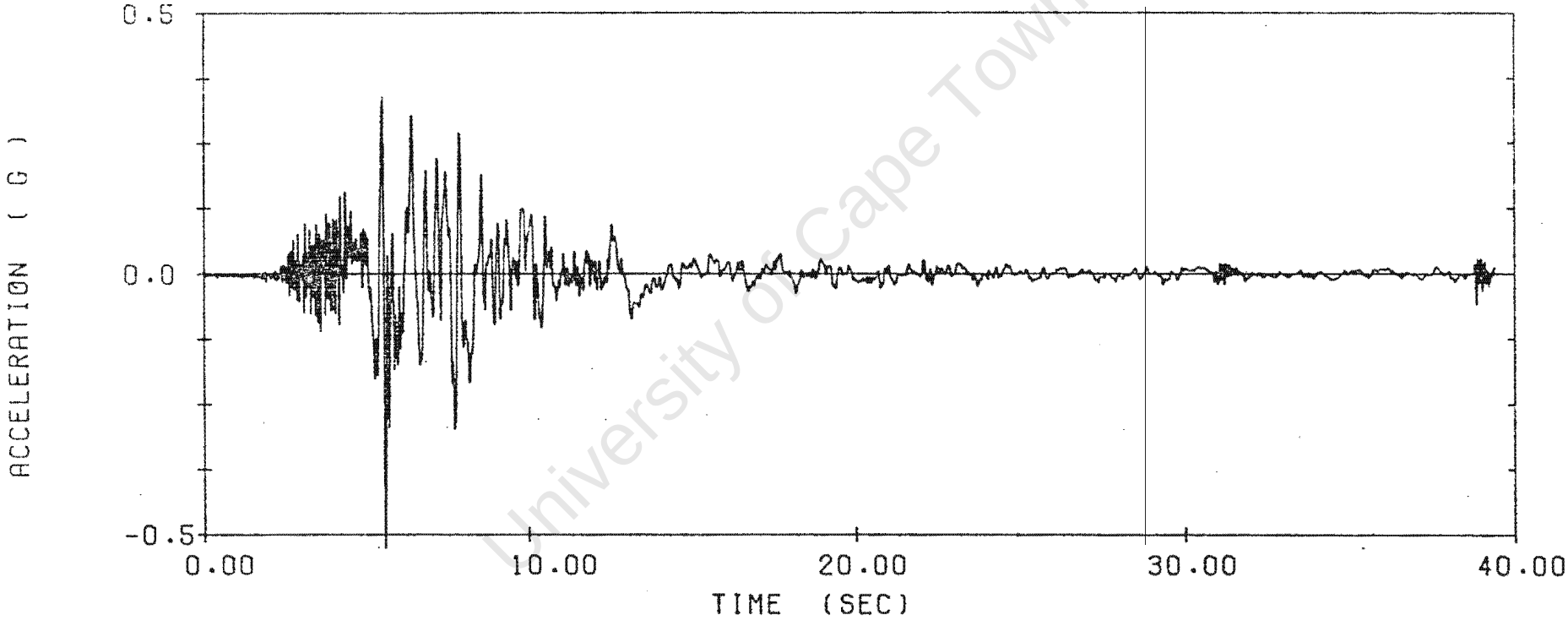

IMPERIAL VALLEY EARTHQUAKE 15/10/79 ST. 952 H 140 DEG

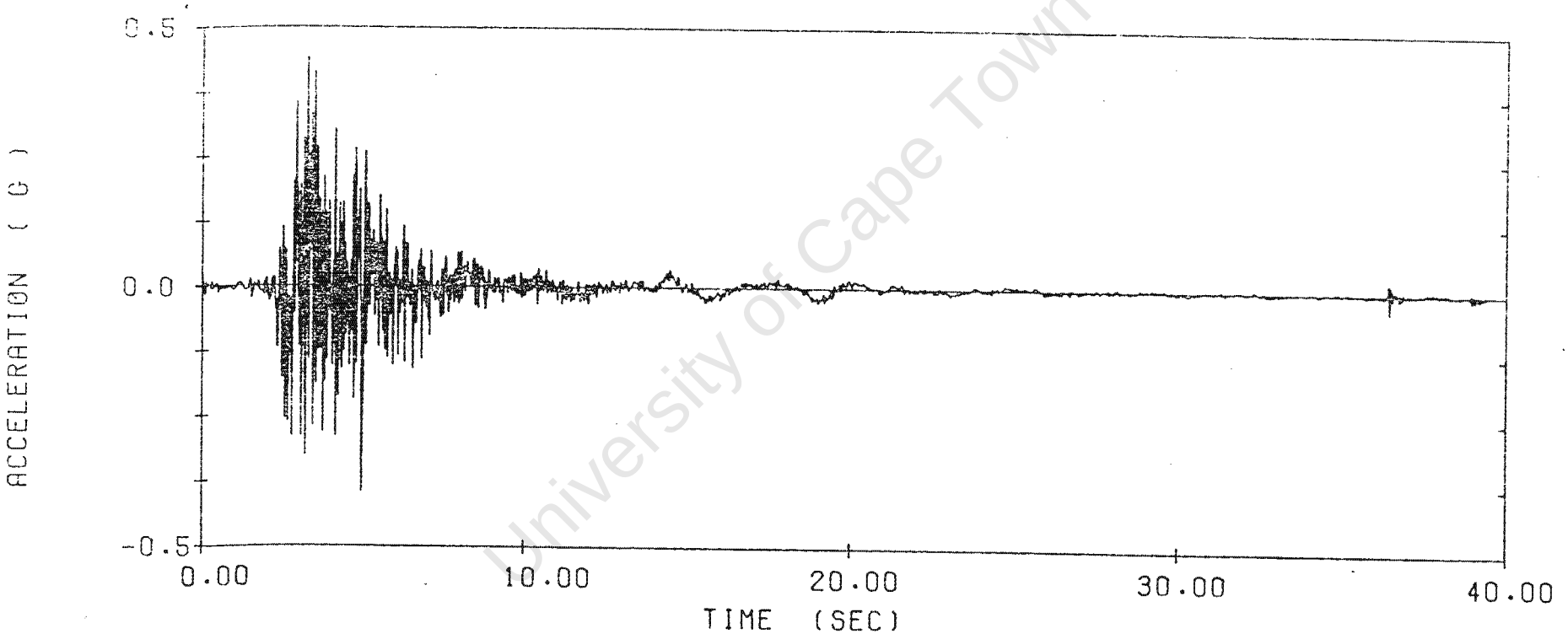

IMPERIAL VALLEY EARTHQUAKE 15/10/79 ST. 952 VERTICAL

NØSTRUM

NØNLINEAR STRUCTURAL MECHANICS RESEARCH UNIT
UNIVERSITY ØF CAPE TØWN

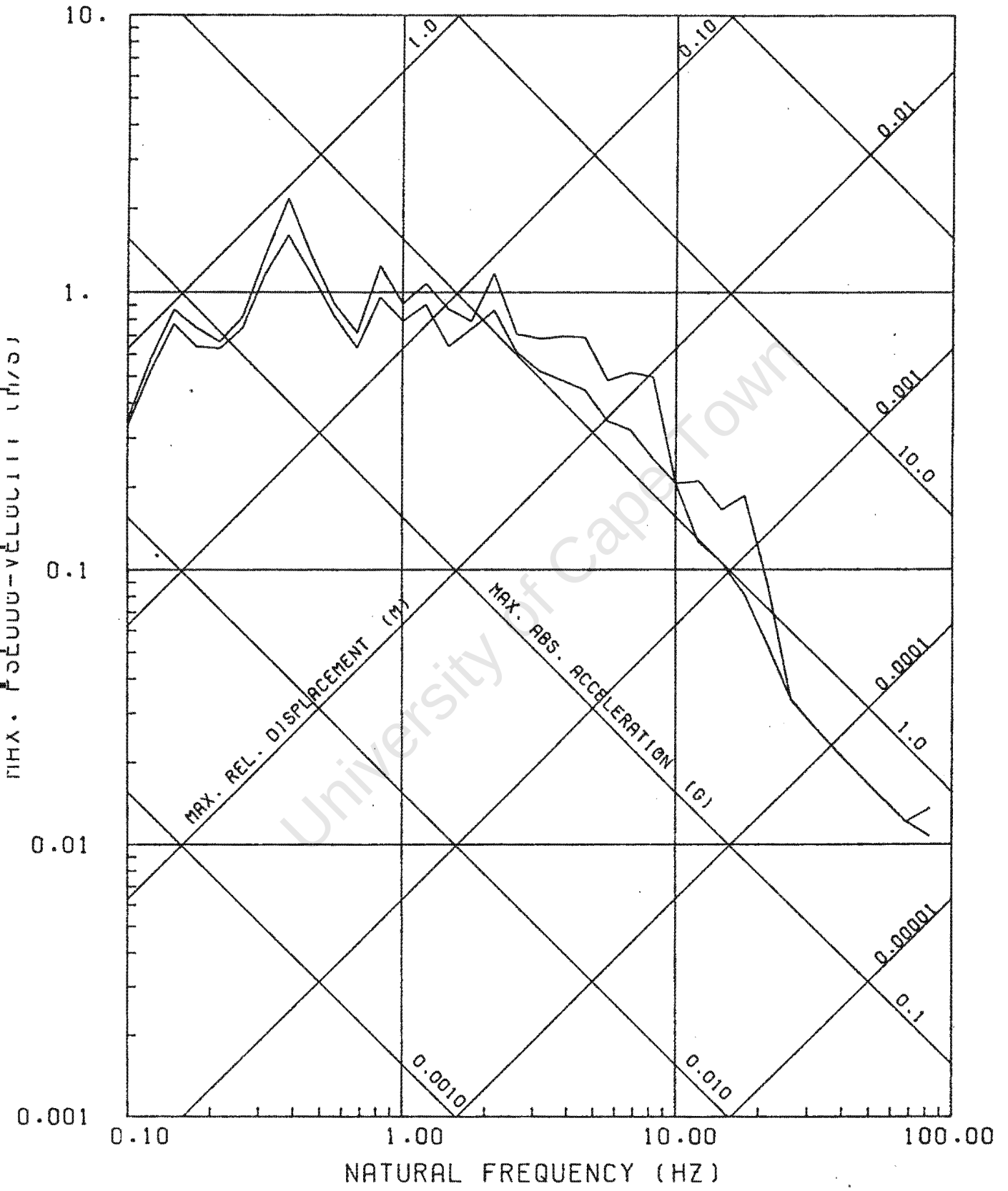

RESPONSE SPECTRA -IMV79/952-3 18SEC

DAMPING : 0%,2%

NØSTRUM

NØNLINEAR STRUCTURAL MECHANICS RESEARCH UNIT
UNIVERSITY ØF CAPE TØWN

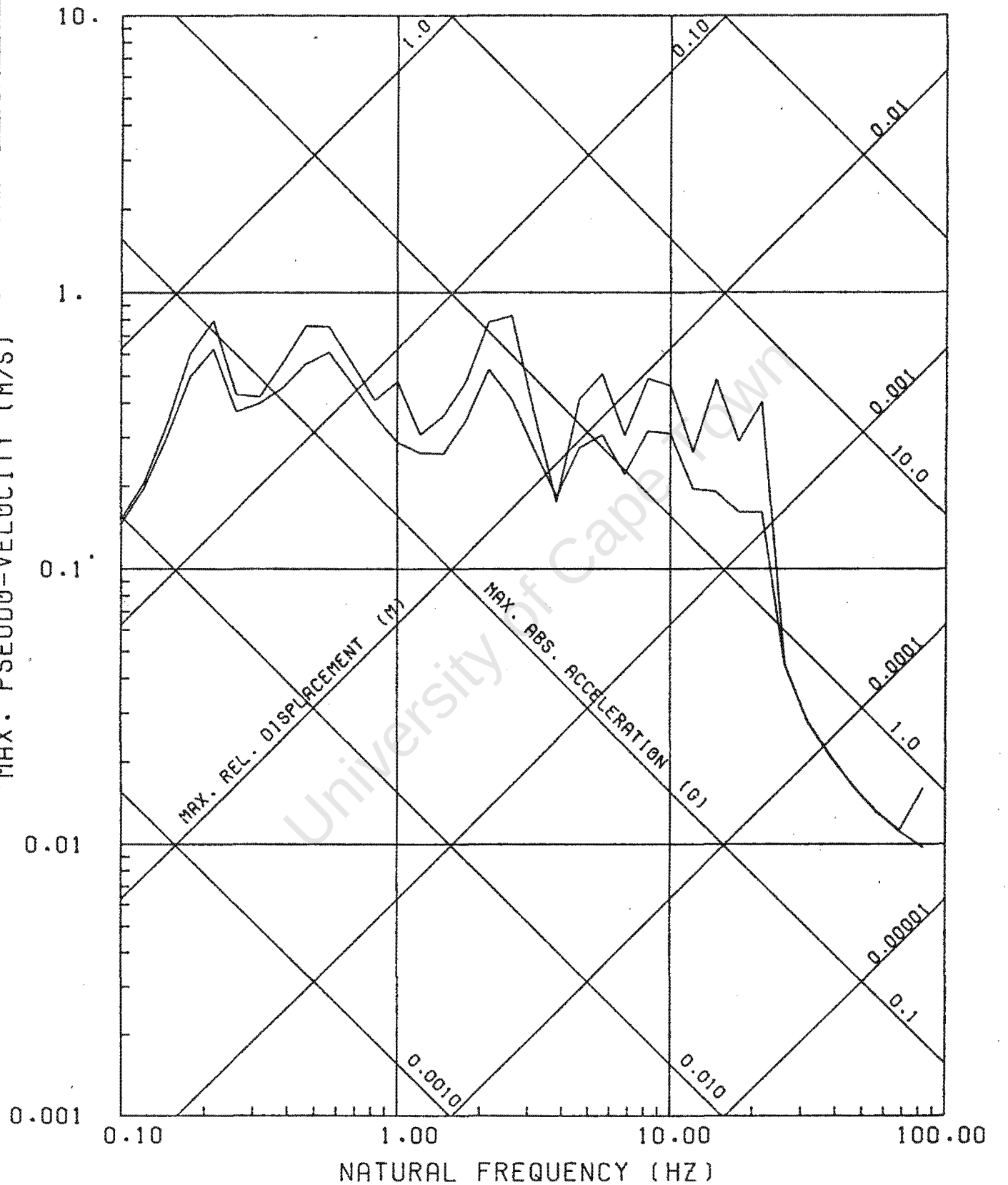

RESPØNSE SPECTRA -IMV79/952-2 18SEC

DAMPING : 0%,2%

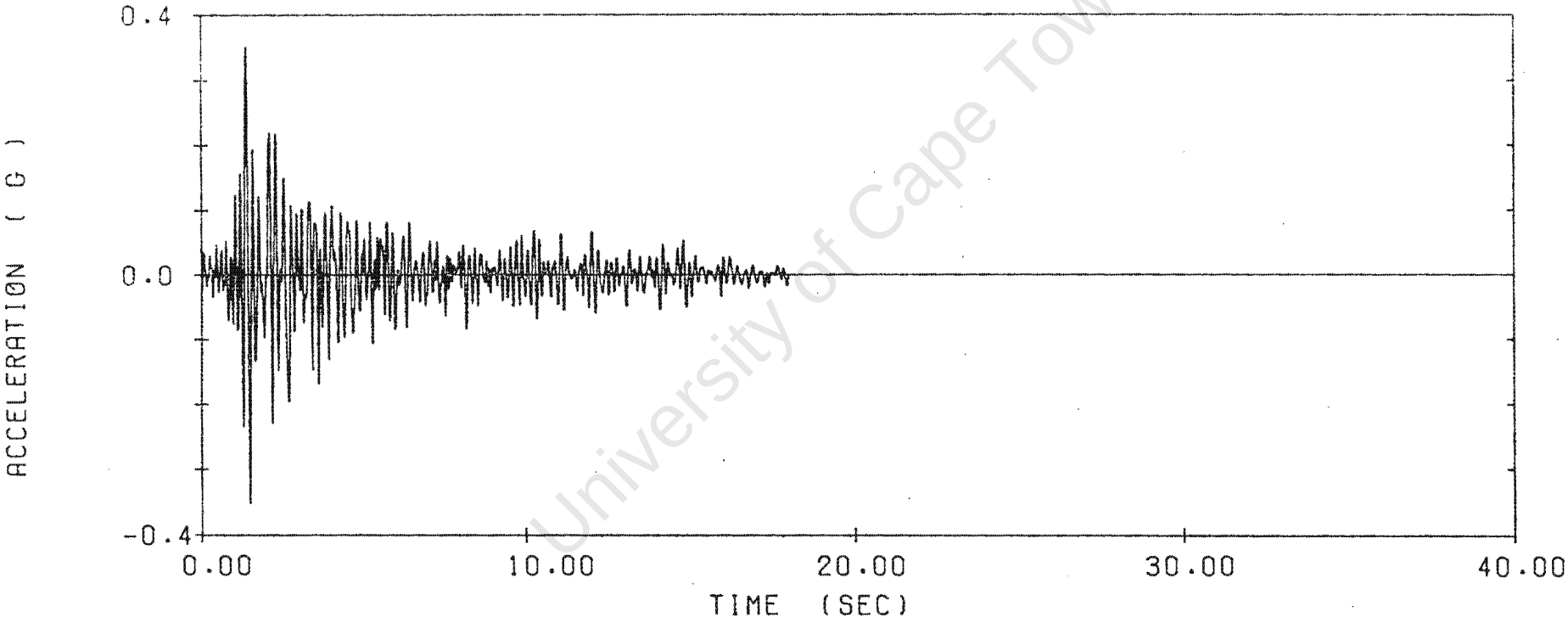

SAN FERNANDO EARTHQUAKE 09/02/71 ST 128 HOR N21E

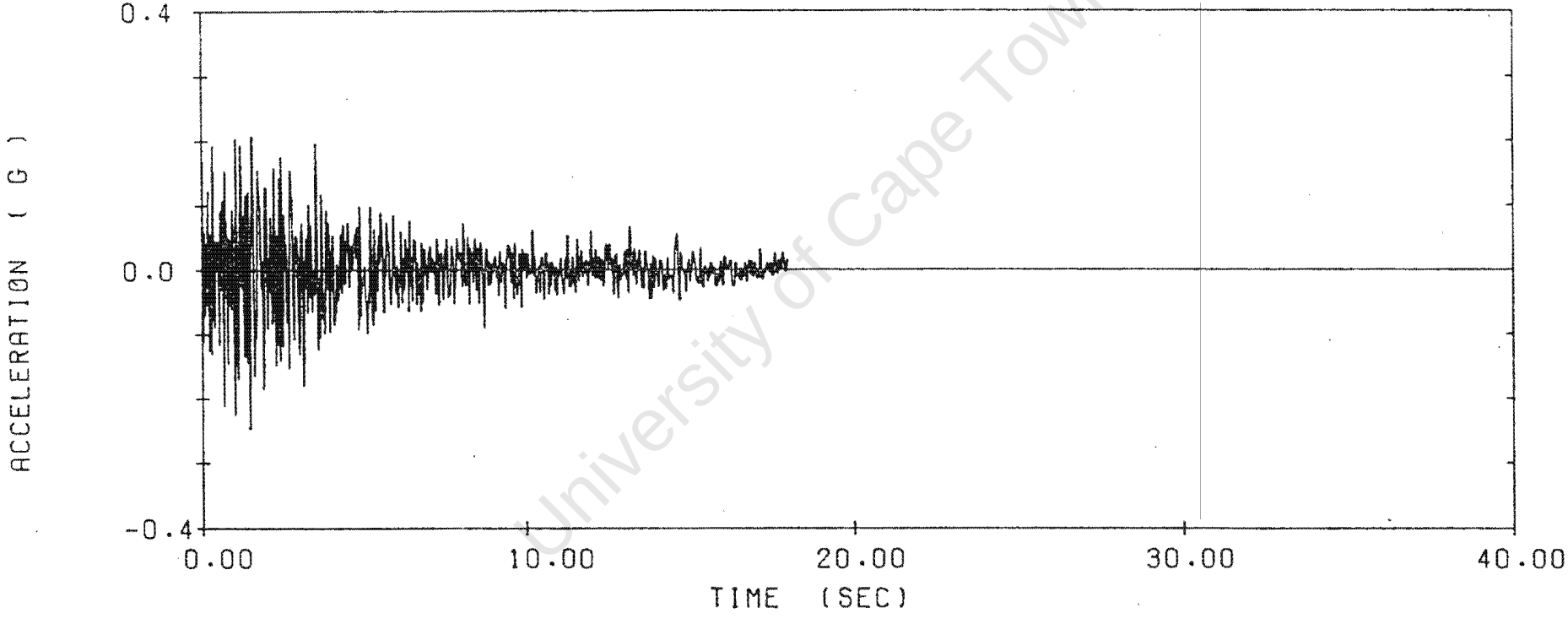

SAN FERNANDO EARTHQUAKE 09/02/71 ST 128 VERTICAL

NØSTRUM

NØNLINEAR STRUCTURAL MECHANICS RESEARCH UNIT
UNIVERSITY ØF CAPE TØWN

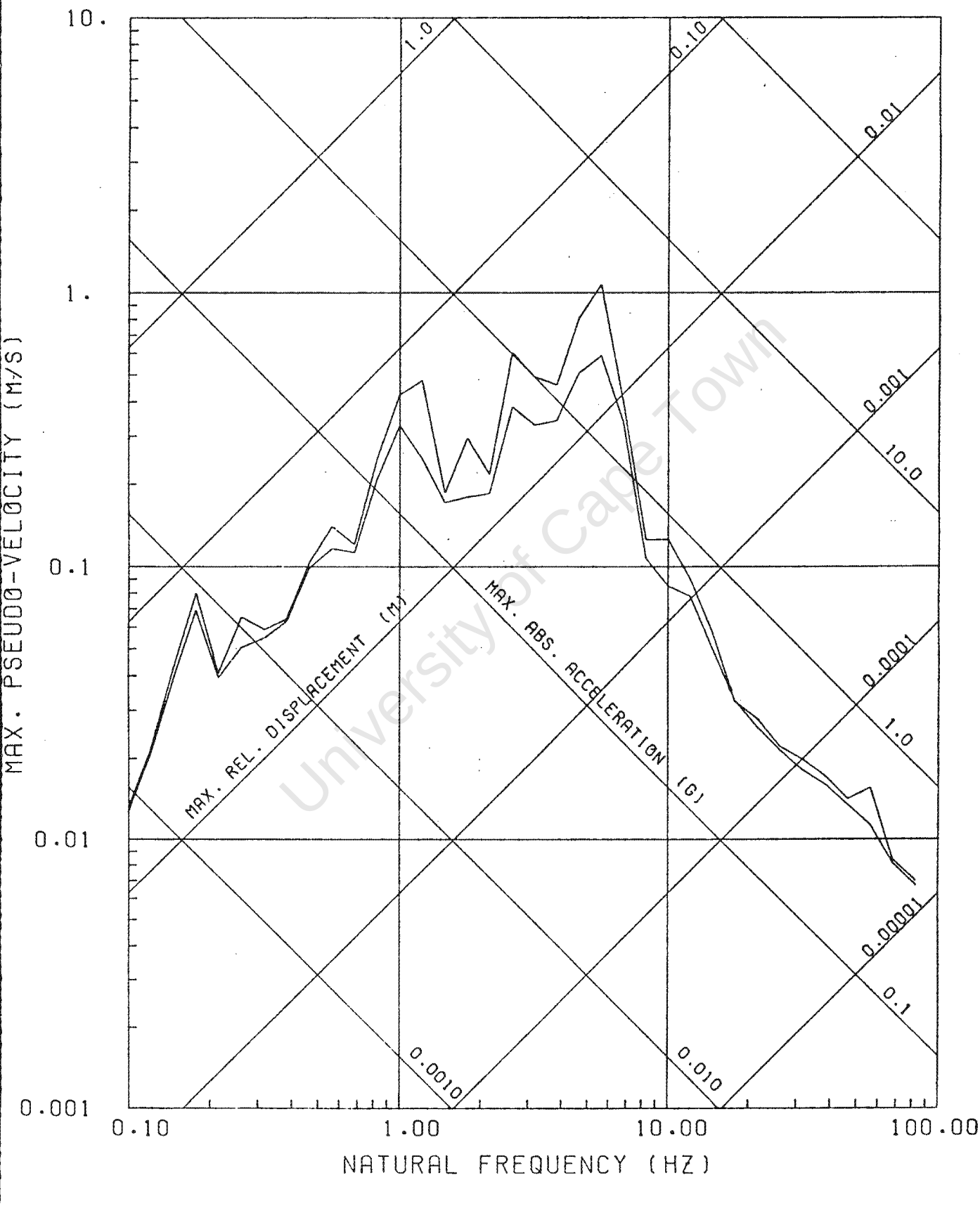

RESPØNSE SPECTRA -SNF71/HØR 18.0 SEC

DAMPING : 0% 2%

NOSTRUM

NONLINEAR STRUCTURAL MECHANICS RESEARCH UNIT
UNIVERSITY OF CAPE TOWN

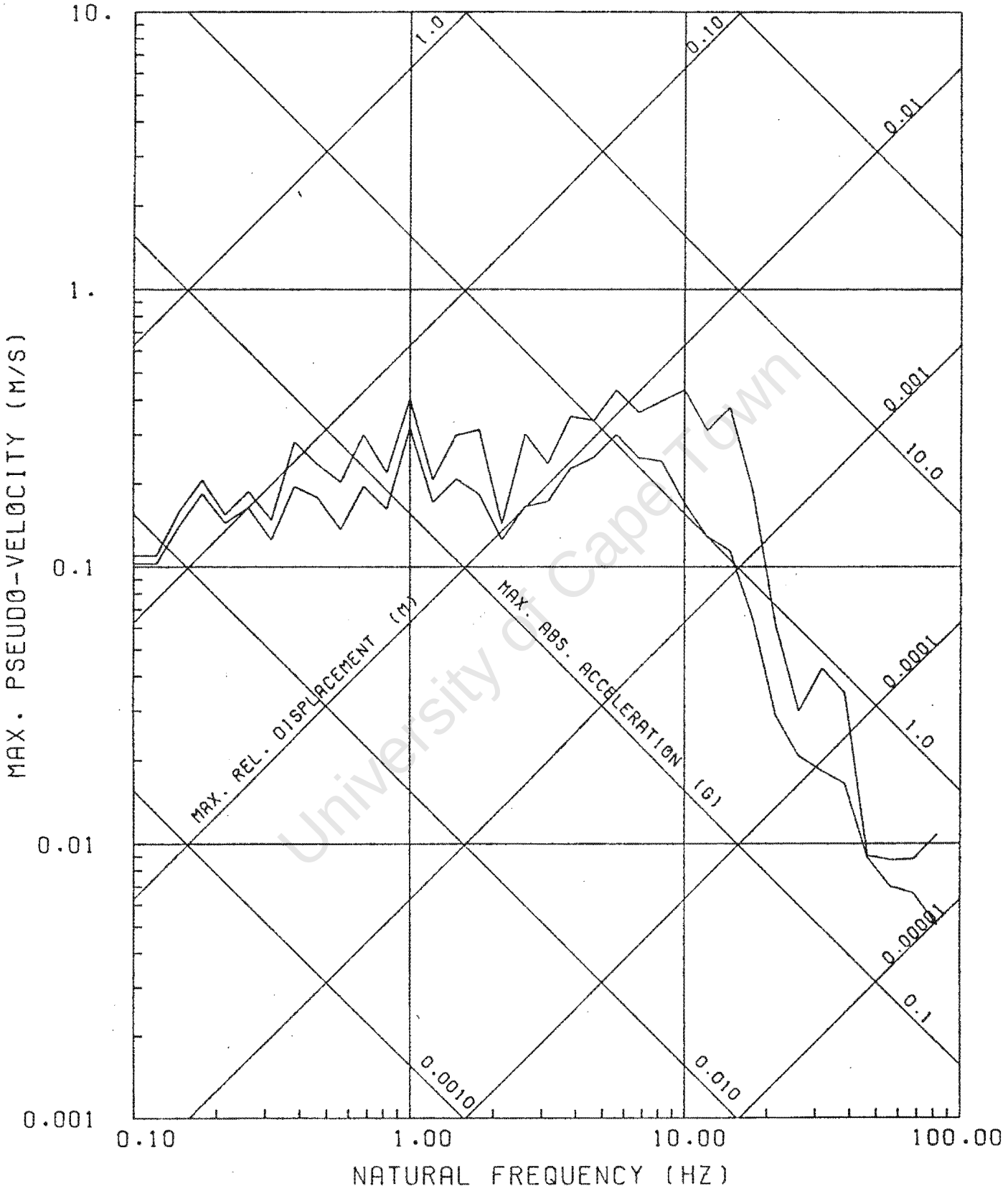

RESPONSE SPECTRA -SNF71/VER 18.0 SEC

DAMPING : 0%.2%

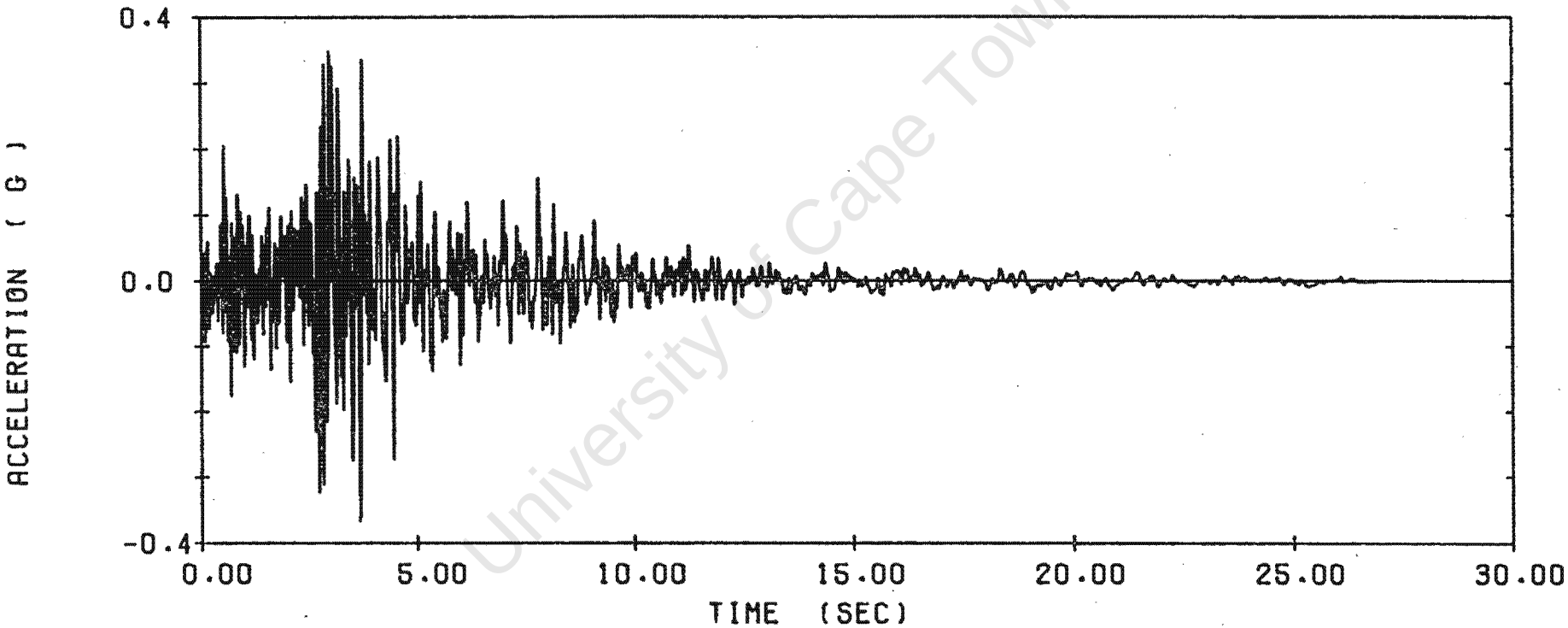

COYOTE LAKE EARTHQUAKE 1979 STATION 1408 H 230 (* 4.3)

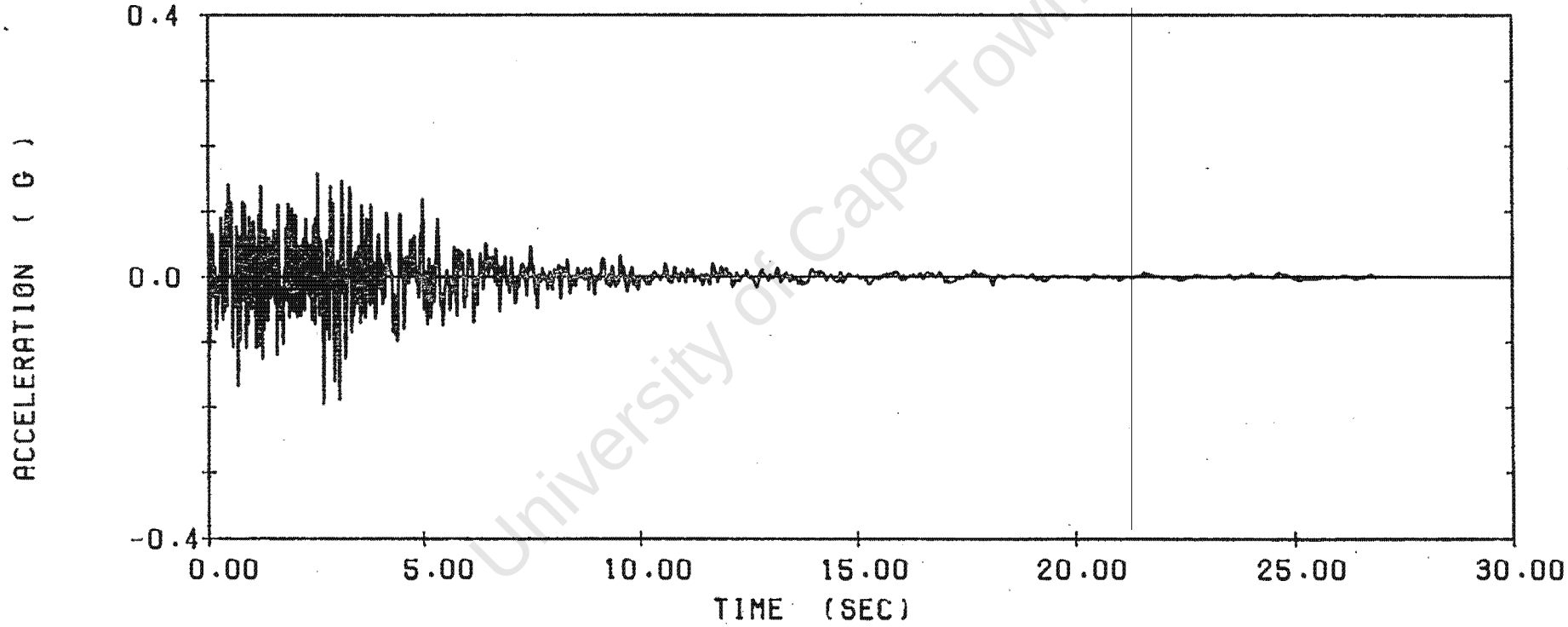

COYOTE LAKE EARTHQUAKE 1979 STATION 1408 UP (* 3.3)

DAMPING : 2%

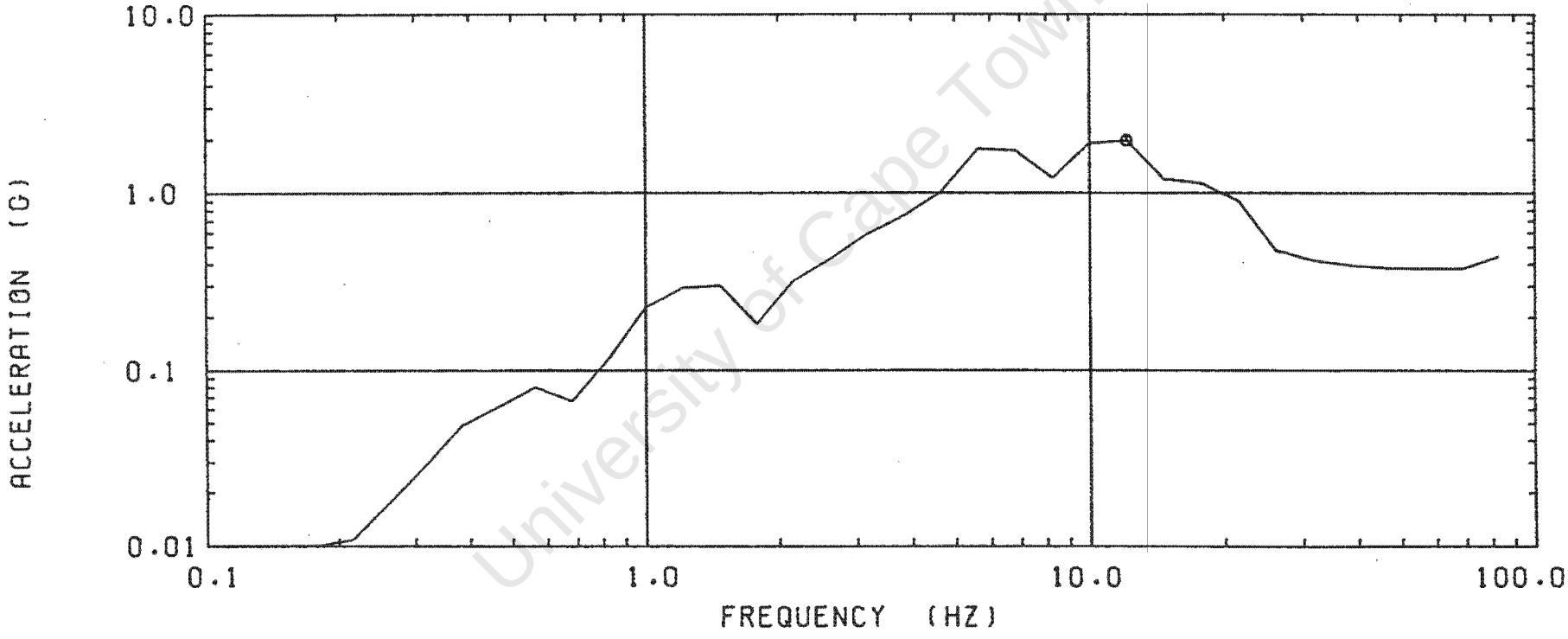

ACCELERATION SPECTRA HORIZONTAL 230 (*4.3 1200 STEPS)
COYOTE LAKE EARTHQUAKE STATION 1408 MAXIMUM ACCELERATION 1.961 @

DAMPING : 2%

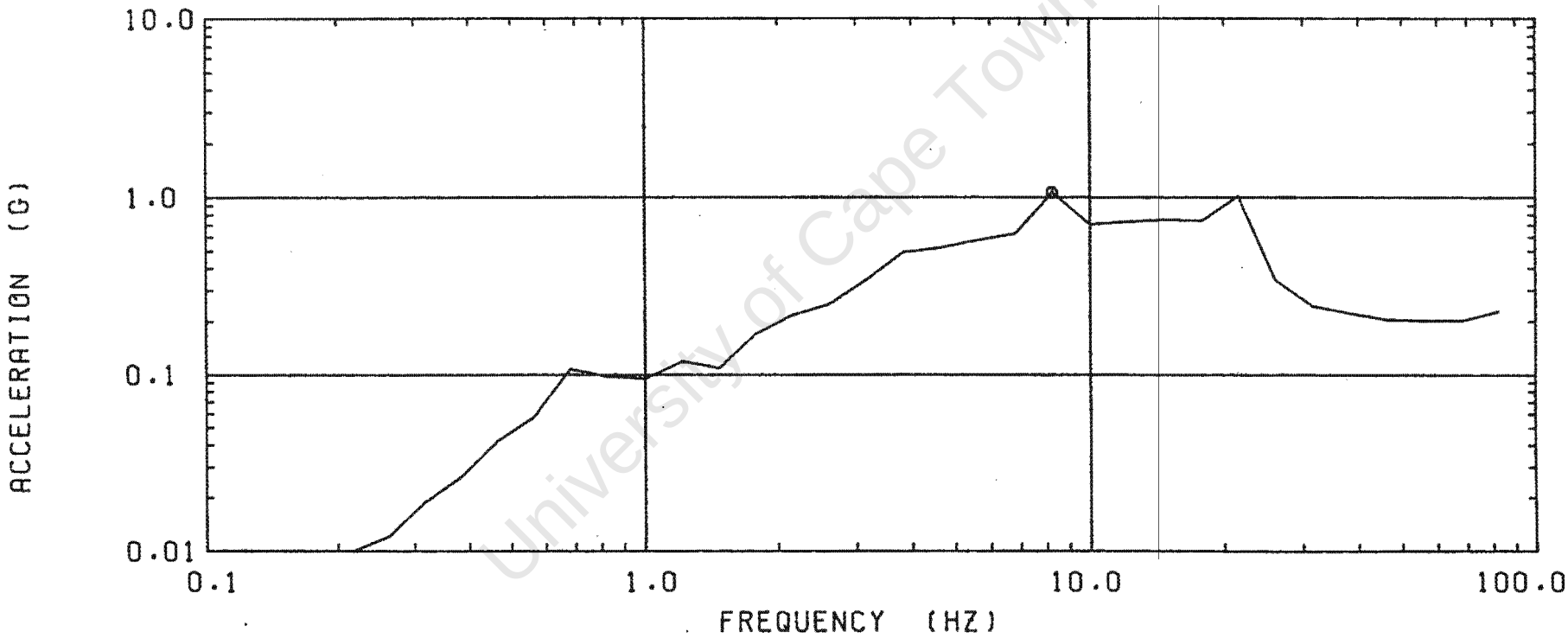

ACCELERATION SPECTRUM VERTICAL (*3.3 12.0 SEC)
COYOTE LAKE EARTHQUAKE STATION 1408 MAXIMUM ACCELERATION 1.058 G

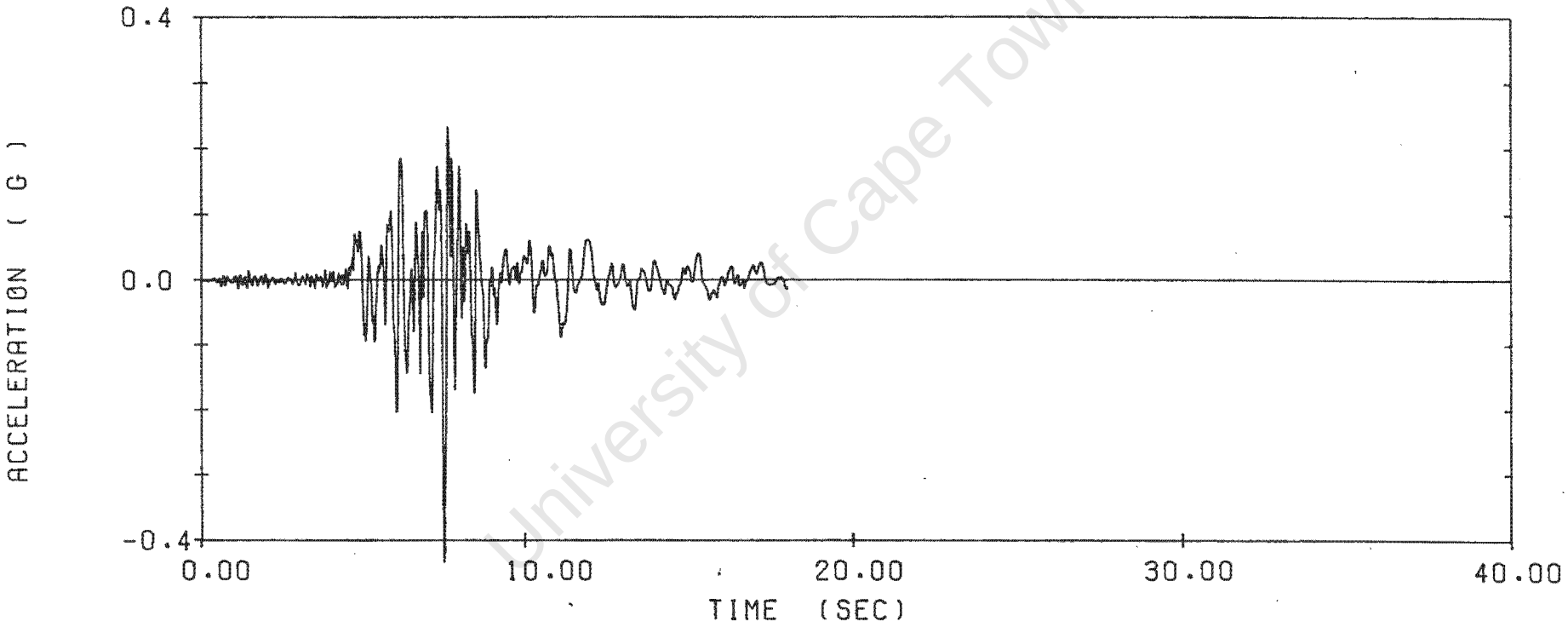

PARKFIELD EARTHQUAKE 27/06/66 ST 014 H0R N85E

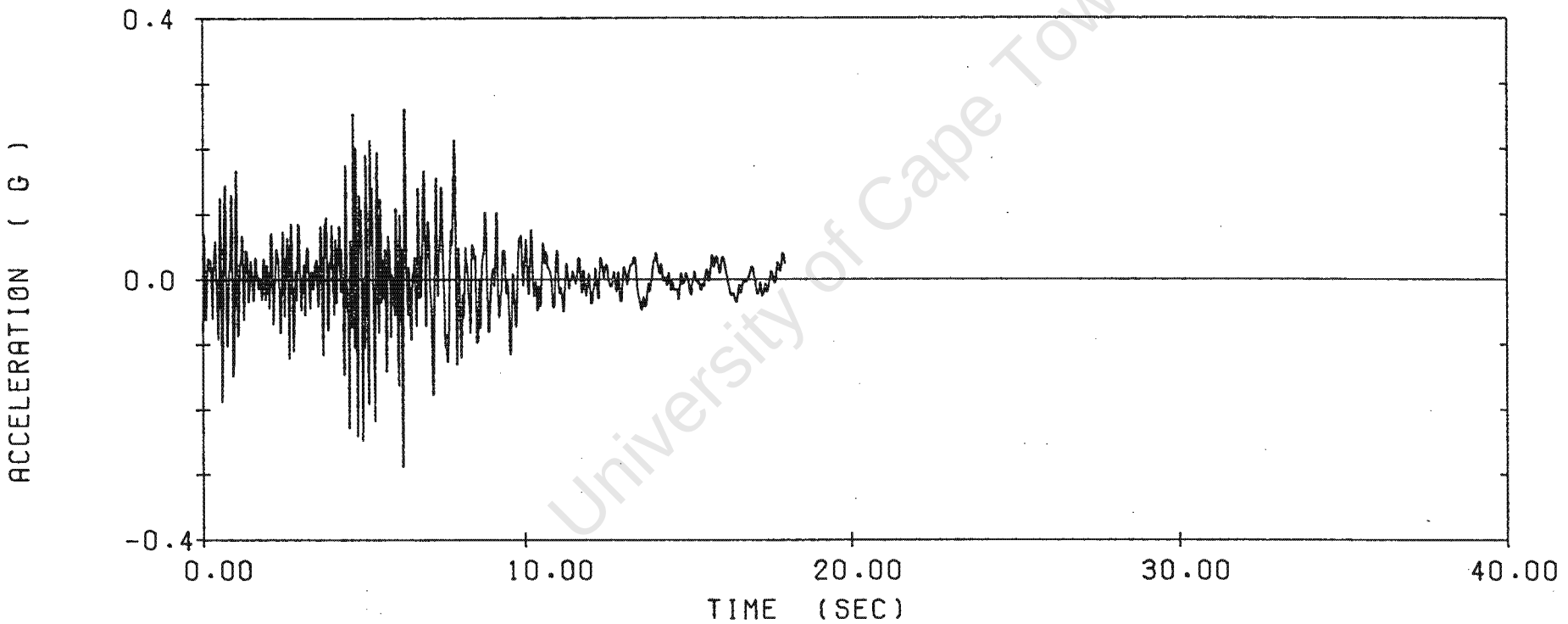

PARKFIELD EARTHQUAKE 27/06/66 ST 014 VERTICAL

NØSTRUM

NØNLINEAR STRUCTURAL MECHANICS RESEARCH UNIT
UNIVERSITY ØF CAPE TØWN

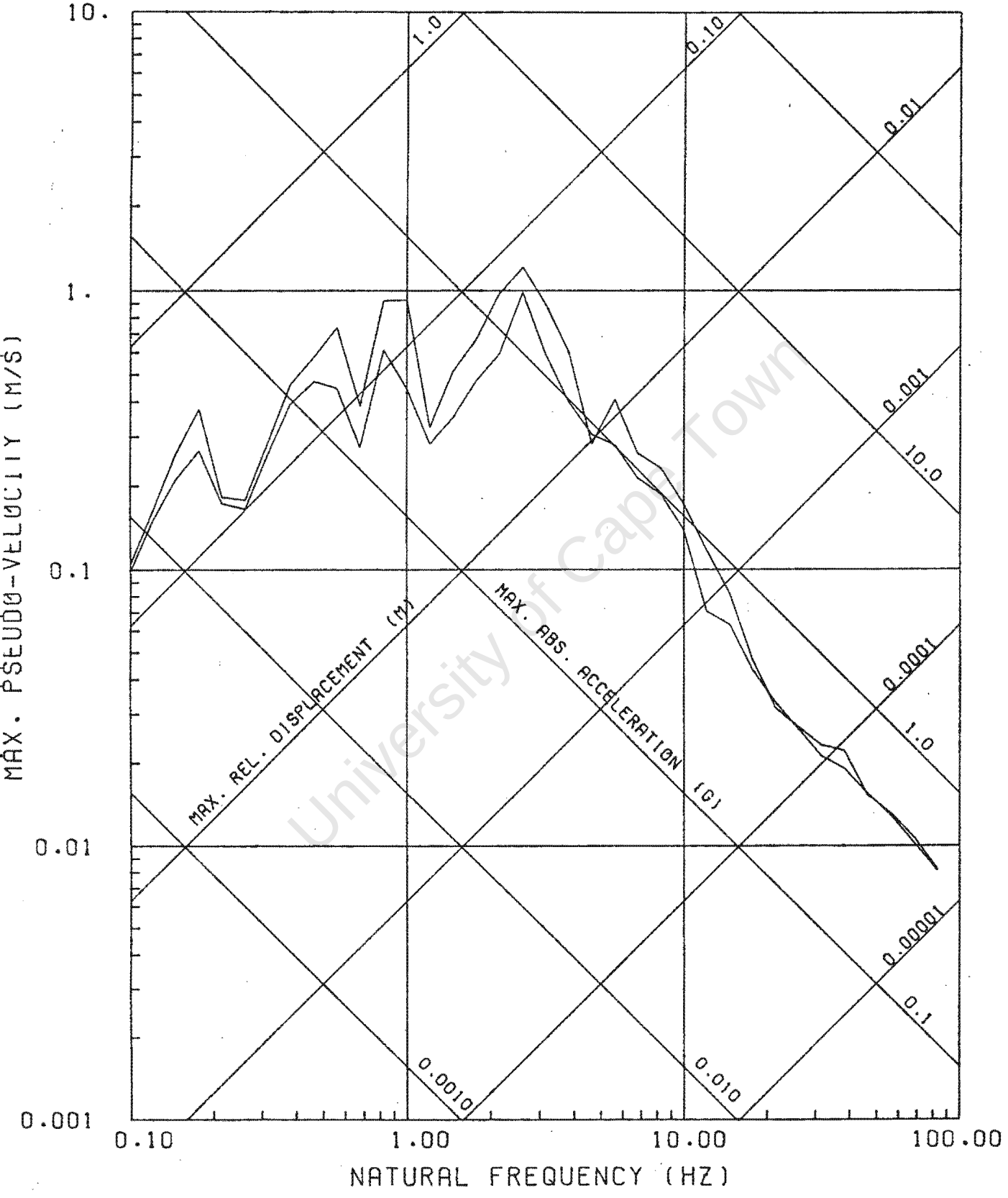

RESPØNSE SPECTRA -PKF66/ ST 014 /N85E

DAMPING : 0%,2%

NØSTRUM

NØNLINEAR STRUCTURAL MECHANICS RESEARCH UNIT
UNIVERSITY ØF CAPE TØWN

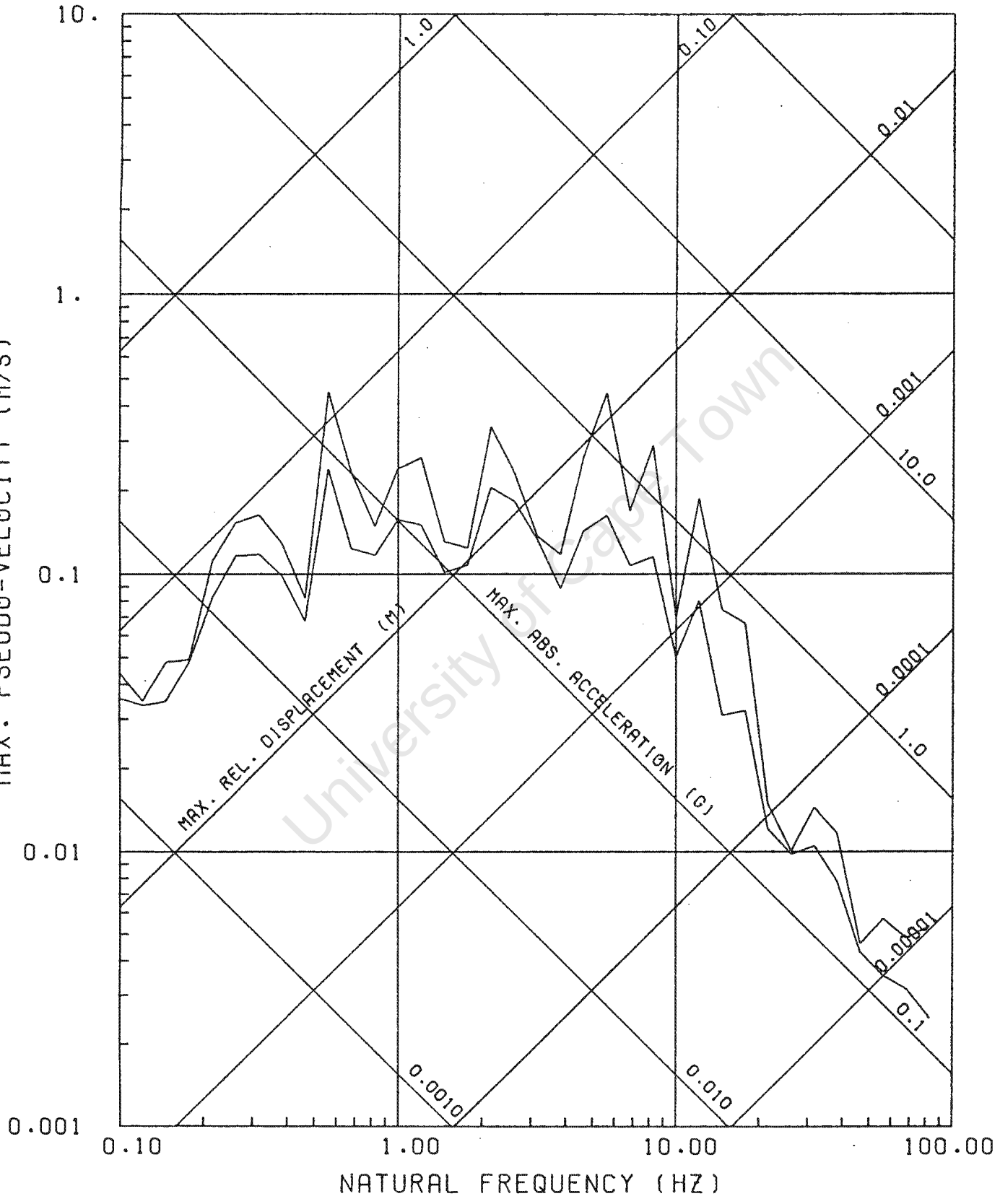

RESPØNSE SPECTRA -PKF66/ ST 014 /VERT

DAMPING : 0%,2%

APPENDIX C

Since this thesis was in partial fulfilment for the degree of Master of Science in Engineering, the remaining work that had to be done in order to fulfil the requirements of the degree was 20 credits of coursework. The coursework was to be related to civil engineering and therefore the courses that were taken, at the University of Cape Town, in 1983 were the following.

NO.	COURSE NAME.	CREDIT RATING
1.	Frame Analysis	2
2.	Introduction to the Theory of Elasticity	2
3.	Plates and Shells	2
4.	An Introduction to the Finite Element Method	2
5.	Finite Element Analysis	3
6.	Numerical Analysis	4
7.	Ship Hydraulics	3
8.	Marine Pipelines	3

A breakdown of the material covered in the courses follows together with the examination papers presented in the course. In the case of Finite Element Analysis, Numerical Analysis, Ship Hydraulics and Marine Pipelines it was necessary to produce a term paper which contributed towards the overall class mark.

1. Frame Analysis

The application of the force method of analysis to framed structures of straight and curved members. The stability of equilibrium of framed structures.

7. Ship Hydraulics

Ship hydrostatics, ship dynamics, added mass. Shiphandling, turning, shallow draught effects. Ship interaction.

8. Marine Pipelines

Types of marine pipes. Ocean wave-induced water motion causing flow forces on exposed pipes. Calculations of forces and ballast required to withstand them. Armor rock stability. Inshore and offshore outfall construction. Outfall systems, hydraulics and dilution calculations.